Masters Theses

Student Theses and Dissertations

Spring 2015

3D numerical modelling of micropiles interaction with soil & rock

Audai Kamal Theinat

Recommended Citation

3D NUMERICAL MODELLING OF MICROPILES INTERACTION WITH SOIL &

ROCK

by

AUDAI KAMAL THEINAT

A THESIS

Presented to the Faculty of the Graduate School of the

MISSOURI UNIVERSITY OF SCIENCE AND TECHNOLOGY

In Partial Fulfillment of the Requirements for the Degree

MASTER OF SCIENCE IN CIVIL ENGINEERING

2015

Approved by

Dr. Ronaldo Luna, Advisor
Dr. J. David Rogers
Dr. Mohamed ElGawady

ABSTRACT

A 5-span bridge along the Foothills Parkway of the Great Smoky Mountains, TN, was recently completed. Two out of the four piers were instrumented to measure the load transfer in the foundations. The foundations consisted of twenty 10-inch micropiles under the pile cap for each pier. Strain gages were installed and monitored at the different stages of construction. The objective of this research is to examine the interaction between the ground and micropiles using the field data performance and numerical modelling. The 3D computer model consists of the micropile foundation within the steep rock bedding planes and overburden soils. The field strains matched with numerical modelling results. In the overburden soil, the load transfer was not significant up to interface friction of 0.3 between the micropile and the ground. In addition, the weathered rock in the cased of the long micropiles transfers significant load although it has small friction with the micropile and this is due to the intermediate value of stiffness. Therefore, the bond zone of the long micropiles carries small percentage of the load. In addition, short micropiles carry much higher because the high stiffness rock is closer to the load source. Also, that load transfer behavior of a single micropiles and group micropiles with S/D=3.9 are almost identical. Parametric study showed that the load transfer mechanism is affected by the friction and the elasticity modulus and any of these factors by itself cannot guarantee a good load transfer. In addition, Poisson's ratio as well as plasticity parameters including friction angle, dilation angle and cohesion showed small effect on the load transfer mechanism.

ACKNOWLEDGMENTS

TABLE OF CONTENTS

LIST OF ILLUSTRATIONS

xi

LIST OF TABLES

1. INTRODUCTION AND PROBLEM STATEMENT

Beginning in 1950s in Italy, use of micropiles has grown significantly in earth structures and slope excavations. The main objective of micropiles is to provide support for foundations in static and dynamic conditions (Armour, 2000). Micropiles are replacement piles, cast in place with a small diameter, which can withstand either axial or lateral loading conditions (Armour, 2000). They are attractive to engineers and clients alike because they provide high load bearing capacity. They can be constructed in difficult access areas, restricted clearance, poor ground conditions while maintaining minimal disturbance to the surroundings. Micropiles are also used effectively in seismic areas, particularly, when a network of micropiles is applied. Advances in drilling equipment and research contributed to the development of this new innovation as a powerful support system in foundation engineering (Cadden et al., 2004).

A micropile's behavior, including the load transfer mechanism and the displacement of micropiles with depth is quite complex and not fully understood. Field monitoring, full laboratory scale testing, analytical methods, and finite element methods are the main methods used to study this behavior.

The finite element method is preferable over other methods; it allows modeling different soil and pile geometries with different boundary and loading conditions. It also takes into account the continuous nature of soil, and it provides a solution at each node and element in the model (Khodair and Abdel-Mohti, 2014).

This research was conducted in an attempt to generate 3D finite element models of the micropiles located underneath Bridge No.2 of the Great Smoky Mountains. The results provide keys to understand the load transfer mechanism of the micropiles and the displacement with depth. The group effect on micropiles was also examined. The results gathered were compared to the monitoring field results taken from strain gauges inserted at various depths.

1.1. BACKGROUND

The growing travel and problems of congestion in the late 1930s created a need for a parkway in the foothills of the Great Smoky Mountains (located in Tennessee). This parkway aimed to provide a scenic view of the mountains, alleviate traffic pressure, and provide an access to other areas of the park (FPMP, 1968).

Construction began on the first section began in 1960 (FPMP, 1968). Unfortunately, the bridge was continuously stalled by funding difficulties; making this bridge the oldest unfinished bridge in Tennessee. One-third of the parkway had been completed and opened to traffic as of 2010.

The parkway is 70 miles long connecting route 129 with interstate 40. The parkway plan has eight sections: 8A to 8H. Both the parkway map and its individual sections are illustrated in Figure 1.1.

The 9.7 miles in Section 8E connects Wears Valley to Carr Creek. It contains 1.6 mile unfinished section that is known as the missing link. The missing link requires ten bridges; two of them have been completed: Bridge No.1 and Bridge No 2 (Bell, 2012).
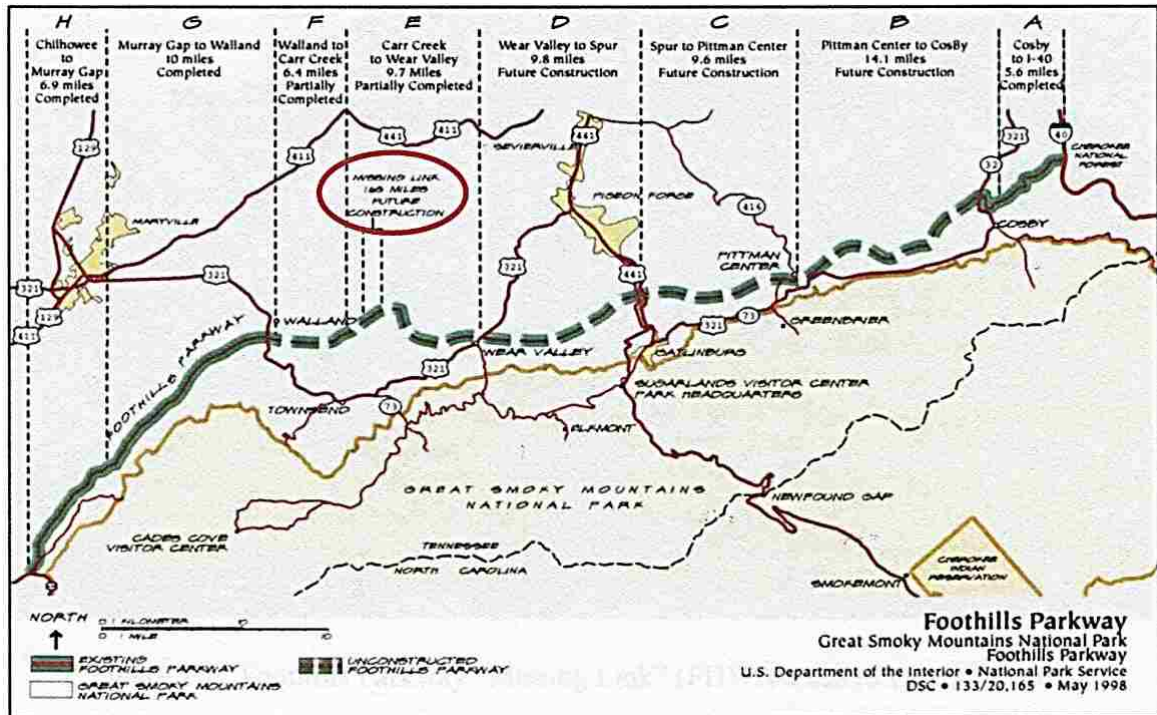
Figure 1.1. Parkway Map (NPS, 1998).

Cooperation between National Park Service and Dan Brown and Associates resulted in a grant to Missouri University of Science and Technology that permitted the installation of field instrumentation underneath Bridge No.2 (Dixon, 2013). This instrumentation was used to collect strain readings at various depths of the micropiles underneath the bridge. Bridge No.2 was completed on December 13, 2012 (Bell, 2012).

1.2. RESEARCH OBJECTIVES

This study included the following objectives:

- Perform a numerical simulation to understand the load transfer mechanism of a single micropile.

- Study the contact and the interaction mechanism of the micropile cased and bond zones with overburden soil, weathered and competent rocks.

- Study the interface friction developed along the micropile in both the cased zone and the bond zone.

- Perform a micropile group simulation to study the group effect on the load transfer mechanism of micropiles.

- Perform a parametric study to investigate the variation in the response of micropiles when different material and loading conditions are presented.

- Study the effect of variation on friction and contact on the load transfer of the micropiles in both the cased zone and the bond zone.

- Compare the field results of the instrumented micropiles with the numerical modeling results.

1.3. THESIS ORGANIZATION

The research presented within this thesis is organized into eight sections. The first section provides a background, objectives, and an overview of the thesis organization. The second section contains a literature review on the load transfer mechanism of micropiles including field and lab testing as well as analytical and numerical methods.

Section 3 contains the results that were gathered from the field instrumentation. These results include information on the site, superstructure, subsurface conditions, the micropiles' design, installation, and instrumentation.

Material and constitutive models as well as the contact and interaction mechanism are discussed in Section 4. Numerical modelling approach is also discussed in Section 4. Numerical simulations of the single behavior of micropiles as well as their response within a group is presented in Section 5 and Section 6, respectively.

A parametric study on the variation of the load transfer mechanism for wide range parameter is discussed in Section 7. The friction variation effect on the load transfer mechanism is addressed in this section as well. This discussion included also friction sensitivity analysis in both the cased and the bond zones.

Conclusions drawn from this research and recommendations for future research are presented in Section 8.

2. LITERATURE REVIEW

Pile foundations are long, slender, prefabricated, or cast-in-place structural members that can support either axial or lateral loads. Piles are used when the upper soil is very weak, the imposed load is very high, and the spread shallow footings cease to be effective. Piles are also considered a good solution when they are subjected to either scour or undermining, the foundation penetrates water, or a large lateral load is expected (Coduto, 2001). Piles are divided into two main categories: displacement piles and non-displacement (replacement piles). Displacement piles displace soil during installation while replacement piles are placed within previously excavated holes (Armour, 2000).

Micropiles are small diameter replacement piles that are grouted and reinforced with steel. They can resist both axial and lateral loads. They can also increase the bearing capacity and reduce the settlement (Juran et al., 1999). Most micropiles can carry compressive and tensile load of 300-1000 kN. In some cases, they can carry more than 5000 kN. Micropiles are typically 100 mm-250 mm in diameter and 20m -30 m long; they are rarely more than 60 m long (Juran et al., 1999, Bruce, 2002). The steel in micropiles comprises more than 50% of the size. Thus, steel has the largest role in the load carrying capacity.

According to Armour (2000), micropiles are used in two main applications: reinforcement and structural support. Reinforcement includes landslide stabilization, soil strengthening, structural ability, and settlement reduction. Structural support includes: retaining of structures and stability, the creation of a foundation for new structures, the

placement of seismic retrofit and the underpinning of existing foundations .Underpinning is an advantage of micropiles due to their small size; they help minimize disturbance during construction and limit the needed clearance (Lizzi, 1982, Armour, 2000).

Additional advantages of micropiles include the following:

- A cost effective method,

- The ability to use in difficult terrain and soil condition,

- Flexibility under seismic loading,

- Easy construction of inclined micropiles,

- Less displaced volume and they can be drilled with no much noise (Bruce et al., 2004). Micropiles, therefore, are often preferred more than conventional piles.

Micropiles are constructed in a three step process; a hole is drilled, the reinforcement is placed, and the grout is applied as shown in Figure 2.1. Micropiles can be classified into two systems; philosophy of behavior and method of construction (Juran et al., 1999). The philosophy of behavior classifies micropiles, according to their design method, into two cases; Case I is the directly loaded piles; individually or in groups, and Case II is the root construction of micropiles; in networks and three dimensional reticulated piles.

Method of construction classifies micropiles based on the grouting method. This method affects the bond between the ground and the grout itself. The method of construction and drilling technique affect the chosen type of the micropile and the load transfer mechanism as shown in Table 2.1 (Armour, 2000).

All methods of construction can be classified into four main categories:

- Type A Micropiles: The grout is placed under gravity. The grout is typically composed of both sand cement mortars as well as neat cement because no pressure is used to inject the grout.

- Type B Micropiles: The grout is injected with pressure between 0.5 and 1.0 MPa. It is applied while the temporary steel casing is being withdrawn from the hole.

- Type C Micropiles: The gout is placed first by gravity, in same manner as that in Type A. Similar grout is injected with a pressure of at least 1 MPa before the grout hardens. This pressure is applied packer.

- Type D Micropiles: the gout is placed first by gravity in same manner as that in Type A. Additional grout is injected at a pressure between 2 and 8 MPa. The pressure is applied with a packer so that horizons can be treated several times.

The effect of the grouting method on the micropiles' in different types of soils can be seen in Table 2.1. A Type D micropile (which utilizes a high amount of pressure) produces the highest friction values.

The temporary steel casing is typically placed before the grouting stage to prevent the hole from collapsing. The casing is removed to allow the load transfer by ground/grout bond in the solid foundation zone/bond zone.

Micropiles design can be classified as either an internal design or an external design. The internal design is the strength of the micropile composite section which depends mainly on the area of the section and the reinforcement strength, In contrast, the external design is the ultimate axial and lateral capacity of micropiles which they depend

on the bond between the soil and the grout and the initial stress state after the installation of the pile (Juran et al., 1999).
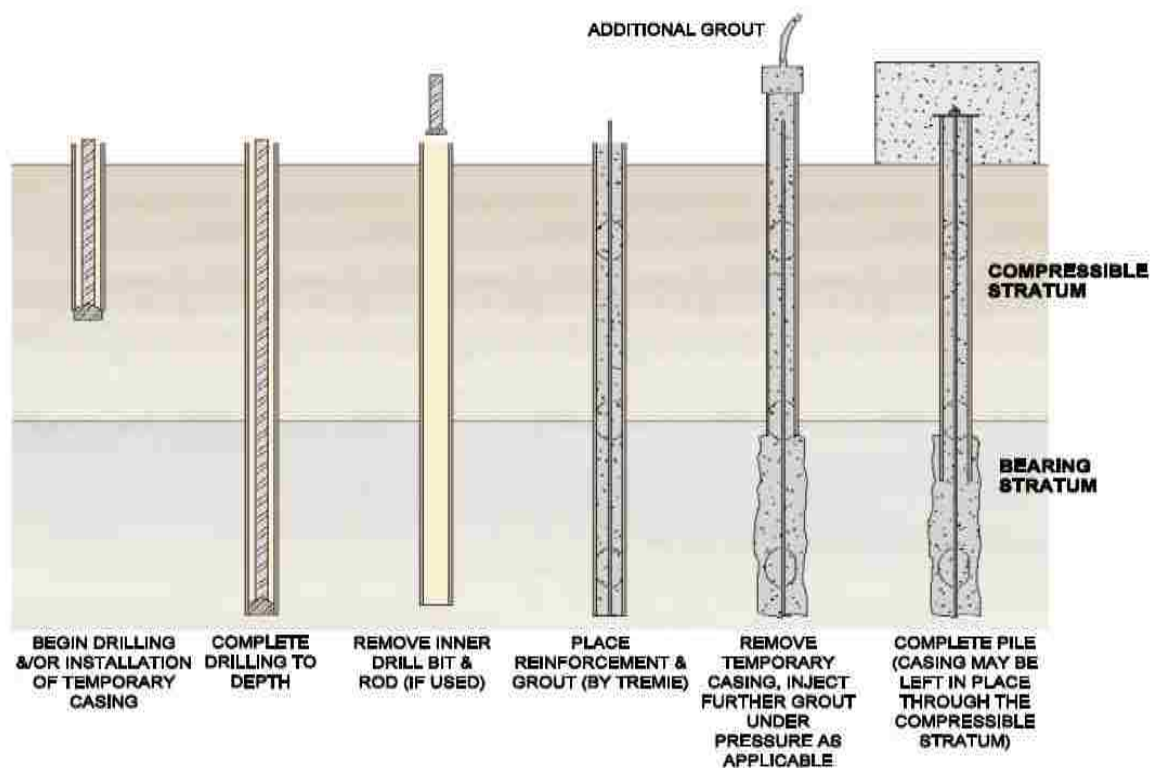
Figure 2.1. Construction Stages of a Micropile (Armour, 2000).

Micropiles' final design should be subjected to field testing to verify both the design assumptions and the installation methods. This testing should include ultimate tests, proof tests, verification tests, and creep tests.

Table 2.1. Grout to Ground Bond for Different Rock and Soil Types (Armour, 2000).

Soil / Rock Description	Typical Range of Grout-to-Ground Bond Nominal Strengths (kPa)			
	Type A	Type B	Type C	Type D
Silt & Clay (some sand) (soft, medium plastic)	35-70	35-95	50-120	50-145
Silt & Clay (some sand) (stiff, dense to very dense)	50-120	70-190	95-190	95-190
Sand (some silt) (fine, loose-medium dense)	70-145	70-190	95-190	95- 240
Sand (some silt, gravel) (fine-coarse, med.-very dense)	95-215	120-360	145-360	145-385
Gravel (some sand) (medium-very dense)	95-265	120-360	145-360	145-385
Glacial Till (silt, sand, gravel) (medium-very dense, cemented)	95-190	95-310	120-310	120-335
Soft Shales (fresh-moderate fracturing, little to no weathering)	205-550	N/A	N/A	N/A
Slates and Hard Shales (fresh-moderate fracturing, little to no weathering)	515-1,380	N/A	N/A	N/A
Limestone (fresh-moderate fracturing, little to no weathering)	1,035-2,070	N/A	N/A	N/A
Sandstone (fresh-moderate fracturing, little to no weathering)	520-1,725	N/A	N/A	N/A
Granite and Basalt (fresh-moderate fracturing, little to no weathering)	1,380-4,200	N/A	N/A	N/A

The ultimate test brings the pile to failure, providing information not only on the grout/ground bond but also on the load at the time of excessive creep deformation. Verification tests ensure that proper installation methods have been applied. Proof tests verify that the production micropiles can carry the designed loads without excessive

movements or long term creep. Creep tests are performed as part of the ultimate test, verification test, or proof test.

2.1. BACKGROUND

Soil structure interaction (SSI) is the behavior of the interface between the structure and the foundation soil. The relative motion between the soil and the foundation, as well as different mechanisms of load transfer, causes high nonlinearity in the behavior. As a result, soil structure interaction and load transfer mechanisms are complex. Field monitoring, full scale load tests, analytical methods and numerical methods are conducted to understand the interaction that takes place between soil and the surrounding structures.

Piles can transfer compressive loads, tensile loads and lateral loads. A compressive load is transferred via two main mechanisms: skin friction and end bearing. Skin friction is produced by results the adhesion and friction that occur between the pile and the surrounding soil. End bearing is the result of the interaction at the bottom of the foundation. A tensile load is transferred via skin friction and the foundation's weight. A lateral load is resisted by the stiffness of the pile and the resistance of the surrounding soils (Coduto, 2001). The load transfer mechanism in a conventional pile for axial compression, uplift, and lateral loading, respectively, is illustrated in Figure 2.2.
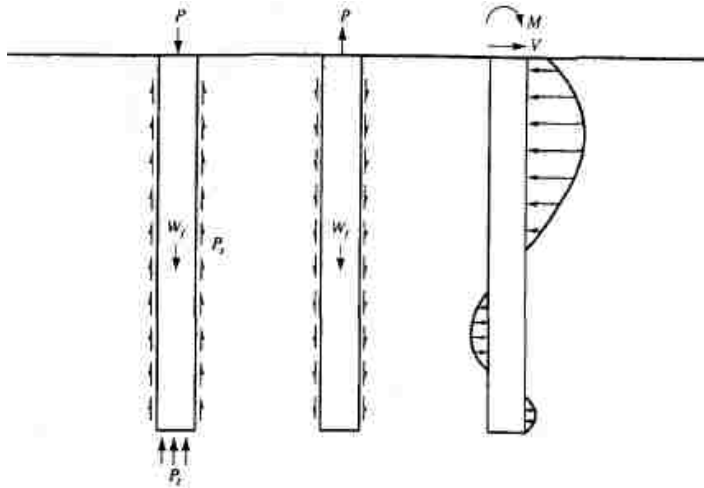
Figure 2.2. Load Transfer Mechanism of a Conventional Pile (Coduto, 2001).

2.2. SOIL-MICROPILE INTERACTION

Micropiles have very small diameters. Therefore, the end bearing capacity is almost negligible, and the load is carried primarily by the friction that is induced in the bond zone. The load is primarily resisted by the steel that occupies more than half of the micropile's volume. The grout transfers the load from the steel bar to the soil by friction. This high friction is generated by the various grouting techniques that allow for generating a strong ground/grout bond. The grout/ground bond, therefore, is highly affected by the grouting and drilling methods, as noted in the previous section (Armour, 2000). Additional factors that affect Micropiles' load transfer mechanism include the initial state of stress, properties of the underlying materials, and if the load is compression or tension; all of these factors would affect the unit of skin friction, fs (Bruce and Juran, 1997).

Steel casing is placed to prevent the hole from collapsing. The casing is typically withdrawn from the strong soil/rock to allow the load to transfer as a result of bonding between the ground and the grout. If the steel casing is removed from the total length, then the total length will interact with soil to become fully bonded as shown in Figure 2.3. This bond is, however, unwanted in the weak soil because the soil will have a downdrag effect and negative skin friction would happen in that region. Therefore, casing is typically maintained in the weak stratum area, and then it becomes partially bonded.
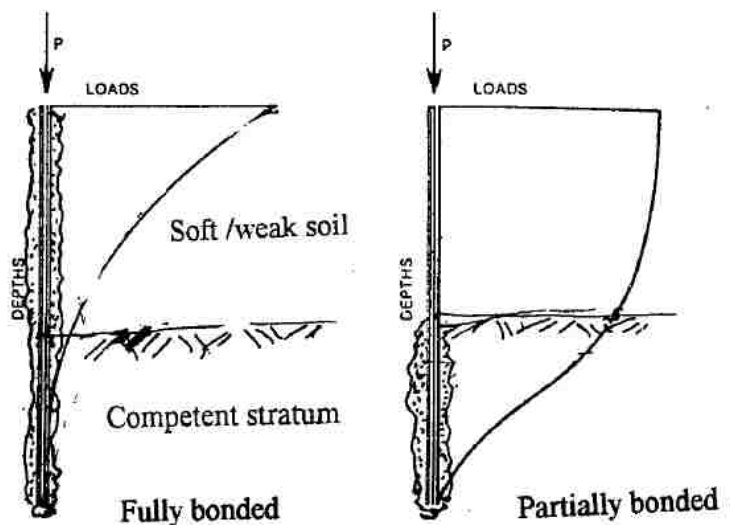
Figure 2.3. Fully Bonded and Partially Bonded Micropiles (Lizzi,1982).

The end bearing is considered to be unimportant in the load transfer mechanism due to the small diameter of the micropile. Juran et al. (1999), however, reported that end bearing would be realistic for moderately loaded micropiles that had been founded on

competent rock. In most cases, therefore, the load is transferred at the bond zone, from the steel bar to the surrounding soil, through the grout, by skin friction when effect from the end bearing is neglected.

2.3. SOIL-MICROPILE STUDY APPROACHES

Previous studies attempted to understand the soil micropile interaction under different loading and geometry conditions. However, nonlinearity in the soil micropile interaction leads to tremendous complexity. Testing and monitoring in the field, full scale laboratory tests, analytical methods, and finite element methods have been used to understand this behavior and allow insights into the micropile performance. Further research is still needed to fully understand this performance.

2.3.1. Field and Full Scale Laboratory Testing. Various tests including both instrumentation in the field and laboratory scale tests were conducted to better understand the load transfer mechanism.

Kershaw (2011) conducted a study on lateral and axial combined loadings. He performed full-scale laboratory testing on micropiles installed in sand. Results showed that deflection was not affected significantly by axial load. Kershaw (2011) also implemented 6 instrumented load tests on micropiles installed in clay. The full scale load tests on clay proved that the axial load can produce a small decrease in both moment and deflection. Kershaw (2011) also deployed P-y curves. P-y curves predicted the load-deflection behavior accurately in clay subjected to lateral and combined loadings. However, the maximum bending moment was over-predicted by p-y curves.

Holman and Barkauskas (2007) used 34 strain gages to instrument 3 micropiles from 2 case histories; two micropiles were brought to plunging failure and one to the impending failure. The load transfer mechanism in the surrounding soil indicated that the micropiles' secant modulus of micropiles decreased as the level of strain increased. Additionally, the load distribution in the bond zone was nonlinear. Strain incompatibility was questionable in the micropiles' composite section.

Russo (2004) conducted a study on micropiles used to underpin existing foundations after a structural collapse in Napoli. Fourteen strain gauges were installed on two instrumented micropiles and embedded in the cement grout. The ultimate bearing capacity of the load tests was not reached in these micropiles. Russo (2004) observed that a larger volume of grout in the lower zones created a negative skin friction which was verified also by finite element analysis.

Han and Ye (2006) instrumented four single micropiles with strain gauges. Two micropile loading tests were under tension, and two were under compression. The strain readings revealed that the micropiles' ultimate shaft capacities under tension were 60% of the micropiles subjected to compression. The tip resistance and displacement were found rate loading independent. Han and Ye (2006) also found the skin friction of micropiles under compression were higher than micropiles under tension.

Qian and Lu (2011) conducted five loading tests on five single micropiles in soft clay: two under compression and the three under tension. The strains' instrumentation readings revealed that the load displacement was linear in both, tension and compression.

The ultimate load capacity and skin friction under tension were approximately 50%-60% of micropiles under compression.

Finno et al. (2002) conducted four axial load tests on micropiles drilled in dolomite in Chicago. The instrumentation involves strain gauges to measure the axial load distribution and characteristics. The results of the load carrying capacity using Davisson's method revealed that micropiles drilled in high RQD have the highest carrying capacity and pile tip movements.

Long et al. (2004) conducted 12 lateral load tests on 50 ft. long loaded laterally micropiles that had been constructed for seismic retrofit. Casing was extended down to a 30 ft. depth. Seven pairs of strain gauges were installed on the two opposite sides of the micropiles' reinforcing cage. Axial tension and compression loading conditions were applied first; a lateral loading condition was applied next. Results were compared to finite element analysis obtained from LPILE. The moment versus depth was drawn, and the resultant curve showed that the highest moment occurred at 5 ft. below the ground's surface.

Richards and Rothbauer (2004) investigated the behavior of micropiles under lateral loading conditions. They used both a lateral jack and a hand pump to perform lateral load tests on micropiles. A dial, a telltale, and gages were installed, and the load was controlled by a resistance load cell. The LPILE, NAVFAC, and CLM were used to match instrumentation results. Richards and Rothbauer (2004) recommended that in order to increase the lateral load capacity, a larger casing should be installed, the diameter or the batter angle should be increased.

2.3.2. Analytical and Finite Element Modelling. The finite element method is a very effective tool in modelling of various engineering problems. It is a numerical technique to find an approximation to complex models by a discrete model which is divided into elements and nodes. Finite element of micropiles was studied with more focus on the seismic behavior numerical modelling of micropiles due to the difficulty to simulate it in the real situation and therefore, most studies on dynamic soil-micropile interaction have been numerical simulation (Turan, 2008). Analytical methods are also used in an effort to develop mathematical models for simulation.

Misra and Chen (2002, 2004) used mathmatical models to simulate soil micropile interaction. They assumed that the load is transferred totally by the skin friction developed in the bond zone. The soil model was assumed to be linear elastic perfectly plastic. The micropiles' input parameters included micropile diameter, the bond length, the debonded length, and micropile's axial stiffness in both the bond zone and debonded zone. The soil micropile's interface was assumed to be homogenous. The input parameters included the ultimate shear strength and the ultimate shear modulus of the micropile-interface as well as the tip soil stiffness. Misra and Chen (2002) also developed scaling factors that influences the model's parameters and the results.

Esmaeili et al. (2012) conducted a numerical study on the performance of micropiles to reinforce high railway embankments supported on loose beds of sand. This study included experimental and numerical modelling of the embankment. An initial numerical study was performed first to optimize the micropiles' location with heights between 5m to 10m. PLAXIS-3D was used to conduct this study. A scaled model

(prototype) with scale factors (shown in Table 2.2) was used next to conduct an experimental study. The loading prototype was selected and interference was minimized between the chamber's sliding surface and side walls. The embankments and bed dimensions are listed in Table 2.3; the entire model is illustrated in Figure 2.4.

Table 2.2. Scale Factors of the Esmaeili et al. (2012) Model.

Description	Scale Factor Y/X
Material Density	1
Length	20
Stiffness	4.47
Displacement	89.44

A jack load capacity of 300 kN was used to apply the load in increments of 2.5 kN above the embankment. Instrumentation tools were installed on the embankment's surface of and on the reinforcing bars to investigate the axial strain of the micropiles, failure loads and displacement of the embankment. PLAXIS-3D was used to conduct three numerical models. An elastic perfectly plastic with Mohr coulomb failure criterion was used to model the soil.

The model was validated by comparing the results of laboratory and numerical modelling. The results of both; numerical modelling and laboratory models showed a percentage difference of 0.89% on the bearing capacity of the micropiles, 16% on the displacements of the bed and the embankment and 4.11% on the axial strain of the micropiles.

Table 2.3. Embankment and Bed Dimensions Used in the Esmaeili et al. (2012) Model.

Parameter	Value (m)
Embankment length	50
Embankment height	10
Slope length	18
Embankment crest	6
Bed depth	16
Depth of modified part of the bed	2
Width of bed sides	7
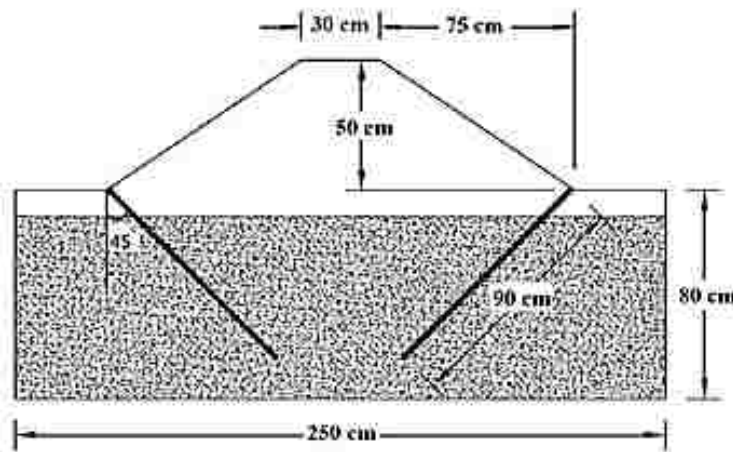
Figure 2.4. Embankment Model of Esmaeili et al. (2012).

A parametric study of the numerical model was conducted on the micropiles' diameter, length, number, and spacing. These results indicated that the spacing is the most efficient factor in increasing the factor of safety; the efficiency factors were 4.6, 3.1, 1.5, and 0.8, respectively, for the spacing, length, diameter, and number of micropiles in the embankment.

Bruce et al. (2004) studied the numerical modelling of micropiles to optimize the micropiles' depth and spacing. This case study was focused on a 16 m high embankment fill in southern Ontario, Canada. Two slopes; slope 1 and slope 2 are located near the CN rail tracks, occasionally experience significant distress. Micropiles were considered the best alternative solution for the following reasons:

- They can be placed in the embankments' upper region, minimizing the removal of tress,
- They are $275,000 less than the next alternative available,
- Disruption is minimized.

Conventional analysis using XSTABL and finite difference approach using FLAC were conducted to optimize the length and the spacing of the micropile wall. XSTABL is used for FLAC's model calibration. Site investigation was conducted; results of soil stratigraphy and engineering properties are shown in Tables 2.4 and 2.5, respectively.

Table 2.4. Layer Soil Thicknesses Used in Bruce et al. (2004).

Description	Top Elevation (m)	Bottom Elevation (m)	Layer Thickness (m)
Gravel Ballast	110.0	108.5	1.5
Sand & Gravel Fill	108.5	106.5	2.0
Silty Sand Fill	106.5	103.5	3.0
Silty Clay Fill	96.5	90.5	6.0
Silty Clay Fill	90.5		10+

Table 2.5. Material Properties Used in Bruce et al. (2004).

Description	Elastic Mod. MPa	Poisson's Ratio	Friction Angle°	Cohesion kPa	Unit Weig. kg/m^3	Dila. °	Bulk Mod. MPa	Shear Mod. MPa	Density kg/m^3
Gravel ballast	142	0.3	40	0	21	5	118	55	2150
Sand/Gravel	98	0.3	31	0	21.5	0	82	38	2200
Silty Sand Fill	54	0.3	28	0	20	0	45	21	2050
Silty Clay Fill	42	0.3	25	0	20	0	28	19	2050
Silty Clay Fill	280	0.3	36	100	23	0	467	100	2250

The spacing between micropiles was 0.5 m along wall and assume a Titan 20/40 injection within 125 mm diameter grout column. The analysis was carried out in the following steps: the critical soil conditions were founded by modelling the slope in FLAC and XSTABL, the micropile wall was then modeled with gradually lowering the internal angle of friction.

The increase in the slope stability was studied by comparing the lowest internal angle of friction necessary for the slope to fail. The results show that when the micropile wall is constructed; a reduction in friction angles of 2 in the silty sand and 3 in the silty clay fill were achieved before the slope began to fail. That would increase the safety factor against slope failure by 1.18. Short term inclominater readings were installed 1m up slope from the micropile wall and frequent readings were being taken to predict the improvement of the slope stability.

Howe (2010) worked to establish the optimum location of micropiles and facilitate the design guidline of the micropiles. Two software were used; SSI2D finite element softwere and STABR limit equilibrium softrware to check the SSI2D results. Soil was modeled as elastic plastic mohr columb failure criteria, also the SSI2D used 6 node triangular and rectangle elements and then the factor of safety was calculated. STABR calculated the factor of safety by searching for the circular slip surface having the minimum factor of safety using Ordinary Method of Slices or Bishop's Modified Method. The analyis was based mainly on three steps; estimation of soil parametrs of existing slopes, performing slope stabilty analysis, and back calculation of the strength parameters until a factor of safety =1 is obtained. The research objective was to apply these models on three case studies:

- A hypothetical case study in the FHWA manual; FHWA design example problem.
- A slope located in littleville landslide on US Route 43 in Alabama; the slope comprmises sandstone and shale where 432 micropiles were constructed; the length was 7m, diameter of 0.114 m and they were battered 30 degrees. The failure surface is assumed to be in the shale stratum
- A root-pile wall constructed for the Pensylvanania Departemnt of Transportation to stabalize a landslide consisted of silty clay and clayey silts mixed with some rock fragments. The failure surface was assumed to be the in the bedrock.

The results of FHWA design example and Pensylvanania landslide were close to the design results after back calucaltion of the strength parameters. However, the results of the US 43 Route were different, mainly, because the actual design has a rock anchor

coming from the pile cap and the micropiles are battered upslope and downslope, which were both not modeled. A factor of safety was also calculated to optimize the locations of the micropiles along the embankemnt. In addtion, the factor of safety was calcualted using many batter angles to determine the optimum batter angle.

Liao et al. (2013) used a loess slope to analyze the behavior of micropile soil interaction and the reinforcement effect of micropiles using FLAC. The soil was modeled as linear elastic perfectly plastic Mohr Coulomb failure criterion. The study was carried out for three cases; slope without micropiles, slope reinforced with one micropile, and slope reinforced with two micropiles. Load of failure was found in all of three cases. The results showed an increase in the load carrying capacity with increasing either the cohesion or friction but larger effect in increasing the internal angle of friction.

Monfared (2012) used ABAQUS to conduct a numerical study on the geometric effect of the inclined micropiles on the load carrying capacity including the diameter, length, and inclination angle of the micropiles. The soil was modelled as linear elastic perfectly plastic Mohr coulomb failure criterion and the micropile as linear elastic model. The properties of the soil and the micropile are shown in Tables 2.6 and 2.7, respectively.

Table 2.6. Material Properties of the Soil Used in Monfared (2012).

Unit Weight (kN/m^3)	Young's Modulus (MPa)	Poisson's Ratio	Cohesion (kPa)	Friction Angle°	Dilation Angle°
16.67	19.6	0.35	9.81	28	3

Model's size was increased until the results remained unchanged. The contact was simulated as surface to surface with finite sliding formulation.

Table 2.7. Material Properties of the Micropile Used in Monfared (2012).

Material	Unit Weight (kN/m^3)	Young's Modulus (MPa)	Poisson's Ratio
Concrete	25	22	0.20
Steel Casing	78	210	0.30

Tangential behavior was defined using "Penalty" contact and the normal behavior using "Hard" contact. The ranges in parameters of this study were 100-125 mm for the micropile diameter, 4-11m in the length and 0º-50º degrees in the inclination angle. The inclination angle was studied on a negative and positive battered micropile. The slip surface of the negative battered micropile deflects downward while the positive battered micropiles deflects upward as shown in Figure 2.5.

The results showed that the negative battered micropiles have higher load bearing capacity than the positive battered micropiles. The increase in the inclination angle caused a notable increase in the load carrying capacity of the negative batter micropiles which the opposite of the effect on the positive batter micropiles which they showed a decrease load carrying capacity. The parametric study on the negative batter micropiles diameter and length showed that the increase in the diameter causes an increase in the lateral load capacity which was much more less by increasing the length.
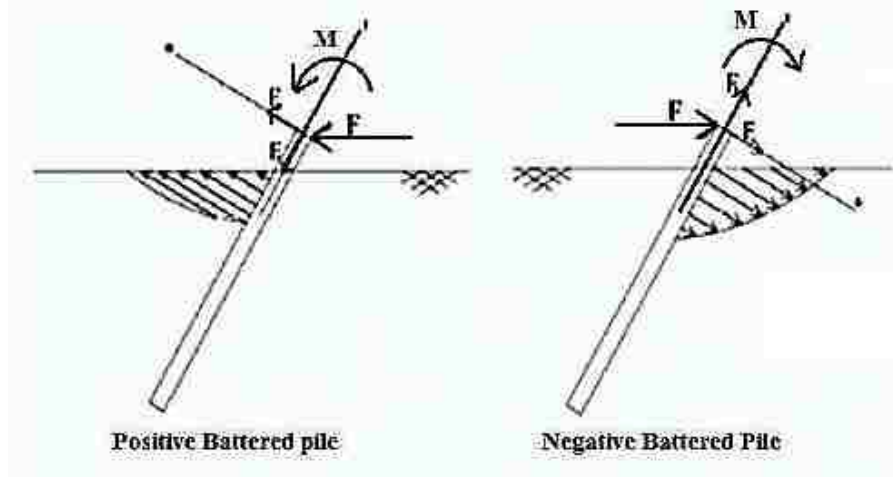
Figure 2.5. Negative and Positive Battered Pile (Monfared 2012).

Juran et al. (2001) conducted centrifugal tests to evaluate the response of a group and network of micropiles under seismic loading. LPILE and GROUP pseudo static analyses were then used to model the centrifuge tests. Piles in the centrifuge tests were made from polystyrene with roughness shaft and they were 5 diameters in length to minimize the influence of the box base. Interface properties were taken by gluing sand particles along the pile with local compaction around the piles to simulate the high ground/grout bond. Strain gauges and accelerometers were used to measure the displacement and the acceleration history measurement.

The model was prepared with latex to line the inside of the box, soil layers were constructed using sand of relative density of 57 and with thicknesses less than 50mm. The model was subjected first to acceleration time history with amplitude of 0.3g and then, 50% and 90% of the failure load. Fourier analysis and p-y curves of the results were analyzed to study the dynamic response and soil micropile interaction. Numerical

analysis using LPILE assumed full fixity at the pile head. The main results of the study showed that the bending moment and displacements values were smaller in 2X(2X1) and 3X(2X1) micropiles arrangement with S/D=3 than single micropiles with S/D=5.

Ghorbani et al. (2014) conducted a 3D study on the seismic response of soil reinforced with micropiles. The soil was homogenous sandy soil. 2X2 with S/D group of micropiles were studied and half of the pile foundation was modelled due to the symmetrical conditions. Distance between the end of the soil mass and the tip of the micropile was taken to be equal the length of the micropile. The lateral boundaries were also taken as 50 times the diameter of the micropile. The soil was modelled using Mohr-Coulomb failure criterion. Soil and micropile parameters used in the model can be found in Tables 2.8 and 2.9, respectively.

Table 2.8. Material Properties of Soil Used in Ghorbani et al. (2014).

Modulus of Elasticity (MPa)	Damping Factor	Poisson's Ratio	Lateral Earth Pressure Coefficient at Rest	Cohesion (kPa)	Friction Angle ∘	Dilation Angle ∘
6	10%	0.46	0.46	0	33	3

Material and geometry damping were considered. Material damping was performed by assuming Rayleigh damping in a time domain. The interface between the micropile and the soil was modeled using contact elements.

Table 2.9. Material Properties of the Micropile Used in Ghorbani et al. (2014).

Mass Density (Kg/m^3)	Axial Stiffness (MN)	Poisson's Ratio	Diameter (m)	Length (m)
6	10%	0.46	33	3

The micropile was assumed as rigidly connected to the pile cap. Lateral boundaries were modelled as viscous elements. The model was verified using a shaking table with inclined micropiles. Sensitivity analyses of the earthquake characteristics, soil properties, superstructure, micropile cap, and micropile structure were all performed to study the influence of each parameter on the seismic response and the soil-micropile interaction.

As expected, it was found that increasing the micropile inclination, diameter, slenderness ratio, friction angle, number of micropiles will improve the seismic response of the micropile. Adding non-linearity in the soil will also improve the seismic response. However, increasing the pile cap thickness, earthquake acceleration, stiffness of the micropiles and the superstructure weight will, all, will have negative impact on the seismic response of micropiles. The pacing ratio of the micropiles had no effect on the response of the micropile under seismic loading. Cosine Amplitude Method, CAM was performed to figure out the most influencing factors and the predominant parameters that affect the response of the micropiles under seismic loadings. Parametric study is shown in Table 2.10. CAM analysis of the shear stress and bending moment are shown in Figures 2.6, 2.7, respectively.

Table 2.10. Parametric Study of Ghorbani et al. (2014).

	Parameter	Symbol	Unit	Range of Variation
Inputs	Thickness of cap	t	m	0.3-0.5
	Peak acceleration of earthquake	a	m/s	0.3-0.5
	Friction Angle	phi	deg	26-45
	Inclination	alpha	deg	0-20
	Mass of superstructure	m	t	40-120
	Micropile diameter	d	m	0.25-0.45
	Number of Micropiles	N	dimensionless	3-5
	Predominant frequency of superstructure	f	Hz	0.4-156
	Slenderness ratio	SR	dimensionless	20-60
	Spacing ratio	s	dimensionless	4-6
	Relative stiffness	E	dimensionless	120-3666
Outputs	Maximum shear stress	S	100 (kN/m^2)	13.04-207.2
	Maximum bending stress	M	1000 (kN/m^2)	5.77-95.93
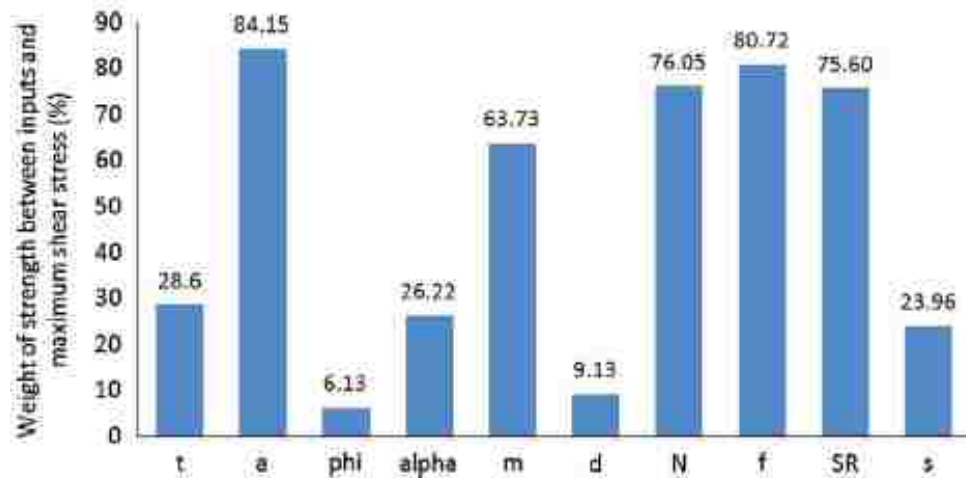
Figure 2.6. Effect of the Parameters on the Shear Stress (%) (Ghorbani et al. 2014).
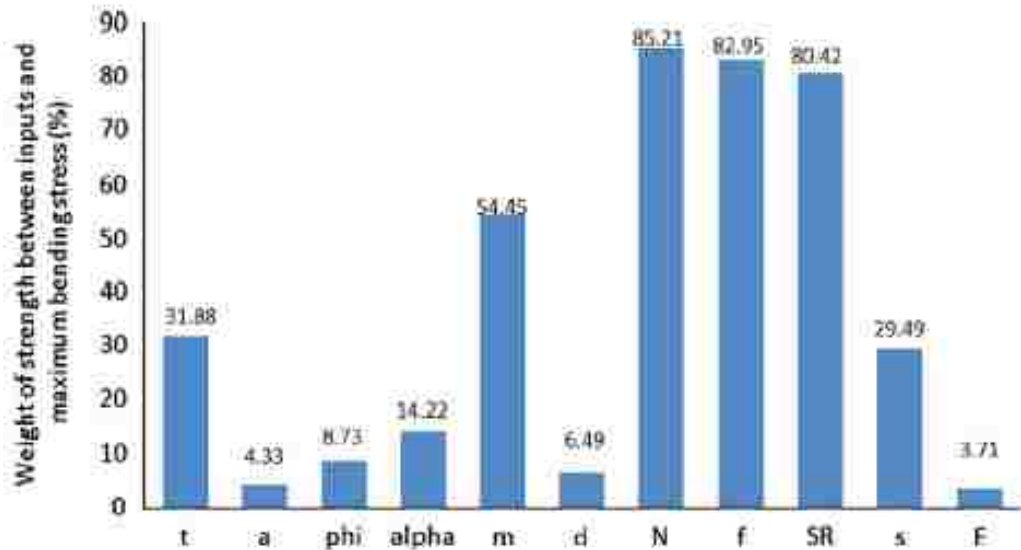
Figure 2.7. Effect of the Parameters on the Bending Moments (Ghorbani et al. 2014).

Turan et al. (2008) conducted a study on the lateral response of micropiles under static and dynamic loading. Pseudo static and dynamic analyses were done on a group of micropiles comprise nine 15 m long and 0.25m diameter. The response of the micropiles was studied without casing and with casing extended down to 5 m deep. The effect of the pile cap flexural rigidity EI and the surface surcharge was also investigated. The pile and the soil were modeled using 8-nodes linear hexahedron. The initial step in each analysis was to perform the geostatic step to establish the initial equilibrium. Separation between pile and soil was not allowed and they were assumed fully bonded.

The seismic loading was simulated by applying acceleration time histories at the base of the model. The soil boundary elements were modeled as infinite elements. The results of the simulation showed that the moments of the piles with casing were higher than the piles without casing and the bending moment values were over 100% increase at

the termination point of the casing. The pile cap flexural rigidity was varied and this variation had no comparable difference on the bending moments of the micropiles. However, the increase in the flexural rigidity results in a decrease in the sliding at the interface between the micropile and the soil; but it became negligible at depths deeper than 2 ft. The effect of the surface surcharge shows that the higher the surcharge around the piles, the larger the bending moment.

Wang and Han (2010) conducted a numerical study to investigate the influence of the micropile inclination and earthquake intensity on the seismic response of micropiles resting on liquefiable soil. The analysis studied two inclined micropiles as shown in Figure 2.8.
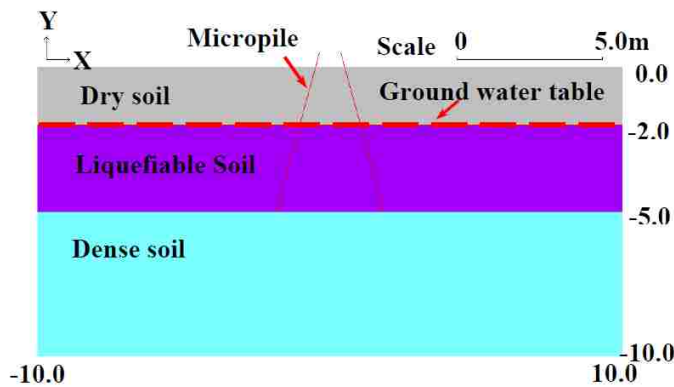
Figure 2.8. Soil Topography Used in Wang and Han (2010).

The analysis was implemented by FLIP program developed by Iai et al. (1990). Sine wave model and earthquake wave model with constant frequency and different amplitude values were studied. The length and diameter of the micropile were 5.7 m 0.2 m. the micropile was modeled using linear beam elements. The superstructure was modeled as rigid body. Springs elements were used to simulate the interaction between soil and micropiles. The soil strata include 2 m dry soil, 3 m liquefiable soil and dense soil underneath. The results showed that for the sine wave model; bending moment, deflection and acceleration values increase with increasing the input motion under constant pile inclination. For the earthquake model, the higher the inclination the smaller values of lateral displacement and bending moments. The results also showed that displacement between micropile and soil increases with increasing the inclination and the intensity.

Ousta and Shahrour (2001) also examined a micropile's seismic response. The numerical model was implemented using PECPLAS. The soil-fluid coupling was modeled using u-p formulation of the displacement and pore-pressure of the fluid phase (Zienkiewicz et al. 1980). Soil behavior was modeled using cyclic elastoplastic MODSOL consecutive model. The micropile was modeled as linear elastic material and the interface was assumed as perfect. The finite element mesh used was 852 of 20 nodes elements. The base layer was assumed as rigid and impervious, water table coincide with the ground surface, and periodic conditions were applied at the lateral boundaries. The seismic loading was applied at the base of the soil. Group of micropiles 2X2 was also studied with spacing S/D=3. It was found that micropiles affect the earthquake induced pore pressure and that micropiles mounted in loose to medium sandy soil will increase

pore water pressure which decreases the soil modulus and increases the bending moment. It also was found that positive group effect was observed up to S/D=6.

Sadek and Shahrour (2004) developed and verified a 3D embedded beam element numerical model. The model was used to perform a seismic study on the effect of head and tip connection on group of 4 vertical and inclined micropiles using PECPLAS. The soil was assumed as elastic with Rayleigh material damping. Micropiles were modeled as 3D beam elements. Boundaries were placed at huge distance to minimize the boundary effect. The seismic loading was applied at the base of the soil mass. It was found in this study that the pin connection decreases the moment and the axial force and that was more significant with the inclined piles.

Wang et al. (2009) used PLAXIS to conduct a study on the effect of micropile reinforcement on soil under static and dynamic conditions. The soil properties are listed in Table 2.11. The micropiles were 14 m length and 0.2 m in diameter and they were modeled using 5 nodes beam element. The interface was assumed as interface elements with thicknesses equal to 0.1 and 0.01 of the length. The bottom boundary was assumed fixed in all directions and the lateral boundaries were assumed to move only in the vertical direction. Mesh was generated and it was more refined at the pile-soil interface areas. During the dynamic analysis, the bottom boundary was change to have predefined displacement of 0 m while the lateral ones were prescribed to be 0.01 m. As expected, this study showed that reinforcing soil with micropiles has a great influence on seismic mitigation of soil embankments.

Table 2.11. Soil Properties Used in Wang et al. (2009) Model.

Soil type	Unsaturated Unit Weight (kN/m^3)	Saturated Unit Weight (kN/m^3)	Cohesion (kPa)	Friction Angle	Young's Modulus (MPa)	Poisson's Ratio
Fill	16	20	1	30	8000	0.3
Clay Silt	16	18	5	25	10000	0.35
Soft Soil	17	18.5	7	20	5000	0.35
Coarse Sand	17	20	1	34	30000	0.3

This study was conducted to analyze the effect of harmonic and seismic loads on the seismic behavior of micropiles mounted in sandy soils. The numerical analysis was conducted using Plaxis. The soil was modelled as linear elastic. Micropiles were modeled using elastic beam elements. The 40 ton superstructure was connected to the pile cap using 1m massless pile. The boundaries effect were minimized by increasing the distance between the lateral boundaries and the piles to 50 times the diameter. The 2D analysis was implemented on 2X2 micropiles. It was found that the increase in the acceleration amplitude increases the displacement, bending moments, axial force and shear force. It also was found that Rayleigh damping causes reduction in the seismic energy, displacement and the horizontal acceleration of micropile cap. It also caused reduction in the amount of internal forces in the micropiles and the cap but negligible effect in the vertical acceleration.

2.4. SUMMARY

This field is not fully understood. Further research is still needed, particularly, in the nature of the friction and contact between soil and the micropile. The load transfer mechanism in the both the cased zone and the bond zone still need further research. The interaction between the micropile and the rock should be investigated further.

3. FOOTHILLS PARKWAY BRIDGE NO.2 MICROPILES

Monitoring of Bridge No.2 foundations was conducted to understand the load transfer mechanism of micropiles mounted deep in Metaconglomerate and Metasandstone rocks. Using strain gauges, the strains along the length of micropiles were measured at different stages of construction. In this section, the site description as well as the micropile design and installation will be presented. Field instrumentation data will be presented as well.

3.1. SITE DESCRIPTION AND BRIDGE CONSTRUCTION

The Foothills Parkway Bridge No.2 is a 70 miles scenic parkway located in Blount County. The parkway connects the route 129 with interstate 40 in the northern boundary of the Great Smoky Mountains along Tennessee-north Carolina border. This location is roughly 12 miles southwest of Pigeon Forge, Tennessee (Kershaw, 2011).

The Foothills Parkway lies on the slopes of the secondary ridges of the Great Smoky Mountains. The land rising from an elevation of 857 feet at its southern terminus to 2600 feet at the look rock, web and green mountain. The slope varies 30-34^0 of the mountain topography. The countryside is a dense woodland of hardwoods and pines (FPMP, 1968).

The demand for the increase in recreational traffic created a need for the parkway to handle the congestion. In addition; the proposed parkway was intended to provide

access to several areas of the parkway. The Parkway design theme required a design with a good quality by presenting a scenic, historic and cultural character. It was also designed to meet variety, accessibility, design, safety, adaptability, aesthetic, conservation objectives, compatibility with other recreation, and competing uses where other requirements should not interfere with the recreational function of this Parkway (FPMP, 1968).

The parkway overall plan had eight sections; 8A to 8H shown in Figure 3.1. Section 8E, 9.7 miles long, connects Wears Valley to Carr Creek. 8E section has unfinished part, 1.6 miles long, known as the missing link, which requires ten bridges; two of them was completed; Bridge No.1 and Bridge No.2. The 790' Bridge No.2 was constructed using cantilever construction method, it involves a symmetrical erection of cantilever segments around the piers. Temporary post-tensioning tendons were used to attach all cantilever segments with the supported bridge pier. When all segment piers were stressed, a closure joint made of concrete was made at the mid-span. All construction stages were made with great caution to avoid disturbance and aesthetic issues to the surroundings (FHWA, 2012).

The five span of Bridge No.2 has four piers as shown in Figure.3.2; each pier has twenty micropiles inserted deep down to the rock. During the process of completing the construction of the missing link, Missouri University of Science and Technology installed strain gages to the micropiles and measurements were taken to examine the performance under different loading conditions; during construction, after completing the bridge and under live load conditions (Dixon, 2013).
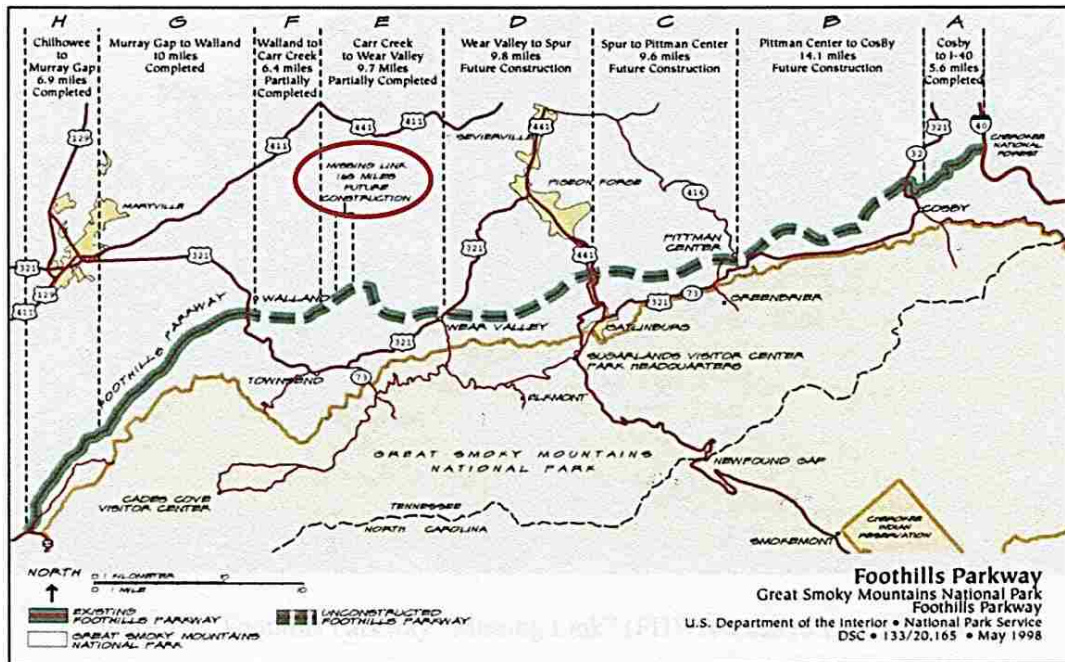
Figure 3.1. Map Showing the Sections of Parkway and the Missing Link (NPS, 1998).

Figure 3.2. Bridge No.2 Side View, Elevation and Surroundings.

3.2. SUBSURFACE CONDITIONS

Pier No.1 and Pier No.2 were chosen for the purpose of this study, the subsurface conditions were defined by Dan Brown and Associates. Pier No.1 has six surrounding borings; 2-2A, 2-2B, 2-2C, 2-3A, 2-3B, and 2-3C, 2-3B. Pier No.1 is located at the southeastern side of Bridge No.2 and closest to the abutment (Siegel & Thompson, 2010).

Pier No.2 borings are 2-4A, 2-4B, 2-4C, 2-5A, 2-5B, and 2-5C. The boring's locations are shown in Figure 3.3.
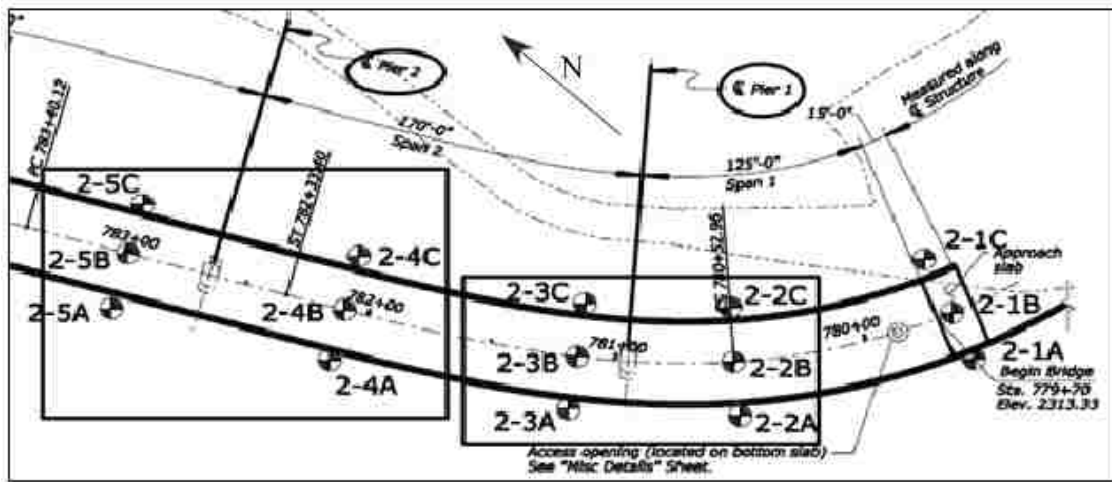
Figure 3.3. Boring Logs Location of Pier No.1 and Pier No.2 (Siegel & Thompson,2010).

The ground in the area of Pier No.1 and Pier No.2 is characterized by 4' to 50'overburden soil of sand and gravel overlying Metaconglomerate and Metasandstone rock. The rock is comprised of weathered and competent rock, which they can be distinguished from each other by RQD values and RQD recoveries.

Conglomerate and sandstone belong to the same family of sedimentary rocks i.e., clastic family. However, they differ by the sediment size from gravel (conglomerate) to sand (sandstone), when they are subjected to high amount of heat and pressure, they are changed to a more compact, denser and stronger type of rocks (Metaconglomerate and Metasandstone).

These type of rocks belong to the non-foliated family of metaphoric rocks, which they are homogeneous and massive rock. Therefore, there is no significant difference in the properties upon testing them in different direction (Foster 1978, Hoskin 2005, West 2010). Rock Quality Designations (RQD) and, unconfined compressive strength (UCS) tests of the rock were conducted frequently.

Water level was encountered at 10.5' to 73.8' below the ground surface, the water level is shallower in the regions of shallower bedrock (Siegel & Thompson 2010). The 3D graphical representations of the subsurface conditions are shown in Figure 3.4 and Figure 3.5. They were generated using 12 boring logs and 20 drilling memos of the micropiles' installation.

The red color represents the sound Metaconglomerate and the Metasandstone which they have a high RQD and high recoveries. The yellow color represents the weathered rock of the same types of rocks. The overburden soil is represented by the green color. Grey color represents the drilled platform and the concrete that was used to provide the level topography under the foundation.
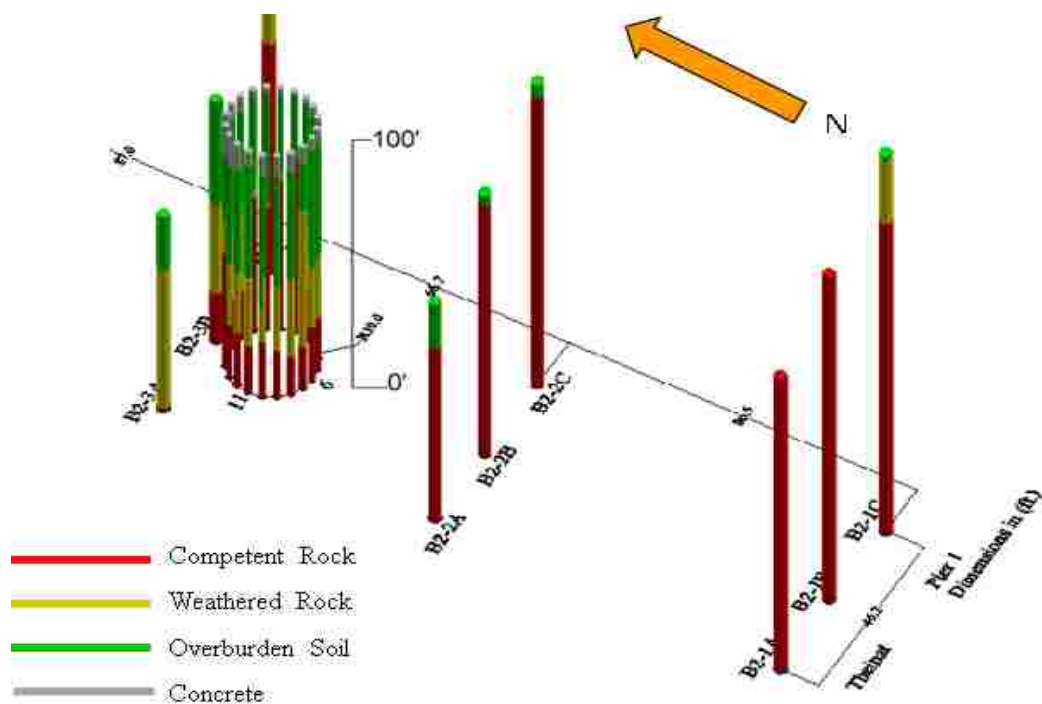
Figure 3.4. Stratigraphy Characterization of Pier No.1, Southwest 3D View.
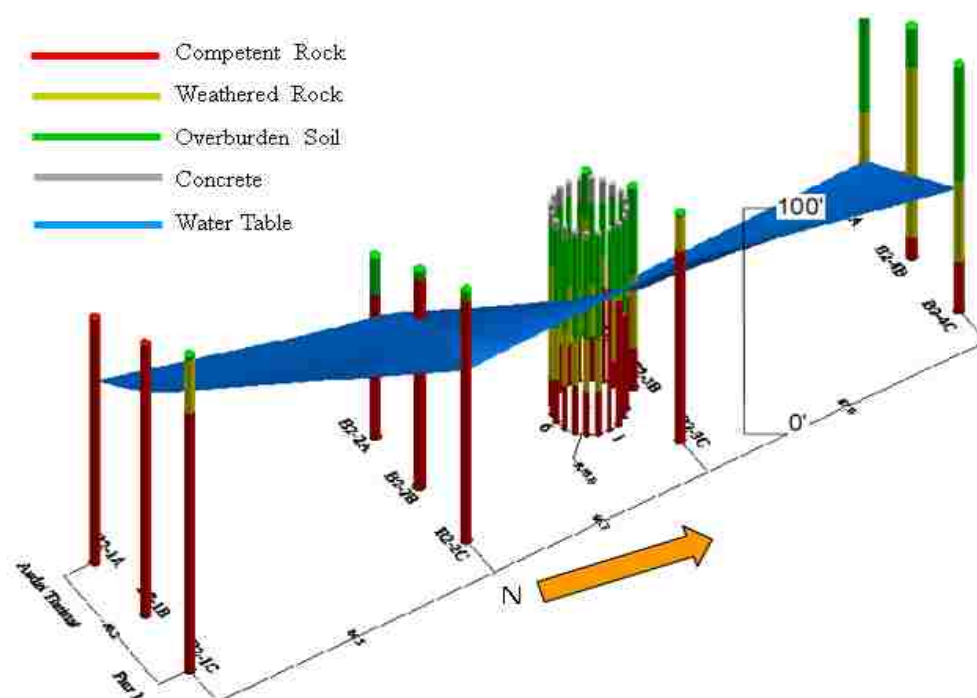
Figure 3.5. Stratigraphy Characterization of Pier No.1, Southeast 3D View.

3.3. SUBSURFACE FIELD AND LABORATORY TESTING

Subsurface field testing includes Standard Penetration Tests (SPT) for the soil, and Rock Quality Designation for the rock cores (RQD). SPT tests were conducted at 5' interval and it shows high blow numbers in most of the regions. RQD starts with very low values near the top of the rock and reaches 100 at deeper levels.

Soil laboratory tests include moisture content, Atterberg limits, and grain size analysis. The moisture content of the soil is around 10%, LL=27, PL= 8. The grain size distribution is around 45% gravel, 35% sand and 20% clay and silt. The soil classification varies between SC and SM.

The Unconfined Compression Strength (UCS) tests of the rock (Metaconglomerate and Metasandstone) has an average of 46,000 kPa and an average unit weight of 26 kN/m^3.

3.4. MICROPILE DESIGN AND INSTALLATION

Micropiles were considered as the best alternative to support the foundation of Bridge No.2. The main reasons were structural capacity, terrain difficulty, cost efficiency and the minimal disturbance during construction.

The implemented foundation design was a 20' diameter, 5' thick pile cap connected to twenty micropiles (Siegel & Brown, 2010). A platform is also connected to

the cap as shown in Figure 3.6. The platform function was to install the micropiles and to provide a level topography underneath the cap (Corvern Engineering, 2010).

The plan view of the foundations, shown in Figure 3.7, includes twenty micropiles located 8.5' away from the center of the micropiles.
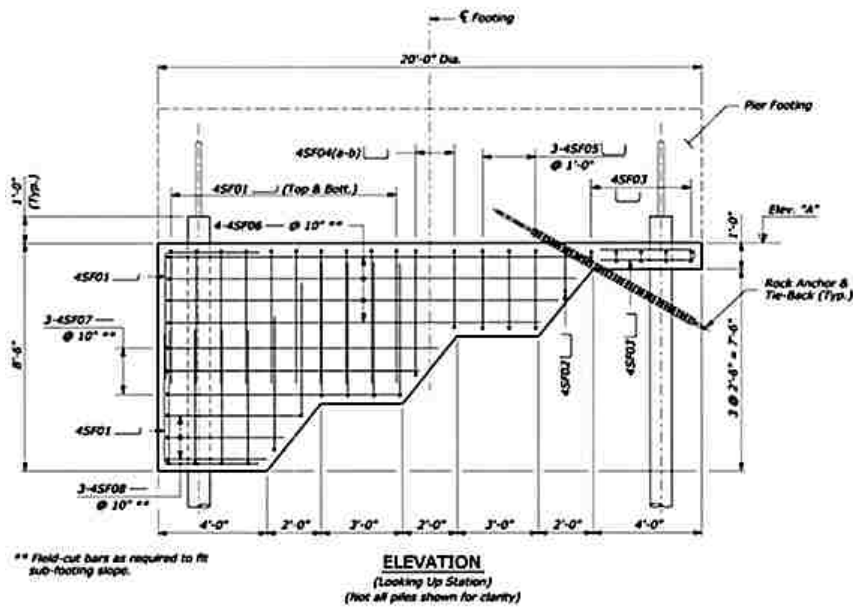
Figure 3.6. Drilled Platform (Corvern Engineering, 2010).

The installation of the 154 ton micropiles were conducted using percussive drilling methods with internal flush. The power was applied using high pressure/high volume compresser of 900 cfm.
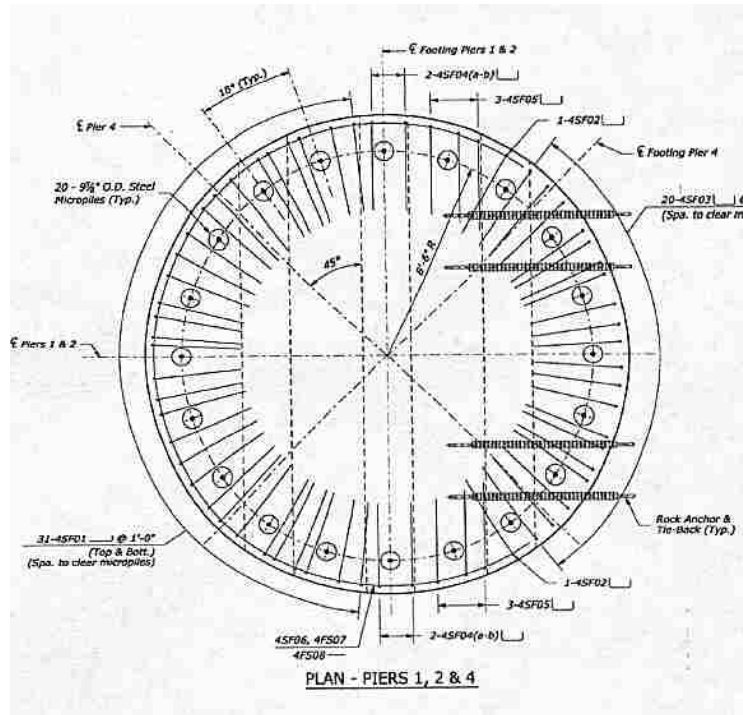
Figure 3.7. Footing Plan (Corvern Engineering, 2010).

The micropiles consists of a 2.5" central steel bar encircled by an 8.681" grout. A 0.472" outer steel casing was placed in the cased zone of the micropile as shown in Figure 3.8. The micropiles were required to carry the maximum estimated load estimated by GROUP, a software developed by ENSOFT (Siegel & Brown 2010). The parameters of the model used in GROUP at Pier No.1 are shown in Table 3.1 which they were used to develop the p-y curves. The Unconfined Compressive Strength (UCS) used in the analysis of Table 3.1 was conservative where the actual values are higher.

The maximum axial tension load, axial compression were found to be 7.4 kips,

310 kips, respectively, which the micropiles were designed to satisfy these extreme

loading conditions.
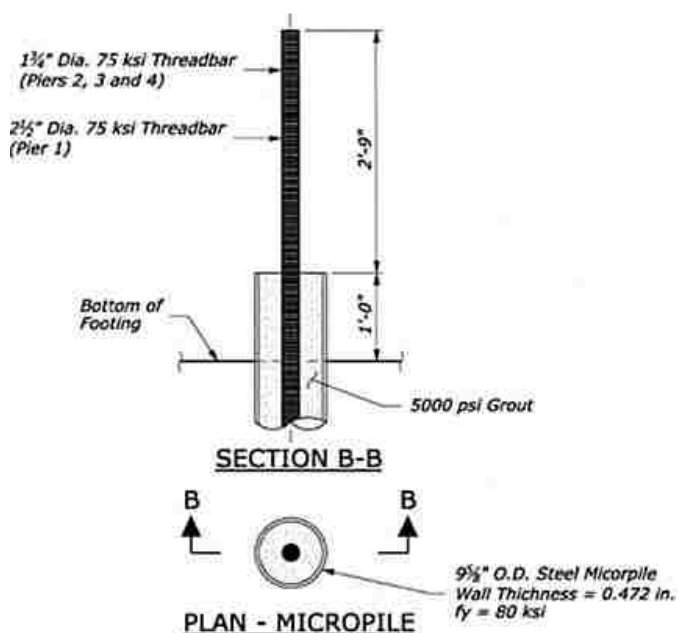
Figure 3.8. Micropile's Cross Section (Siegel, 2010).

Table 3.1. Parameters of the GROUP Analysis (Siegel, 2010).

Layer	Thickness (ft.)	p-y Curve	Strength	Unit Weight	Modulus
Overburden Soil	38	Sand	$\Phi=28°$	120 pcf	K=25 pci
Rock	NA	Weak Rock	$q_u=1000$ psi	150 pcf	$E_i=175$ ksi

Based on the geological conditions as well as the estimated loading conditions,

the bond length was selected to satisfy the nominal grout to rock bond of 100 psi (Siegel

& Brown, 2010). Based on this; the length of the micropiles varied based on the location and the geology of the micropile.

- Pier No.1: The design called for a minimum of 15' into the bond zone of the sound rock. Due to variability of the stratigraphy and the depth of the rock below the ground surface, the length of the micropiles varied. Therefore, Pier No.1 has short micropiles as well as long micropiles. Short micropiles are Micropiles No.1, Micropile No.18, Micropile No.19 and Micropile No.20 and the rest sixteen micropiles are long. The short micropile hits the competent rock at shallower depth while the long micropiles hits it at deeper depths. The long micropiles also have intermediate weathered rock layer. Short micropiles total length is around 50'; 35' in the soil/casing zone and 15' embedded in the rock/bond zone. The long micropiles are around 95' total length; 75' in the soil/casing zone and 20' embedded in the rock/bond zone.
- Pier No.2: All the micropiles are long, they are around 100' total length; 80' in the soil/casing zone and 20' embedded in the rock/bond zone

The steel used in center bars of the micropiles must be compatible with stiffness of the grout to insure a strain compatibility between the steel in the center and the grout of the micropiles (Siegel & Brown, 2010).

To account for the steep slope in Pier No.1; rock anchors were installed as an additional resistance of the anticipated lateral load. The anchors were parallel to the sloping topography to have a maximum conditions of stability. The rock anchors

locations can be found in Figure 3.6 and 3.7. The nominal tensile strength of the rock anchors is 18 kips +/-.

Micropile design verification was conducted to ensure meeting the required load carrying capacity and other design criteria (Siegel & Graham, 2010).

The strain gauges were attached to the central reinforcing bars of the instrumented micropiles in Pier No. 1 and Pier No. 2. A terminal box was installed outside the pile cap and the strain gauges were then connected to the terminal box by wires according to their locations (Kershaw, 2011).

3.5. INSTRUMENTATION, DATA COLLECTION AND REDUCTION

Micropiles instrumentation included installing strain gages at various depths along the instrumented micropiles of Pier No.1 and Pier No.2. Micropiles No.1, No.4, No.11 and No.16 were instrumented at Pier No.1 while Micropile No.1, No.6, No.11, and No.16 were instrumented at Pier No.2 as shown in Figure 3.9 (Dixon, 2013).

Instrumentation plan included the following components:

- Concrete embeded strain gages; Geokon Model, 4200.

- Miniature surface mounted VW strain gages; Geokon Model, 4151.

- Terminal box outside the surface of the pile cap; Geokon Model, 4999.

- VW readout device; Geokon Model GK-404.
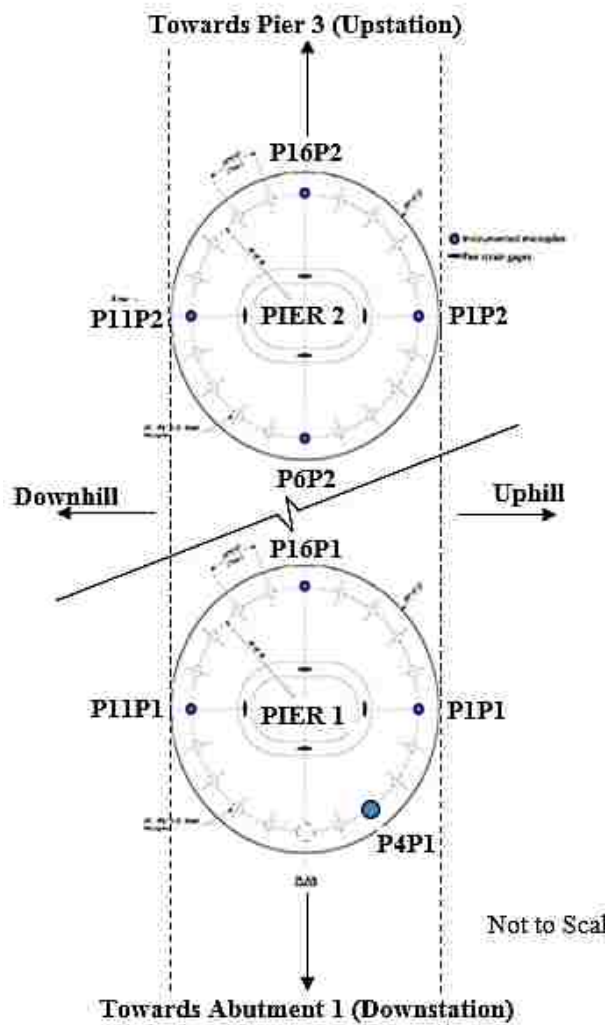
Figure 3.9. Instrumented Micropiles in Pier No.1 and No.2 (Dixon, 2013).

The strain gages were installed and mounted to the micropiles' central bar as shown in Figure 3.10.

A steel wire was tensioned between two barbell shaped ends, the deformation that occurs between these two barbell causes change in the frequency vibration and untimely strain readings variations. All environmental changes such as rainfall, temperature

variation and seasonal changes may affect the readings of the strain gages due to their effect on the frequency vibration (Kershaw, 2011).
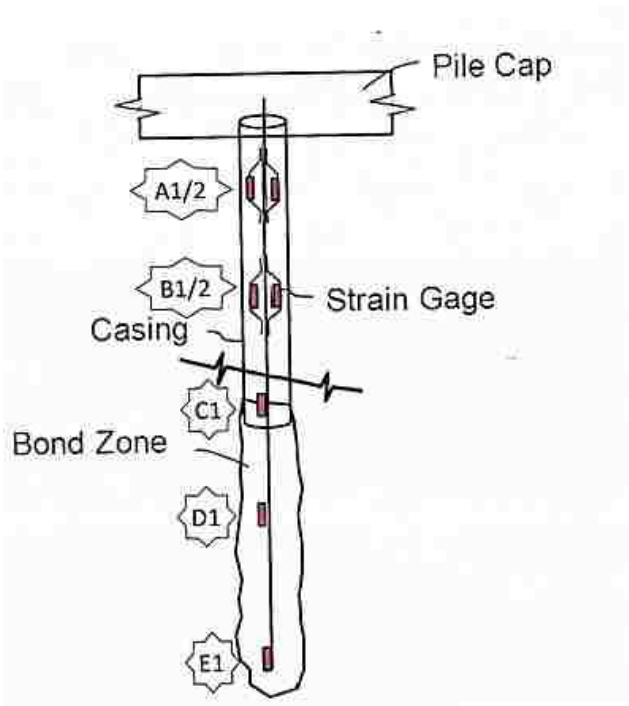
Figure 3.10. Location of the Strain Gages along the Micropile (Kershaw, 2011).

Pier No.1 consisted of the pile cap, 6 columns and 21 cantilever segments. Pier No.2 consisted of the pile cap, 5 columns segments and 21 cantilever segments, the columns and cantilevers are shown in Figures 3.11, 3.12.

Readings were taken after each cantilever segment construction. Continued monitoring of the bridge was done upon completion the bridge and under live loadings. Four trucks were placed at different positions (Kershaw, 2011).
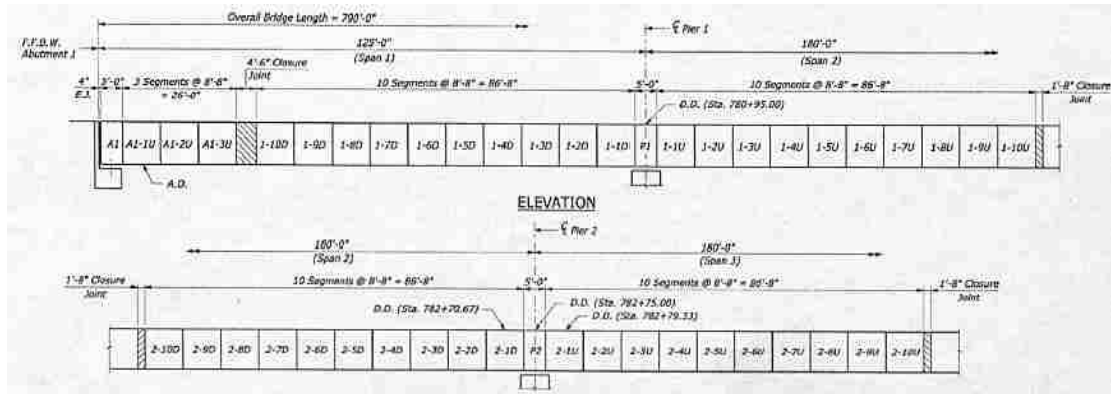
Figure 3.11. Cantilever Segments Construction (Corvern Engineering, 2010).
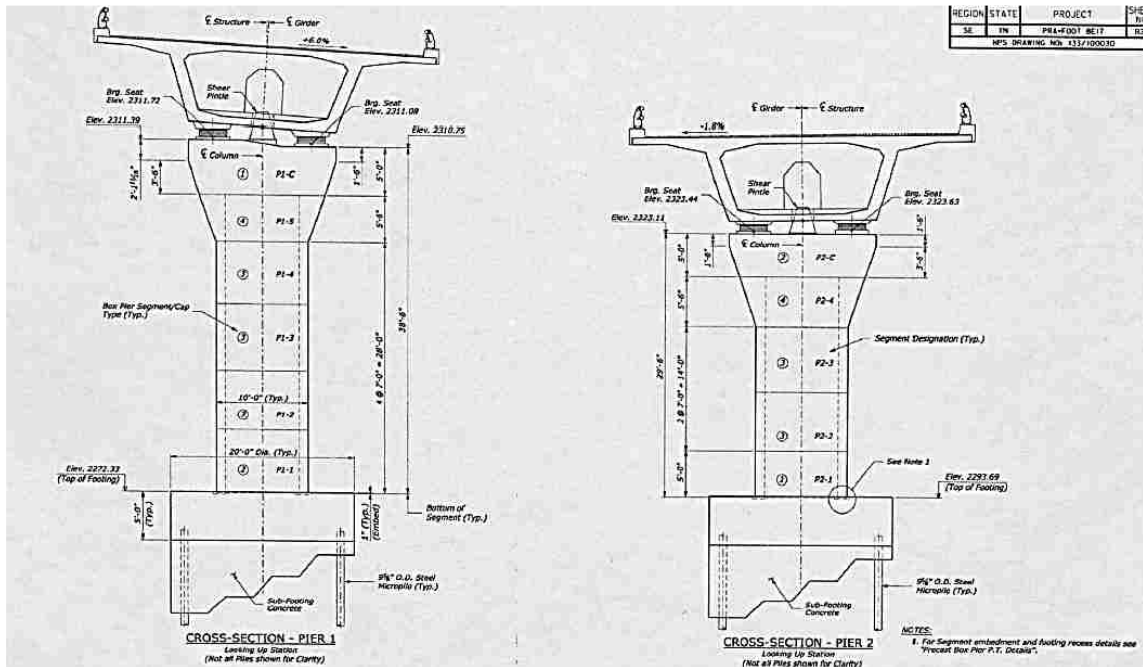
Figure 3.12. Column Segments Construction (Corvern Engineering, 2010).

Strain readings of Geokon 404 readout device can then be taken. The distance between the strain gages and the center of the micropiles is measured as shown in Figure

3.13. Subsequently, the equivalent axial stiffness EA and EI presented in Table 3.1, 3.2 and 3.3 were used to calculate the load and the moments from the strain readings.

Table 3.2 shows the geometrical and the properties of the micropiles. Table 3.3 and 3.4 show the properties of the micropile section when it is transformed to one uniform steel section, a uniform concrete section, or a uniform composite section that preserve the real geometry but have a different axial stiffness than concrete or steel.
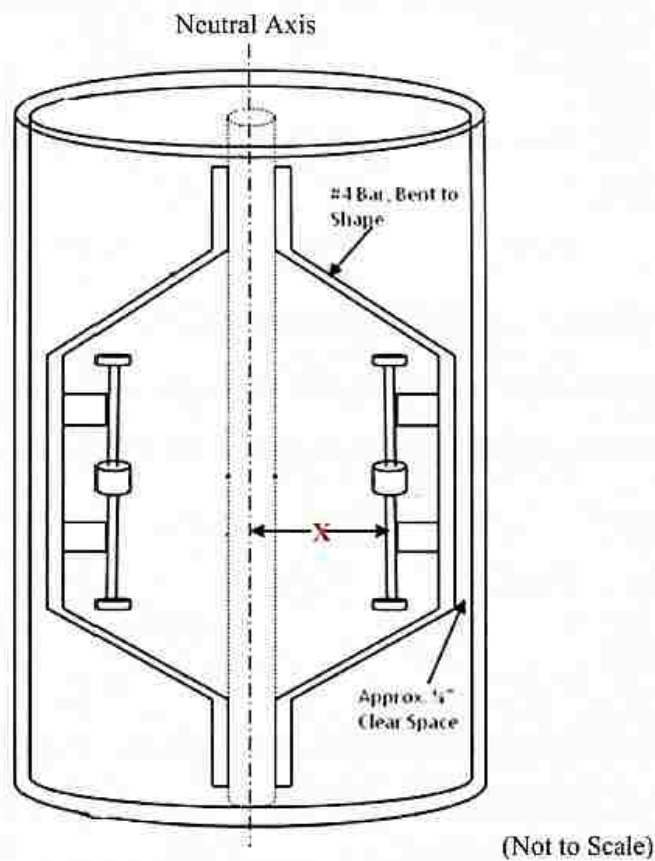
Figure 3.13. Strain Gages Location (Kershaw, 2011).

Table 3.2. Micropiles' Properties.

Property or Dimension	Value	Unit
OD_{casing}	9.625	in.
Id_{casing}	8.681	in.
$(Dia)_{bar}$	2.5	in.
E_{steel}	29000	ksi
f'_c	5	ksi
E_{grout}	4030	ksi

Table 3.3. Micropile Cased Zone Properties.

Property or Dimension	Value	Unit
A_{casing}	13.57	in^2
A_{bar}	4.91	in^2
A_{grout}	54.28	in^2
η	7.20	
$A_{trans,steel}$	26.02	in^2
$A_{trans,grout}$	187.25	in^2
$A_{composite}$	72.76	in^2
$E_{composite}$	10373	ksi
$I_{composite}$	421.28	$in.^4$

Table 3.4. Micropile Bond Zone Properties.

Property or Dimension	Value	Unit
A_{casing}	0.00	in^2
A_{bar}	4.91	in^2
A_{grout}	67.85	in^2
η	7.20	
$A_{trans, steel}$	14.34	in^2
$A_{trans, grout}$	103.17	in^2
$A_{composite}$	72.76	in^2
$E_{composite}$	5715.00	ksi
$I_{composite}$	421.30	$in.^4$

3.6. FIELD INSTRUMENTATION AND MONITORING PROGRAM

The final completion date of the bridge was on December 31, 2012. The final reading were taken on the morning of December, 18, 2012 before the live test data had been taken (Dixon, 2013).

3.6.1. Pier No.1: Micropile No.1, No.4, No.11 and No.16. The load at the top of Pier No.1 footing was estimated to be 2,306 kips after completion of the bridge construction. Strain readings were taken at every load increment where a column or segment was placed, as discussed earlier. Micropile No.1, No.4, No.6 and No.16 were instrumented. As shown in Table 3.5, Micropile No.1 is the short Micropile among all the micropiles in Pier No.1 and this is due to the shallow rock depth encountered at that location as shown in the 3D stratigraphy shown previously in Figures 3.4 and 3.5.

Table 3.5. Cased, Bond and Total Lengths of Pier No.1's Instrumented Micropiles.

Micropile	Total Length (ft.)	Cased Length (ft.)	Bond Length (ft.)
No.1	43	28	15
No.4	93	73	20
No.11	91	73	18
No.16	93	70	23

Total length of Micropile No.1 is 43', 15' is embedded in the rock. The load transfer distribution during construction of Micropile No.1 is shown in Figure 3.14. The dashed red line is the load design envelop, Pc, estimated by GROUP analysis. The solid lines, Rcc and Rcu, are the structural capacity of the micropiles based on analytical

methods for the cased zone and the bond zone, respectively. GROUP analysis and the

analytical method of the micropiles were implemented by Siegel & Brown (2010).
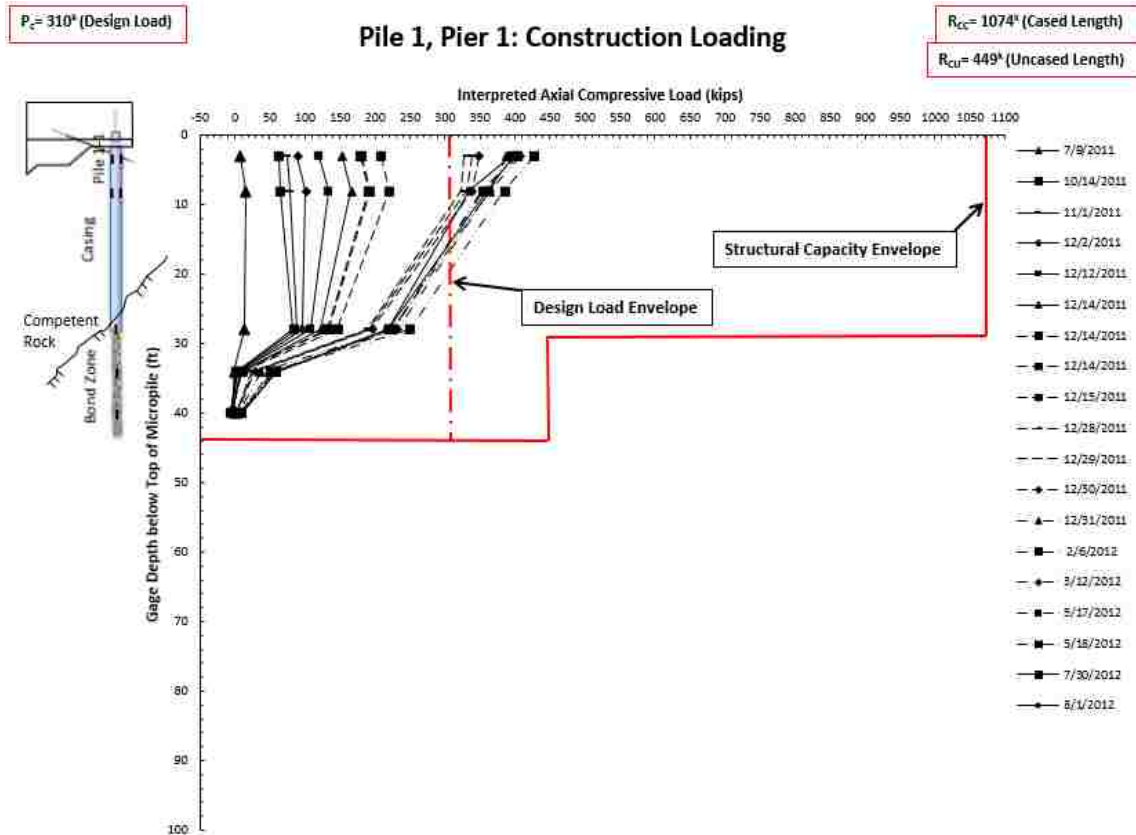
Figure 3.14. Load Transfer of Micropile No.1, Pier No.1 (Dixon, 2013).

Micropile No.1 carries more load than the other micropiles. The strain gages were

connected by straight lines to show the load transfer path. As shown in the figure, load is

transferred in the cased and the bond zones. Theoretically, the load should not be

transferred in the cased zone. However, as the time and the load increase, more load is

transferred in the cased zone. The load is, then, transferred efficiently in the bond zone.

Load transfer of Micropile No.11, Pier No.1 is shown in Figure 3.15. Load transfer of Micropile No.11 was different from Micropile No.1. As it appears, the micropile considers an inverse transfer mechanism. In the cased zone, the micropile is subjected to an additional load from the ground and then, start to transfer the load to the ground effectively in the bond zone. The micropile may considered some downdrag that might be the reason behind the additional load from the ground. However, soil is not compressible (gravel, sand and few silt) and the downdrag somehow is unlikely to occur.

The load is applied over the cap and drilled platform, this load is transferred to micropile by the strong bond between the micropiles and the pile cap since the cap has higher stiffness, larger load and strong bonded with micropile. Therefore, there is no guarantee that the load has increased at the end of the concrete. Therefore, a strain gage was necessary to see the load transfer.

The strains gauges readings may also were biased due to weather and loading condition. Their location near stress concentration areas of the pile cap is an additional concern.

In the concrete platform region, the load is transferred from the ground to the micropiles because the micropiles collect load from the cap and the platform. This is discussed in details in Section 4.3.1.1 "Cased Zone-Concrete Platform Interaction".
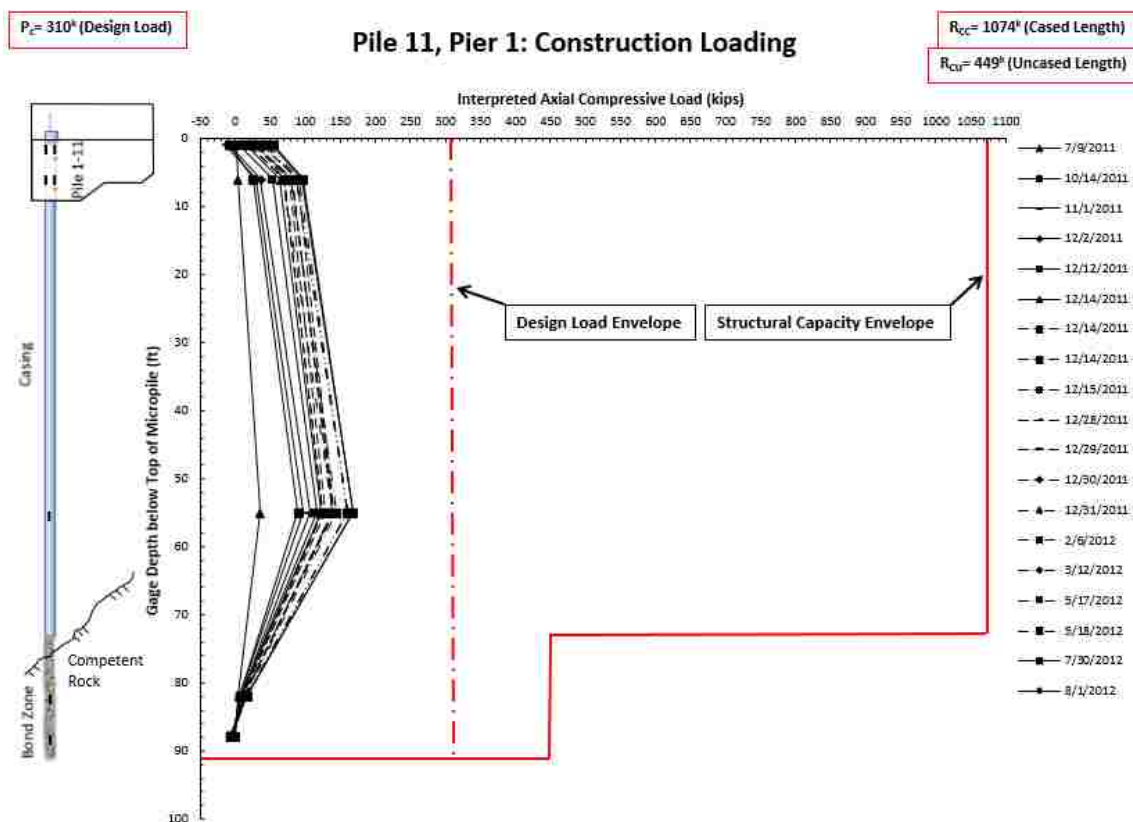
Figure 3.15. Load Transfer of Micropile No.11, Pier No.1 (Dixon, 2013).

Micropile No.4 load transfer is shown in Figure 3.16. The load transfer shows that only small load is transferred from the ground to the micropile. The rest of the cased zone length of the micropile as well as the bond zone did not consider a downdrag. However, the load is transferred effectively in the bond zone.

Micropile No.4 has strain gage in the overburden soil and therefore, the behavior can be predicted more than Micropile No.11. The load of the micropile is increased in the concrete, transfer some of it in the cased zone and then all the remaining load in the bond zone.
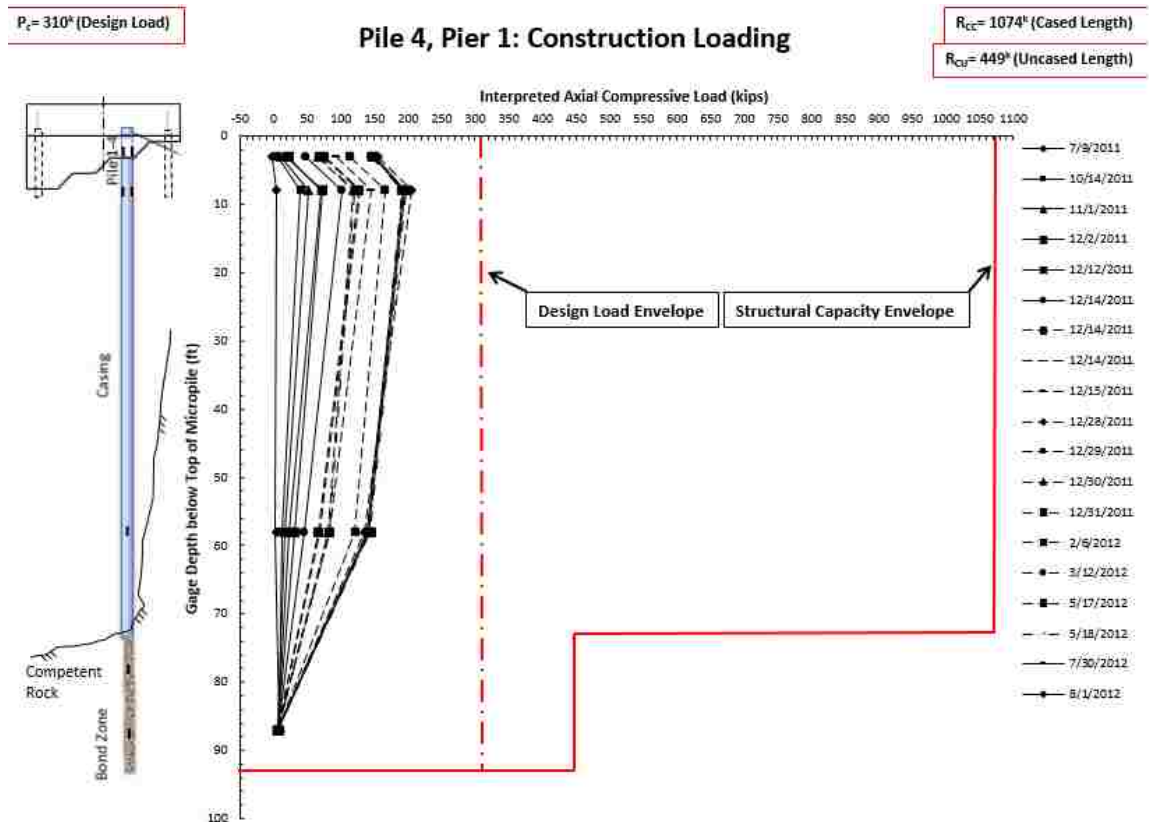
Figure 3.16. Load Transfer of Micropile No.4, Pier No.1 (Dixon, 2013).

Another micropile that was instrumented in Pier No.1 is Micropile No.16. The load transfer mechanism is shown in Figure 3.17. It is close to Micropile No.4 behavior.

Tension was observed in the lowermost strain gages in some of the micropiles, the possible reasons are:

- Curing of the grout made some possible tension across the barbell ends of the strain gages.
- A gap is existed between the rock and grout at the bottom of the micropile.
- Tension readings may be within the range of errors in the load measurement.

- The load is completely transferred, and the pile feels confinement stress from the ground that may bring the end of the micropile to tension.

This issue will be discussed in terms of the numerical modelling introduced in the next sections of this thesis.
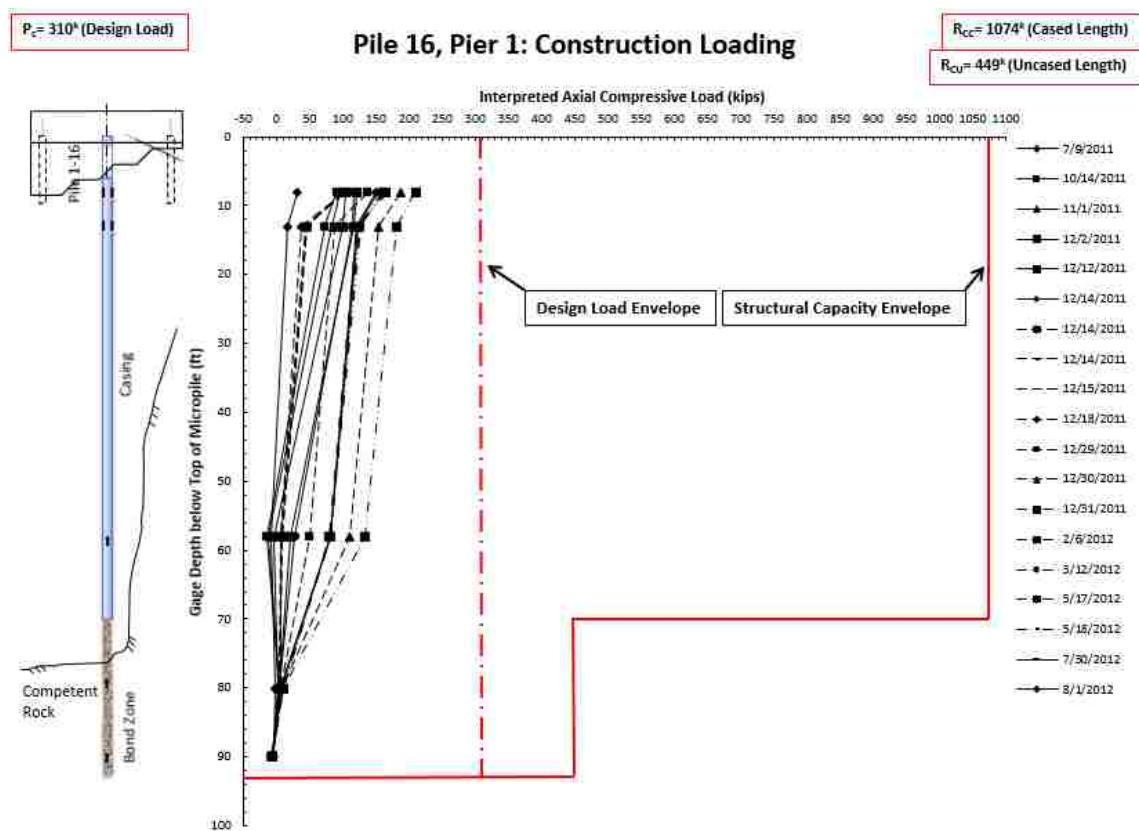
Figure 3.17. Load Transfer of Micropile No.16, Pier No.1 (Dixon, 2013).

Micropile No.16 has both of the strain gages in the overburden soil and therefore, it shows agreement to the conclusion made earlier.

3.6.2. Pier No.2: Micropile No.1, No.6, No.11 and No.16. Pier No.2 consists of five column segments (instead of six in Pier No.1) and twenty cantilever segments. Therefore, this pier is carries less load than Pier No.1. The total load was estimated to be 2,236 kips. The terrain is less steep and the Pier has two lateral rock anchors instead of the four in Pier No.1.

The lengths of Pier No.2 micropiles are shown in Table 3.6.

Table 3.6. Cased, Bond and Total Lengths of the Instrumented Micropiles in Pier No.2.

Micropile	Total Length (ft.)	Cased Length (ft.)	Bond Length (ft.)
No.1	98	80	18
No.6	99	75	24
No.11	106	85	21
No.16	98	80	18

Micropile No.1's behavior of Pier No.2 shown in Figure 3.18 shows similar behavior to Micropile No.11 of Pier No.1. The load is transferred effectivity at the bond zone. However, it considered some downdrag in the cased zone.

Although the weathered rock is located in the cased zone, but it transfers the load effectively. The high stiffness of the weathered rock needs a minimum friction to transfer the load. This issue will be discussed extensively in the next few sections.
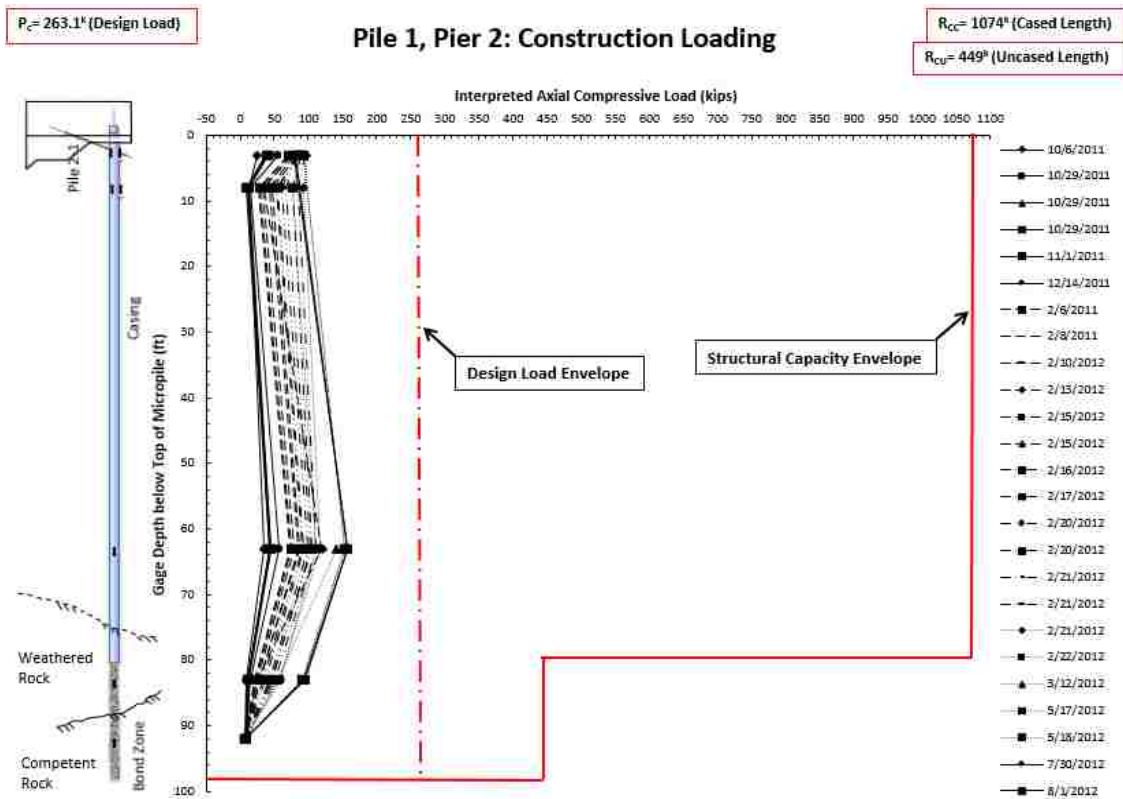
Figure 3.18. Load Transfer of Micropile No.1, Pier No.2 (Dixon, 2013).

Load transfer mechanism of Micropile No.11 in Figure 3.19. It also has a strain gage in the concrete and one in the overburden soil. This confirms that the load is increasing and this is due to the pile cap that gives load to the micropile. After that, it transfer most of the load in the weathered rock. The remaining load is transferred in the bond zone of the micropile.
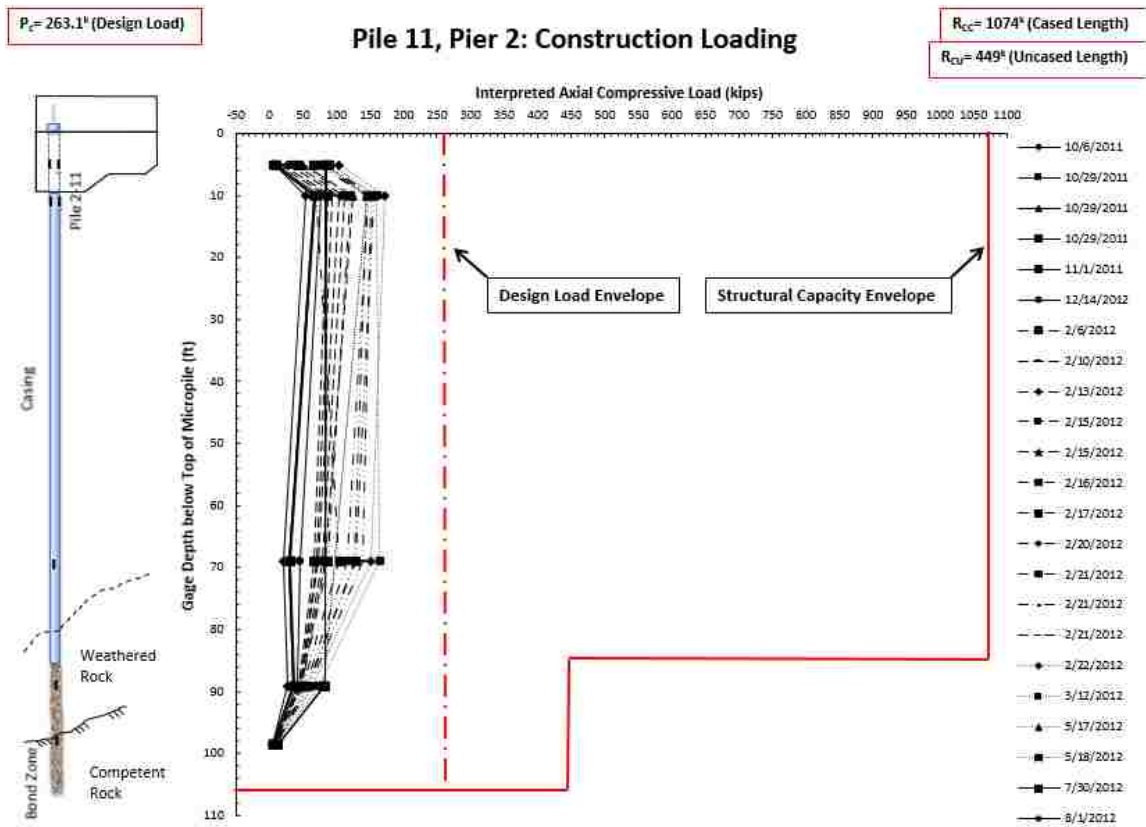
Figure 3.19. Load Transfer of Micropile No.11, Pier No.2 (Dixon, 2013).

The load transfer of Micropile No.6 is shown in Figure 3.20. It appears that the load is not completely transferred as shown at the end of the micropile.

Micropile No.16 load transfer is shown in Figure 3.21. The transfer is efficient at the weathered rock layer and continue throughout the bond zone until it transfer most of the load into the ground.
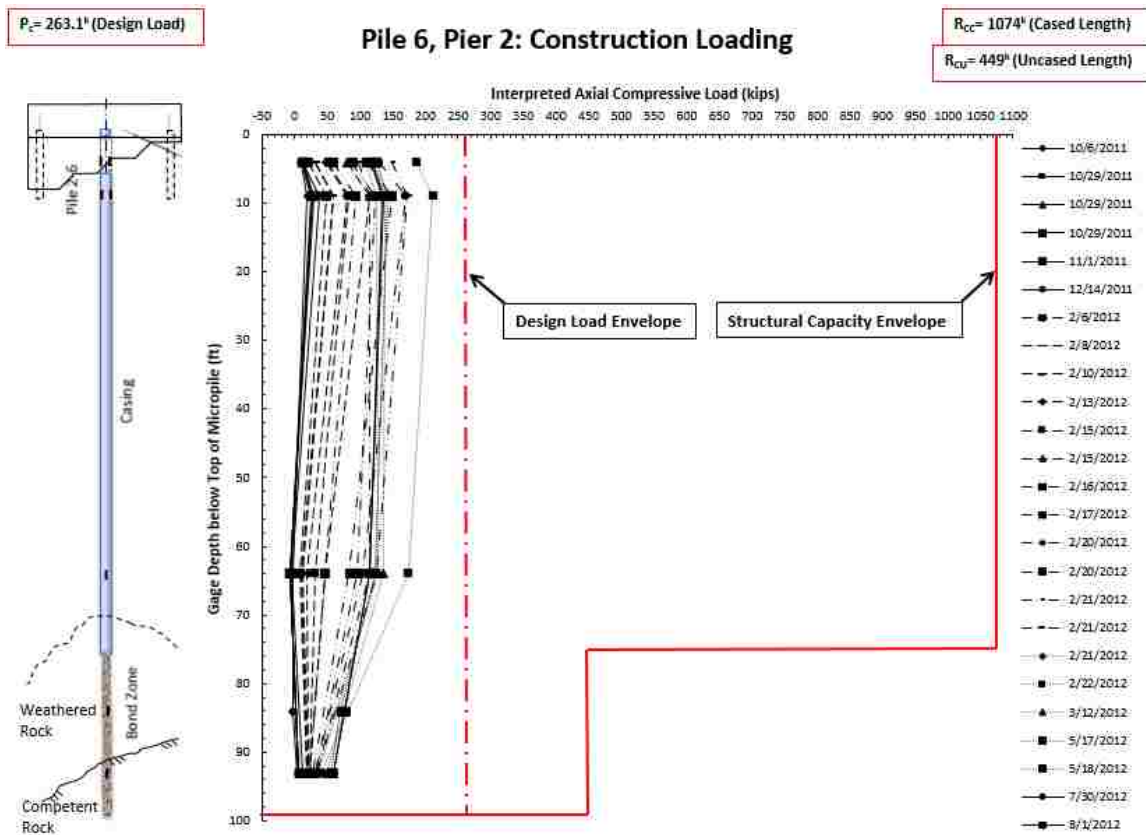
Figure 3.20. Load Transfer of Micropile No.6, Pier No.2 (Dixon, 2013).

Generally, Pier No.1 and No.2 load transfer mechanism shows the following mechanism;

First, the load is collected from the pile cap and the drilled platform and transferred to the micropile. So the load of the micropile is increasing in that area. All micropiles that have one strain gage or both in the concrete proves this.

Next, some of the load transfer occur in the overburden soil and then, it is transferred efficiently in the weathered rock and competent rock.
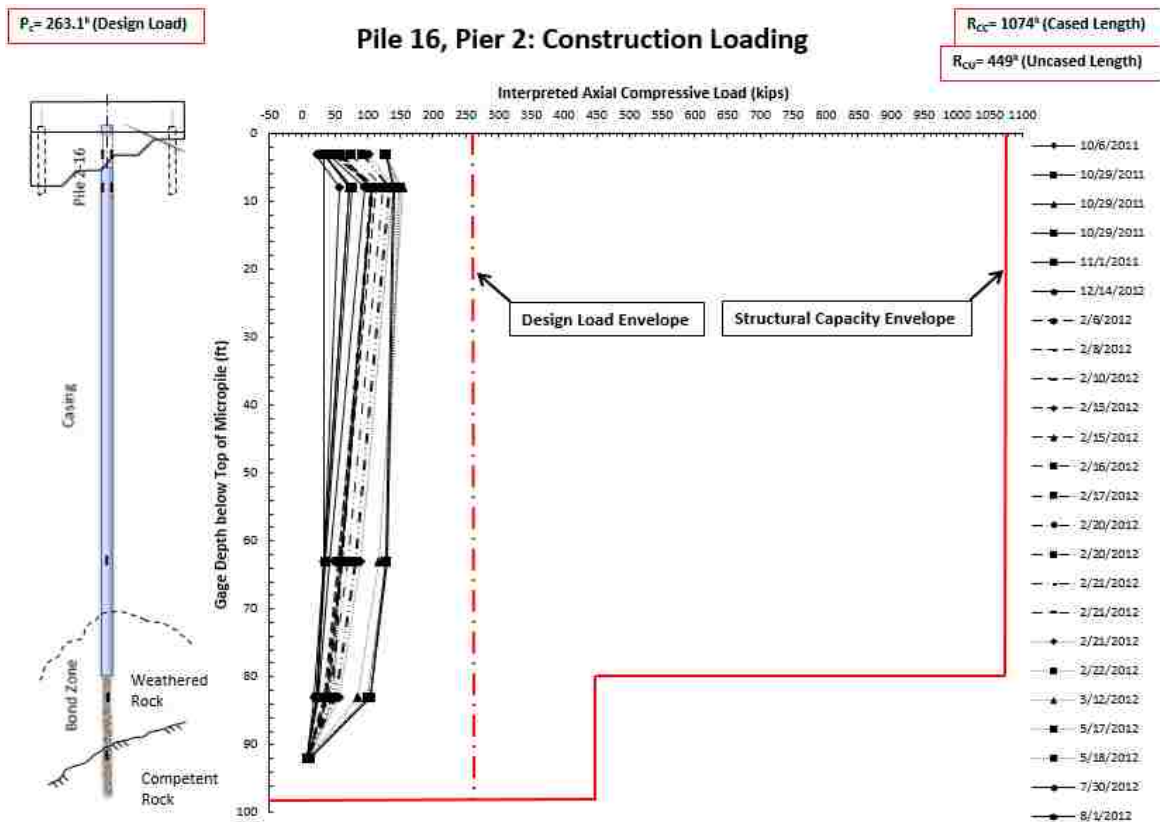
Figure 3.21. Load Transfer of Micropile No.16, Pier No.2 (Dixon, 2013).

The field instrumentation data will be used in the numerical modelling of the micropiles as will presented in next few sections. The numerical modelling results will be compared to the field results at different construction loading conditions.

The field results have limitations; strain gauges are affected by environmental conditions and stress concentrations. Therefore, more strain gauges should be placed at different locations along the micropile to have multiple data for the strains.

Numerical modelling can overcome the shortcomings of the field strain gages. However, the numerical modelling should be verified by a good and realistic field data.

As a result, a combined field and numerical modelling analysis can best understand the load transfer mechanism and this is the objective of this thesis.

4. NUMERICAL MODELLING OF BRIDGE NO. 2 MICROPILES

The finite element method is a very effective tool in modelling of various engineering problems. It is a numerical technique to find an approximation to complex problems by a discrete model which is divided into elements. Each finite element represents a portion of the physical model and they are joined by nodes. Nodes and elements form the mesh. The density of the mesh varies based on the length of elements, the number of nodes and the detail level of the model. All calculations are implemented at the nodes to find the displacement as the primary variables followed by subsequent calculation to find other variables.

Numerical modelling provides a powerful tool to investigate the interaction between the ground and the structures, especially, the studies that cannot be done on real scales such as the dynamic analysis.

Numerical modelling has many advantages over the other methods; to name a few; the ability of modeling different pile and soil geometries with various boundaries and loading conditions, the ability of finding solutions at any point/node in the model and most importantly the ability to account for the continuity of soil behavior. (Khodair and Abdel-Mohti, 2014).

In this analysis, the non-linear numerical modelling will be implemented using ABAQUS standard; a software developed by SIMULIA. ABAQUS is considered as one of the most powerful tools in FEM analysis. It has great efficiency in model development,

importing and exporting the data, modelling of the contact between bodies, easy sharing of the models, data, and results.

ABAQUS standard is a wide range application that can solve linear and nonlinear problems by solving any system of equations implicitly at each increment after forming the global stiffness matrix. This is unlike ABAQUS explicit which does not require forming the global stiffness matrix and solving a large system of equations but, rather, the solution is advanced kinematically in each increment (ABAQUS, 2011). ABAQUS standard is favorable in static simulations.

As mentioned before, Bridge No. 2 has four piers. Pier No. 2 micropiles are longer than Pier No.1. Pier No.2's micropiles has similar length and soil characteristics. Pier No.1 has larger variation and more steep. Therefore, four micropiles in Pier No.1 are short while the other micropiles in Pier No.1 are long. Pier No.2 Micropiles, however, are all long. In this study, the numerical modelling analysis includes the following approaches:

• Numerical modelling of a single micropile. This includes a short micropile (Micropile No.1 in Pier No.1) that encounters the rock at shallow depth and a long micropile (Micropile No.16 in Pier No.1) that encounters the rock at deeper levels.

• Interaction of Micropile No.1 (short micropile) and Micropile No.16 (long micropile) within the two adjacent micropiles. The objective is to study the interaction of the micropiles together. This will not include a pile cap to check if there is any overlap without load that comes from the cap to the soil.

- Group behavior of Micropile No.16 within the two adjacent micropiles. This includes a pile cap.

- Numerical modelling of Pier No.2 with all micropiles.

Micropile's single behavior as well as interaction of three micropiles (without pile cap) will be studied in this section. The rule of the pile cap in the load transfer mechanism as well as the group effect of the micropiles will be discussed in Section 6.

All of the aforementioned approaches will explain micropiles' and they will be beneficial as design guidelines on the load transfer mechanism of micropiles.

Finite element analysis' general steps is shown in Figure 4.1. The 3D geometry of the micropiles and the ground was developed where the micropiles was defined by multiple parts. The different parts were necessary to define different contact algorithms. Then, the different parts collected to form one Assembly. The ground and the micropile were also divided into partitions to define different materials.

The contact algorithm was selected to define the interaction between the parts in the assembly. Next, the loading and the boundary conditions were defined, the loading including the gravity and the structure load. Mesh was then selected and refined until the difference in the results were within few percent. Post processing was conducted to find the strain, stresses and the displacement.
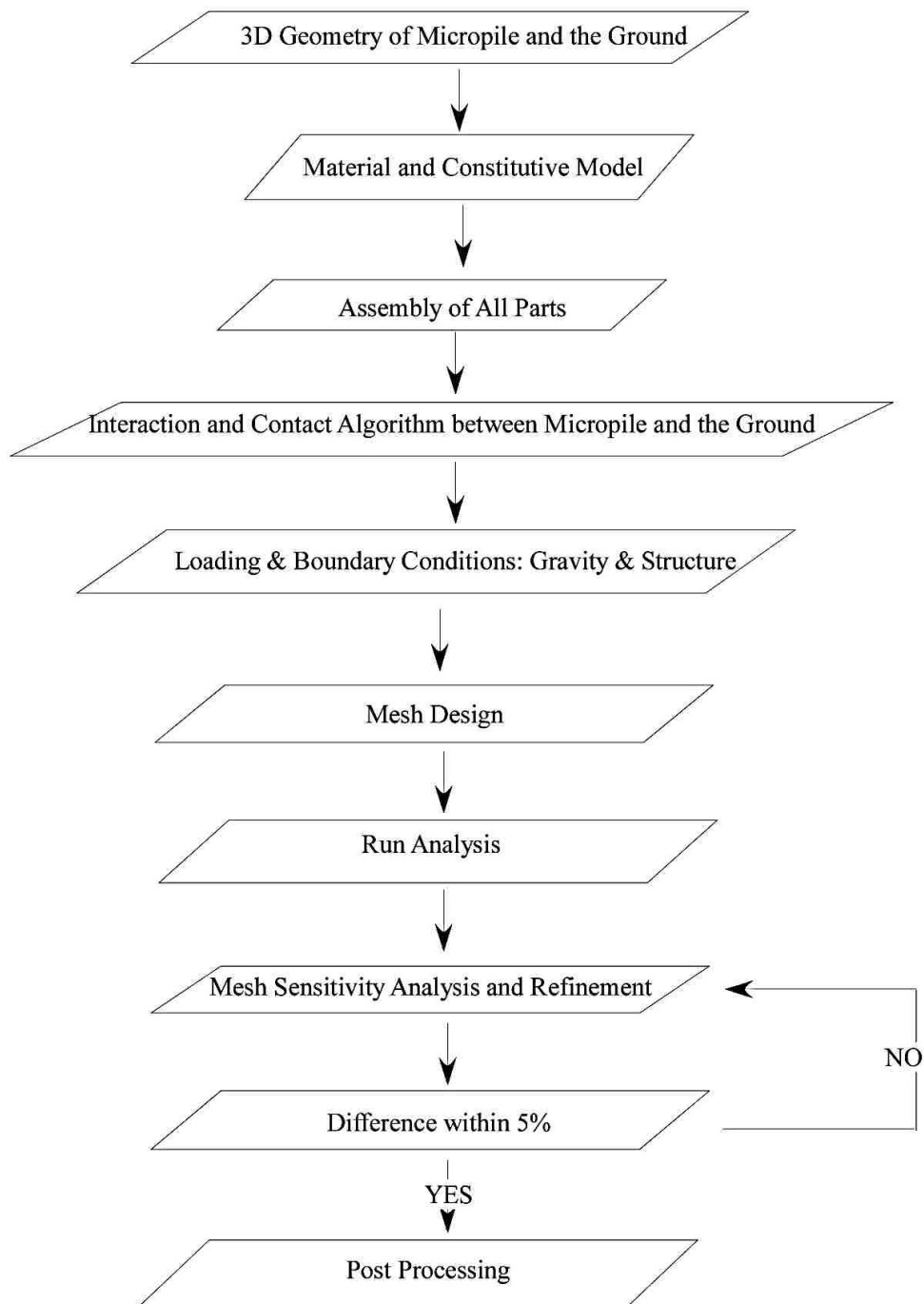
Figure 4.1. Numerical Modelling Approach of Bridge No.2's Micropiles.

In this section, the numerical approach, material and constitutive model. The interaction and contact algorithm between different parts of the micropiles and the ground is presented as well.

4.1. CONSTITUTIVE MODEL AND PARAMETERS

The selected constitutive model should capture the main characteristics of the material mechanical behavior which is unlike the minor characteristics that they might be neglected.

The Mohr Coulomb constitutive model is a non-associated flow rule, linear elastic-perfectly plastic model which omits the contribution of any intermediate stresses other than the principle ones. The elasticity is defined by two parameters; Young's modulus and Poisson's ratio. The failure criteria is defined by the friction angle and cohesion. Dilatancy angle is an additional parameter to describe the use of non-associated flow rule due to irreversible change in volume and the plastic change of the ground (Lade, 2005, Ti et al., 2009). As will be shown shortly in the results, the most important is the behavior of rocks in the low stratum because it is responsible for most of the load transfer mechanism.

A typical stress strain diagram is shown in Figure 4.2. Mohr coulomb assumes elasticity in the first portion which is more pronounced for rocks under higher confined stresses, Figure 4.3 (Bell, 1980). Therefore, Mohr Coulomb becomes closer to simulate

the Metaconglomerate and Metasandstone which they are very confined in the area of

Pier No.1.
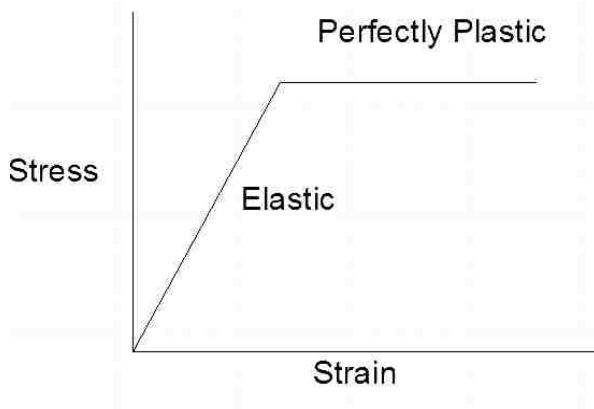
Figure 4.2. Mohr Coulomb Stress-Strain Diagram.
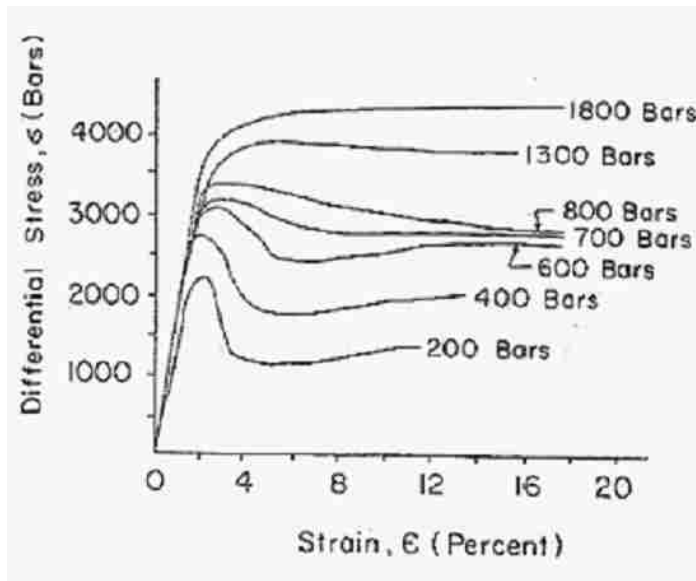
Figure 4.3. Stress Strain Diagram of Rock with Different Confining Stresses (Rahn, 1996).

Correlations between the measured properties and the parameters needed in the model are reported in the literature.

4.1.1. Soil Parameters. Elastic and plastic parameters of soil include the following:

▪ Elastic modulus. Kulhawy and Mayne (1990), Braja (1999) correlated SPT values and the elastic modulus for sand and sand with fines according to the following formula;

$$\frac{E}{Pa} = rN_{60}$$
Eq. 4.1

r coefficient varies between 5 and15. However, gravel accounts for 50% soil composition in Pier 1. Braja (1999), Bowles (1988), Kezdi (1974) and Prat (1995) reported that for sand with gravel soil, modulus of elasticity varies between 100-320 MPa (2090 -6690 ksf).

▪ Poisson's ratio. Kulhawy and Mayne (1990) correlated the friction angle with Poisson's ratio by the following formula;

$$\upsilon = 0.1 + 0.3 \, \phi_{rel}$$
Eq. 4.2

Where $\phi_{rel} = \dfrac{\phi_{tc} - 25}{45 - 25}$
Eq. 4.3

ϕ_{tc} is the friction angle of triaxial compression.

As will be shown next, the friction angle is estimated to be 35º-45º. Therefore, υ is estimated to be 0.25-0.40. The results can be validated with the reported range of this kind of soil in (Kulhawy and Mayne,1990).

▪ Friction angle. Meyerhof (1956), Terzaghi (1967), Peck, Hanson et al. (1974), Kulhawy and Mayne (1990), Das (2002) reported ranges for different types of soil with

different SPT numbers. For SPT numbers , N, between 10-60, the friction angle varies between 35º-45º.

▪ Cohesion of soil. Small cohesion can be assigned to this soil since clay accounts in the compsition of the soil as reported by Siegel (2010). Small number, 2 kPa (50 kPa), can simulate this composition and avoid probable tension that may happen to the elements in the model.

▪ Dilation angle. Dilation angle was correlated in some places as two third of the friction angle or the friction angle substracted by 30 (Youssef-Abdel-Massih and Soubra, 2008). This suggest, that the dilation angle can varies from 5º-15º. This can be checeked by the range based on the soil type given by (Vermeer and De Borst, 1984).

▪ Unit weight. The unit weight is estimated to be 20-21 kPa (125 -135 psf) below ground water table and 16-20 kPa (100-130 psf) above ground water table. The water table shown in Figure 4.3 at Pier No. 1 is located at height of 55' below the ground surface.

4.1.2. Rock Parameters. Elastic and plastic parameters of rock include the following:

▪ Elastic modulus. Elastic Modulus can be correlated to available data of unconfined compressive strength and rock quality designation. RQD data was recorded every 5 ft. Correlations reported in the literature to estimate the intact and the deformation modulus. Intact modulus will be extracted first followed by the deformation modulus.

• Intact rock modulus, Er. Intact rock modulus can be correlated with the unconfined compressive strength.

$$Er = MR\sigma_c \qquad\qquad\qquad \text{Eq. 4.4}$$

where MR is modulus ratio between the unconfined compressive stength and the intact modulus.

Hoek and Diederichs (2006) reported that the modulus ratio, MR for clastic sedmentary rock is betwwen 200-400. Specifically; conglomerate is 300-400 and sandstone is 200-300. For nonfoliated metamprphic rocks such as metasandstone it is 200-300. Unconfined compressive strength varies between 50-100 MPa (1,040-2,080 ksf) at 50' depth. Therfore, the intact elastic modulus is estimated to be in the range of 10 GPa to 30 GPa (208,850-626,600 ksf).

The intact rock modulus is estimated using Figure 4.4 which depends on the depth (Jiang et al., 2009). This suggests that E_r is between 10-30 GPa (208,850-626,600 ksf) at various depth of the ground.
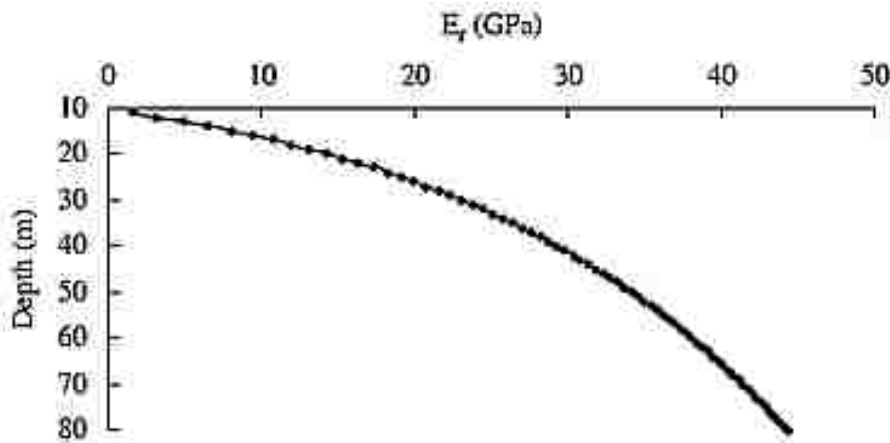
Figure 4.4. E_r Variation with Depth (Jiang et al., 2009).

- Deformation modulus, Em. Can be coerrelated with RQD as follows:

$-E_m = \alpha E_r; \ \alpha = 0.0231(RQD) - 1.32 > 0.15$ (Coon and Merritt, 1970)   Eq. 4.5

-Lower Bound: $\dfrac{E_m}{E_r} = (0.2)10^{0.0186RQD-1.91}$ Eq. 4.6

-Upper Bound: $\dfrac{E_m}{E_r} = (0.8)10^{0.0186RQD-1.91}$ Eq. 4.7

-Mean value: $\dfrac{E_m}{E_r} = (1.0)10^{0.0186RQD-1.91}$ (Zhang and Einstein, 2004)   Eq. 4.8

-Em=(5-20) Er (Farmer and Kemeny, 1992)   Eq. 4.9

Therefore, the deformation modulus is estimated to be 5-15 GPa (104,430-313,280 ksf) and it becomes 20-25 GPa (417,700-522,130 ksf) at deep levels. A limitaiton on the formulas 4.6-4.8 developed by Zhang and Einstein (2004), that when the values of RQD increases, the intact modulus tends to equal the deformation modulus which is unrealistic. West (2010) also suggested 5-10 GPa (104,430-208,900 ksf) for Quartazite rocks.

- Poisson's ratio. A value of 0.25 -0.30 can be estimated for this kind of metamorphic rocks (West, 2010).

- Friction angle. A value of 25º-35º can be estimated from Rahn (1996) and Barton and Choubey (1977).

- Cohesion. A value of 50 -150 kPa (1,044-10,440 psf)can be estimated from Rahn (1996).

- Dilation angle. Vermeer and De Borst (1984) and Ribacchi (2000) suggested that dialtion angle of rock in the range of ϕ-20. This gives 5º-15º for the dilation angle.

- Unit weight. The unit weight was measured to be around 26 kN/m^3 (162 pcf)

(Siegel & Thompson, 2010).

As a result, the ground parameters are as listed in Table 4.1.

Table 4.1. Ground Parameters of Pier No.1.

Soil/Rock	Elastic Modulus (ksf)	Poisson's Ratio	Mass Density (pcf)	Friction Angle(°)	Dilation Angle(°)	Cohesion (psf)
Soil	2,090-6,690	0.25-0.40	130 - 135*	35-45	0.0-15.0	50
Rock	104,450-522,250	0.25-0.30	162	25-35	0.0-15.0	1044-3133

*100-125 pcf below ground water table

4.1.3. Micropile Parameters. The model used for micropiles is linear elastic

model. Parameters needed for this model are modulus of elasticity and Poisson's ratio.

The twenty micropiles have one uniform section.

The material properties of these micropiles:

- E_{casing} and E_{bars}=29,000 ksi

- E_{grout} = 4030.5 ksi based on the following formula,

- E_{grout}= $57\sqrt{f_c'}$ (ACI Committee, 2008)   Eq. 4.10

- Poisson's ratio=0.25, the lower bound for steel and the upper bound for grout.

Micropiles' Parameters are shown in Table 4.2.

Table 4.2. Micropile Parameters of Pier No.1.

Material Properties	E (ksf)	v
Cased Zone	1,493,680	0.25
Bond Zone	822,960	0.25

4.2. MICROPILES -SOIL & ROCK INTERACTION MECHANISM

Contact and interaction mechanisms are the most important in the model since they are responsible for the load transfer mechanism between the micropile and the ground. In this model, the interaction can be classified into the following categories (shown in Figure 4.5);

- Interaction of the pile cap-pile.

- Interaction between steel casing and ground (soil) in the cased zone. This comprises the interaction between the of steel casing - overburden soil, steel casing-weathered rock, and 1 foot extensions of the steel casing into the rock. The one foot embedment is a condition necessary in the design.

- Interaction between the grout and the ground (rock) in the bond zone. This interaction is important as the most of load transfer occurs in this area. It involves the competent material of Metaconglomerate and Metasandstone that will ultimately support the bridge.

- Interaction of the pile tip and the ground that involves no relative movement between the pile tip and the ground, so a constraint is applied.

- Interaction that connects all micropile's parts together.
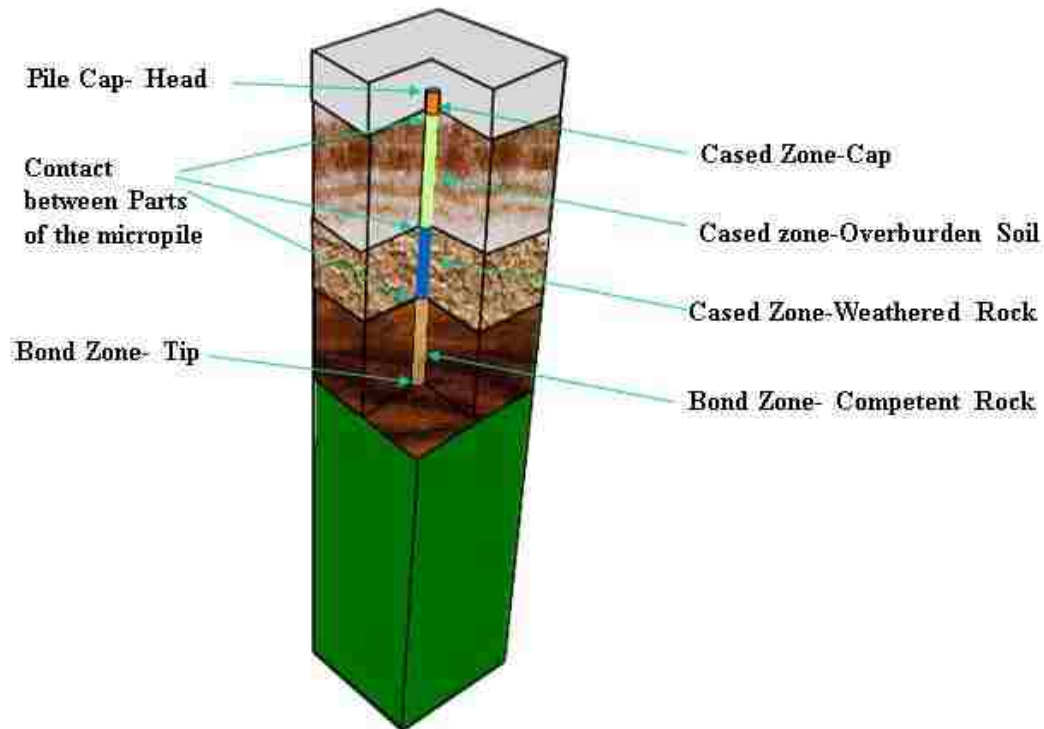
Figure 4.5. Interaction of Ground with the Micropile.

To simulate the interaction, a contact pair, surface-to-surface with finite-sliding tracking approach algorithm was selected for the contact. Surface to surface contact consists of two surfaces, master surface and slave surface. Master surface is taken to be the ground and the slave is the micropile. Master surface nodes is allowed to penetrate the slave surface which requires the micropile to have finer mesh and smaller element sizes than the ground at the contact region, this condition is necessary to avoid penetration of the slave nodes into the master surface (ABAQUS ,2011).

Finite sliding tracking approach implies that the relative motion between the contacted surfaces is tracked all the time. Thereby, area and pressure of the contact are calculated according to the deformed shape of the model (ABAQUS, 2011).

The contact of these two surfaces is of two components; a component normal to the surface and one tangential to the surfaces.

• Normal component: the normal behavior between the micropile and the ground is modelled using "Hard contact". Hard contact applied as long as the clearance or the distance between the surfaces is zero which gives a positive contact pressure value. If the clearance is higher than zero, the contact pressure is negative value and the two surfaces are no longer in contact, this relationship can be shown in Figure 4.6.
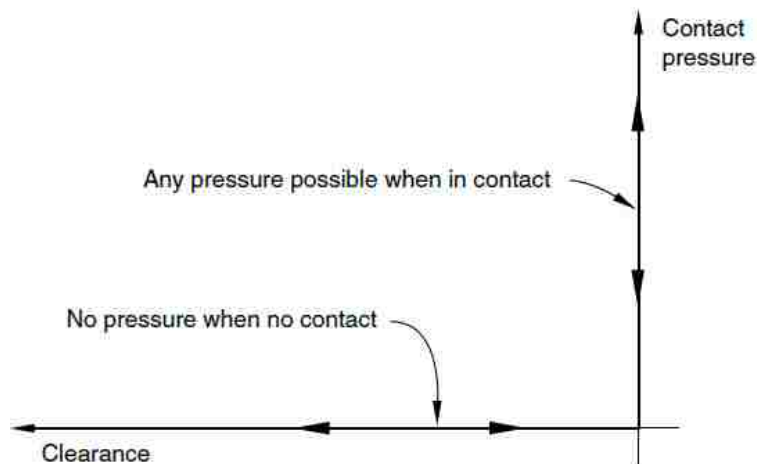
Figure 4.6. Hard Contact Relationship (ABAQUS, 2011).

• Tangential component: is defined as the behavior along the ground interface that involves the relative sliding between surfaces that would transmit shear forces across the interface. Penalty type with coulomb friction model is selected to simulate the shear behavior. Coulomb friction model implies that no load transfer occurs unless the surface traction reaches the critical value of the shear stress as shown in Figure 4.7.

$$\tau_{crit} = \mu P \qquad\qquad 4.11$$

τ_{crit}: critical shear stress

μ: friction coefficient

P: contact pressure
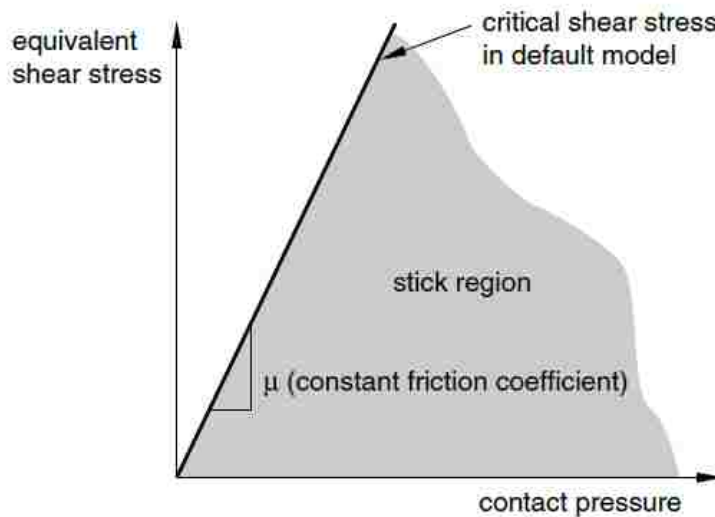
Figure 4.7. Coulomb Friction Model (ABAQUS, 2011).

The friction coefficient is critical parameter in coulomb friction model which depends on the materials of the surfaces in contact. The primary contact surfaces in this

model are steel with overburden soil (Cased Zone) and grout with rock (Bond Zone). The coefficient of friction is different in each interaction.

The friction coefficient should be assumed to simulate the interaction at the cased and the bond zone. The assumed interface friction should consider the installation, drilling techniques as well as the field data that shows the amount of load transfer.

- Installation and drilling techniques: The installation and drilling techniques effect the load transfer mechanism of micropiles. The replacement micropiles installed the micropiles after drilling the soil and removing the material from the hole. This indicates that the interface friction is broken in the cased zone of the micropile. Theoretically, that suggests that the friction should be near to zero at the cased zone. However, as explained earlier in Section 3, this friction can be recovered with time. The amount of friction recovered depend on the ground characterization as will be explained in the next few sections.

The bond zone is not affected by the drilling methods since grout is placed in the hole which enforces a good bond. However, the higher the pressure of the applied grout, the stronger the bond. This was explained in Section 2.

- Load transfer distribution based on field instrumentation: The quantity of the load transfer that was observed in the field indicates the amount of the friction at the interface. Most of the micropiles shows that some load transfer occurred in the cased zone which verifies that the friction is gained with time.

4.2.1. Micropile Cased Zone-Ground Interaction. The interaction between the cased zone of micropile and the ground with micropile is theoretically a frictionless interaction because the soil is drilled and removed prior to pile insertion as was presented earlier, this implies that the shear transfer is zero according to Eq 4.11. The load transfer mechanism with zero interface friction at the cased zone is shown in Figure 4.8. The cased zone area of the micropile is in contact with the concrete platform, the overburden soil and the weathered rock. Each contact will be discussed further in the next sections.
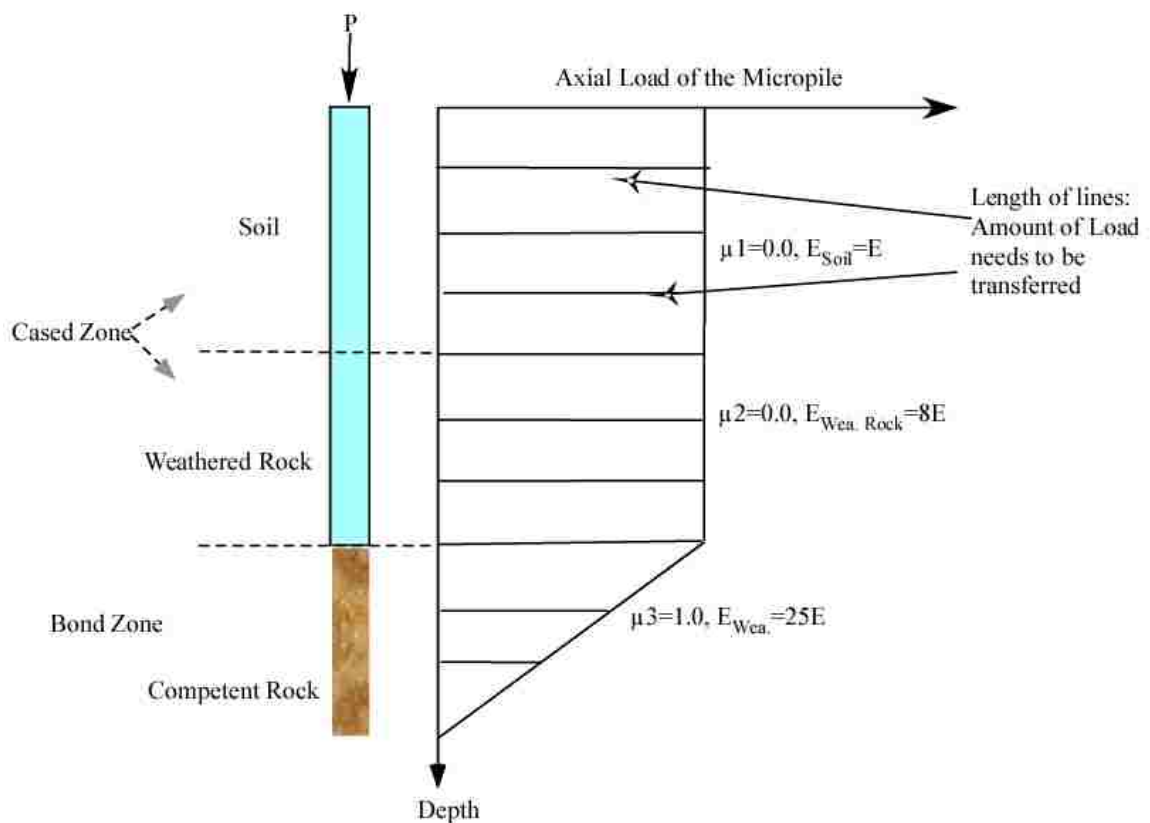
Figure 4.8. Load Transfer Mechanism with No Friction in the Cased Zone.

4.2.1.1 Cased zone-concrete platform. The concrete platform presented earlier in

Section 3 was constructed to provide a level topography under the pile cap and to

drill/insert the micropile into the ground. The installation of micropiles requires drilling

into the platform and installation of the casing. Therefore, the interface friction was

broken at that region. However, after pouring the huge mass of the pile cap, some mortar

may fill the spaces at the interface and subsequently, a friction may be developed. In the

singles micropiles' analysis, the load was applied directly over the micropile not on the

pile cap. Therefore, the concrete platform contact is excluded from the analysis. If the

contact is activated at the concrete drilled platform, it will transfer the load from the

micropile to itself as shown in Figure 4.9.
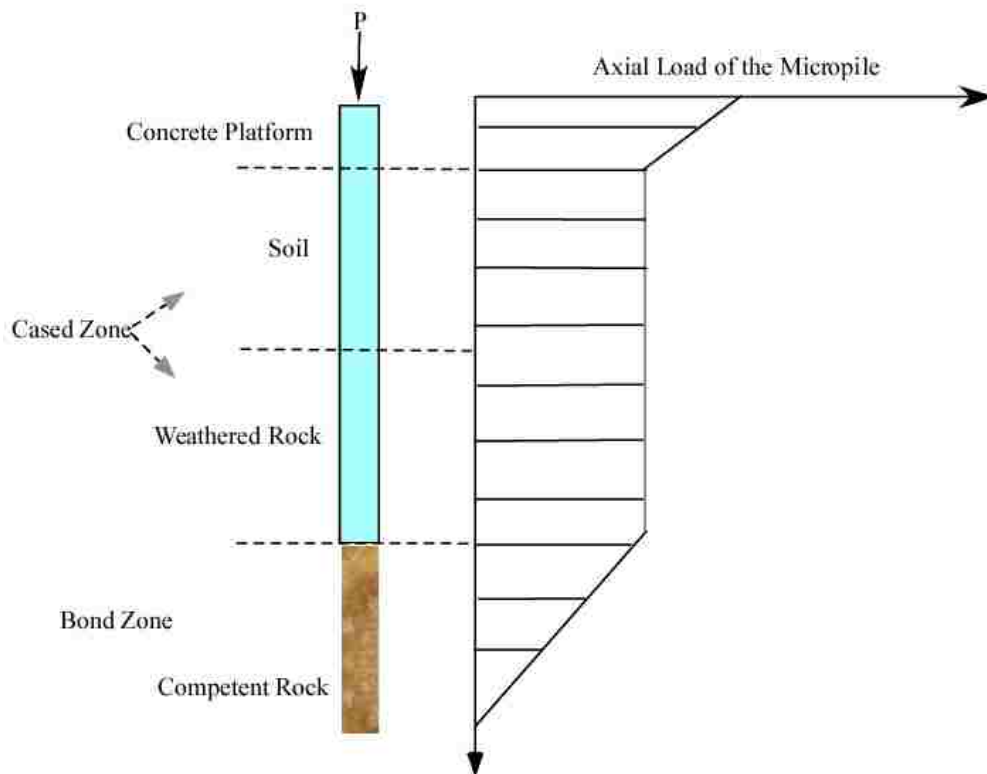
Figure 4.9. Load Transfer of Concrete Platform without a Cap.

In group analysis, the pile cap carries higher load than the micropile at that region. Therefore, it collects the load from the cap and give it to the micropile as shown in Figure 4.9. This is completely the opposite of the single pile analysis without a cap. This result is verified by the field instrumentation of most of the micropiles discussed in Section 3. Most of the micropile show similar trend to Figure 4.10 in the concrete platform region. On the other hand, this behavior does not occur unless there is a friction. That proves that the drilled platform had friction that was added after the pouring of the pile cap.
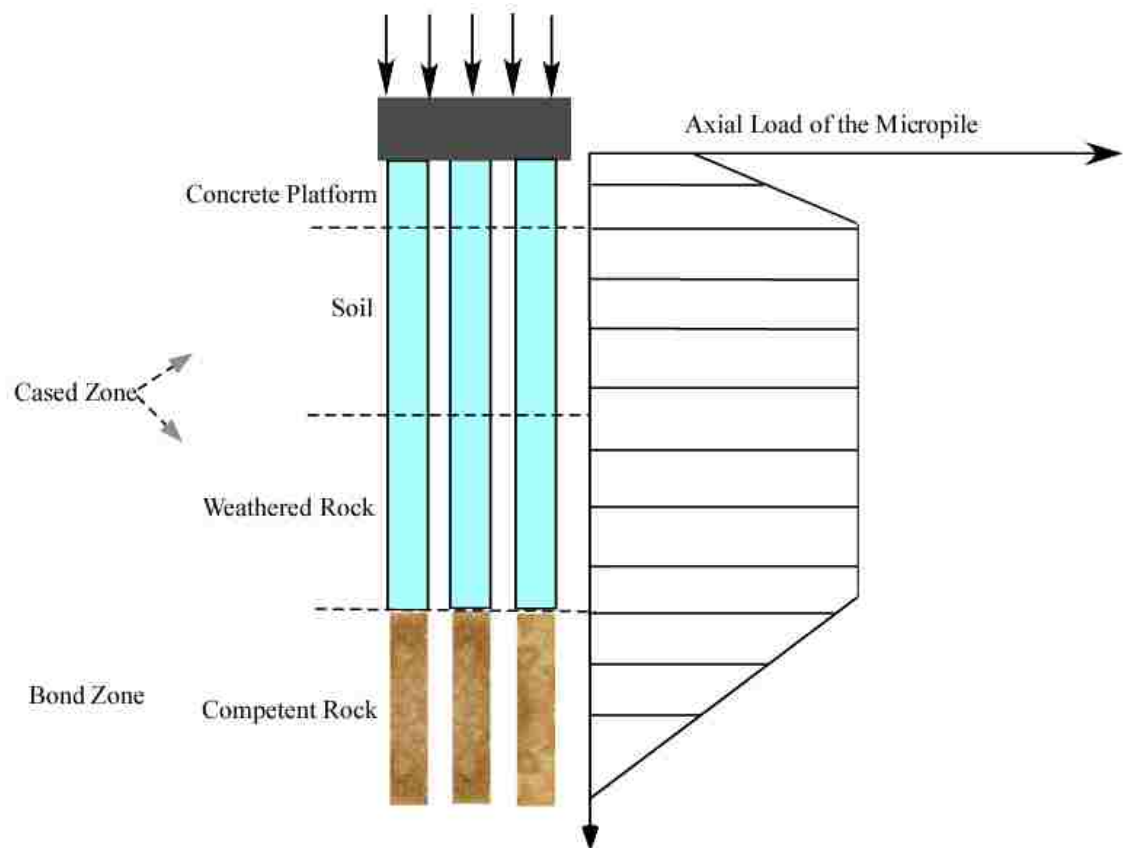
Figure 4.10. Load Transfer of the Concrete Platform with a Cap.

Therefore, the contact between the platform and the micropile should not be activated except with a pile cap. The pile cap was not included into the single analysis of the micropiles due to some reasons:

- The pile cap is not needed in the single micropile, since the function is to distribute the load among all micropiles and reduce the differential settlement.

- To study the load transfer mechanism with cap and without it. This can provides a knowledge on the rule of the cap towards the load distribution underneath it.

In the next few sections, the single analysis is presented as well as group analysis where the contact between the concrete platform and the micropile will be active. Then, the load transfer mechanism will be compared.

4.2.1.2 Cased zone –overburden soil & weathered rock. As explained earlier, the cased zone interaction is a frictionless due to construction and installation method. However, small friction can be gained with time. This depends on the soil characterization. Low plasticity soil such as sand and gravel can gain friction rapidly. The same case with weathered rock. On other side, the surfaces develop friction upon contact.

In addition, any two surfaces can have minimum friction with they touch each other. Therefore, a friction of 0.1 and 0.3 can be realistic values for the interaction of the micropile with soil and weathered rock, respectively. The angles of friction that coincide with these values are 5.71° and 16.7° as indicated in Figure 4.7.

The friction in the cased zone trigger some load transfer. The effect of the friction on the load transfer mechanism is influenced by the stiffness of the ground at that region. This means that the weathered rock will cause more load transfer as shown in Figure

4.11. This will be explained in later sections. The load transfer in the cased zone is also reported by Dixon (2013) which shows that some load transfer occur in the cased zone.
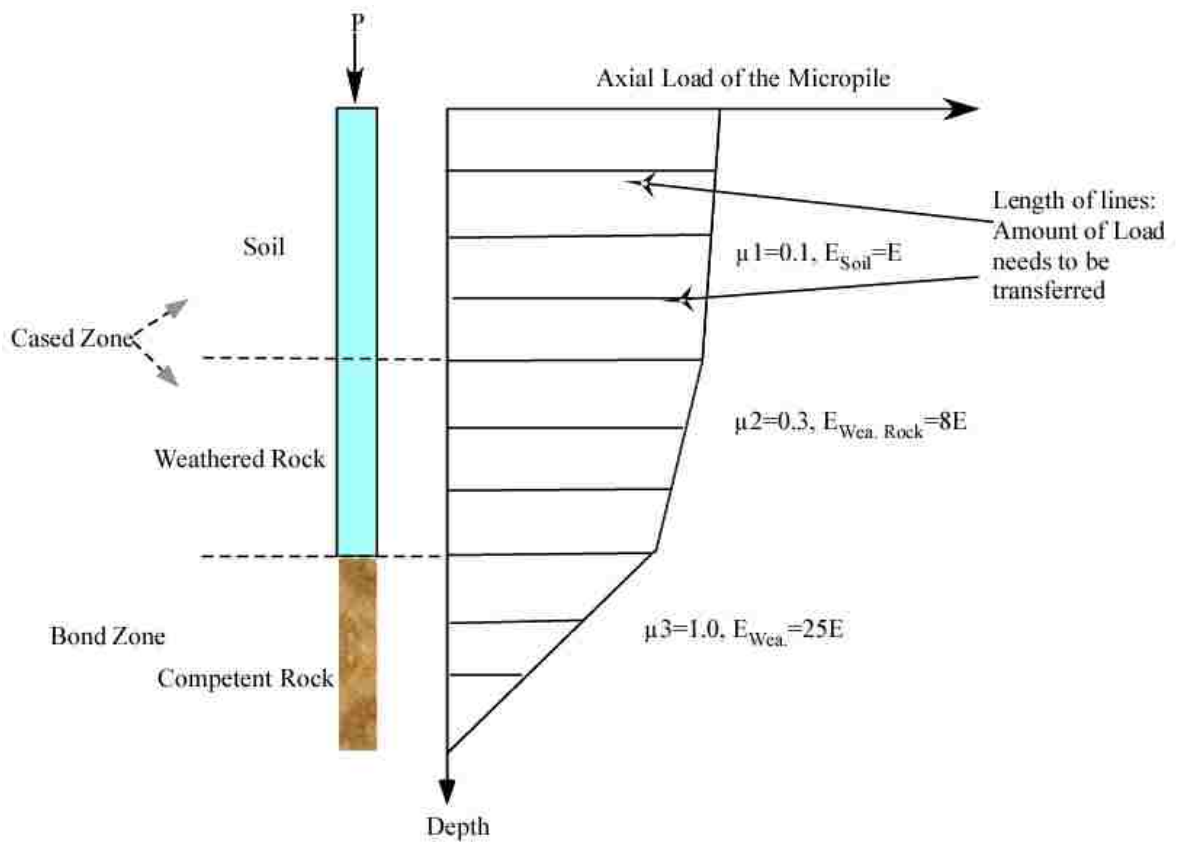
Figure 4.11. Load Transfer Mechanism with Friction in the Cased Zone.

4.2.2. Bond Zone-Ground Interaction. The grout and the rock interaction is gained throughout the period of grout curing. The bond strength depends primarily on the installation method and the ground conditions.

The more pressure applied during grouting, the more strength will be the bond. In the same manner, the higher the stiffness of the ground, the stronger is the bond.

Generally, the bond between the grout and the ground is assumed to be very strongly bonded. As shown in Figure 4.12, most of the load transferred to the ground occur in the bond zone
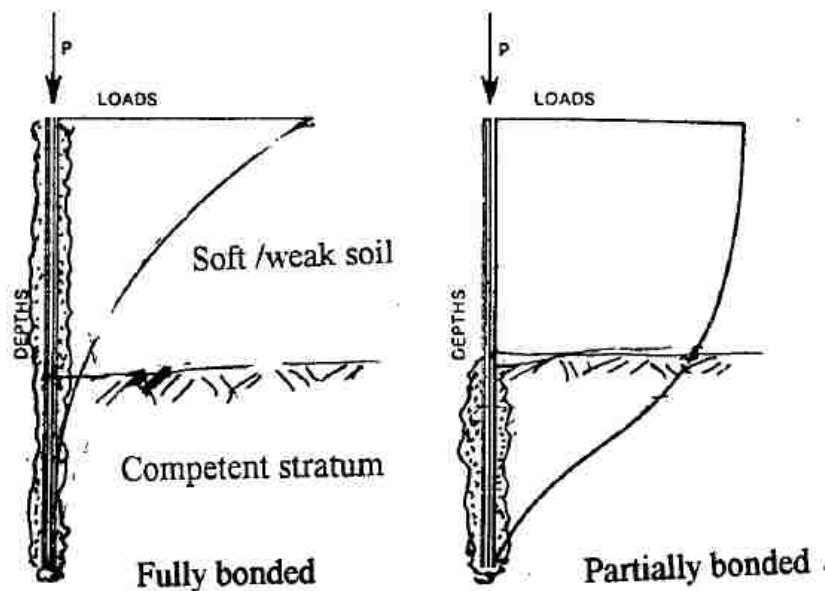
Figure 4.12. Fully Bonded and Partially Bonded Micropiles (Lizzi 1982).

A friction coefficient of 1 can best simulate the strong bond between the rock and the ground. Given all the previous assumptions; coefficient of friction will be assigned for each interaction as in Table 4.3 and as shown in Figure 4.13.

Table 4.3. Friction Coefficients in Micropiles of Pier No.1.

Surface-Surface contact (Pile surface-Ground surface)	Zone	Friction coefficient, μ
Steel-Overburden Soil	Cased Zone	0.1
Steel-Weathered Rock	Cased Zone	0.3
Steel-Competent Rock	Cased Zone	0.3
Grout-Competent Rock	Bond Zone	1

Tie constraint is assumed to simulate the behavior of the interaction mechanism at the interface between the pile tip and the ground. Tie constraint implies that each node in the slave master, micropile, has the same displacement values of the master surface i.e. the ground. Tie also connects the micropiles' parts together to ensure continuity. Tie constraints are shown in Figure 4.13.
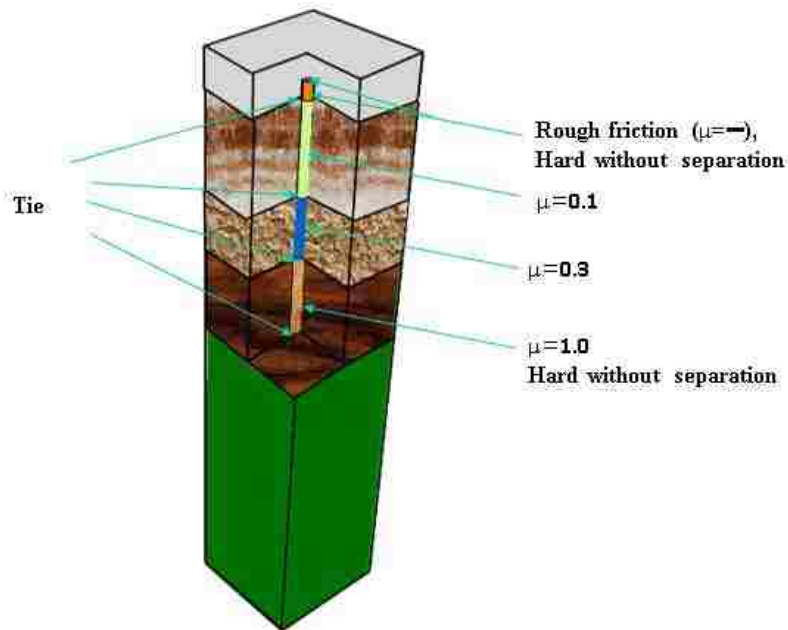
Figure 4.13. The Contact between Micropile and the Ground.

5. SINGLE ANALYSIS OF BRIDGE NO.2's MICROPILES

Single analysis of short micropiles and long micropiles of Bridge No.2 are presented in this section. Among the instrumented micropiles, Micropile No.1 and No.16 are chosen to represent the short and long micropiles, respectively. The study of both micropiles are representative to all micropiles in the bridge.

5.1. NUMERICAL MODELLING OF MICROPILE NO.1

Micropile No.1 represents the short micropile analysis. Micropile No.1 has special characteristics among all micropiles in all piers; it has the shortest length and located in the shallowest area of the bedrock nearest to the right abutment of the bridge. In this section, numerical modelling of Micropile No.1 will be presented as well as the modelling approach and techniques.

5.1.1. Subsurface Conditions and Locations. The stratigraphy shown in Figure 5.1 of Micropile No.1 is characterized as follows:

- In the upper 30': SC-SM overburden soil; 45% gravel, 35% sand and 15% silt.

- Lower than 30': Metasandstone and Metaconglomerate competent rock. The location of Micropile No.1 within other micropiles is shown in Figure 5.2. In addition, Micropile No.1 has the least embedment length in the drilled platform as shown in Figure 5.3.

Figure 5.1. Micropile No.1 Subsurface Characterization.

Legend
Red: Rock, Yellow: Weathered Rock, Green: Overburden soil, Brown: Concrete, Blue: Water Table

Figure 5.2. Subsurface Conditions of Pier No.1.
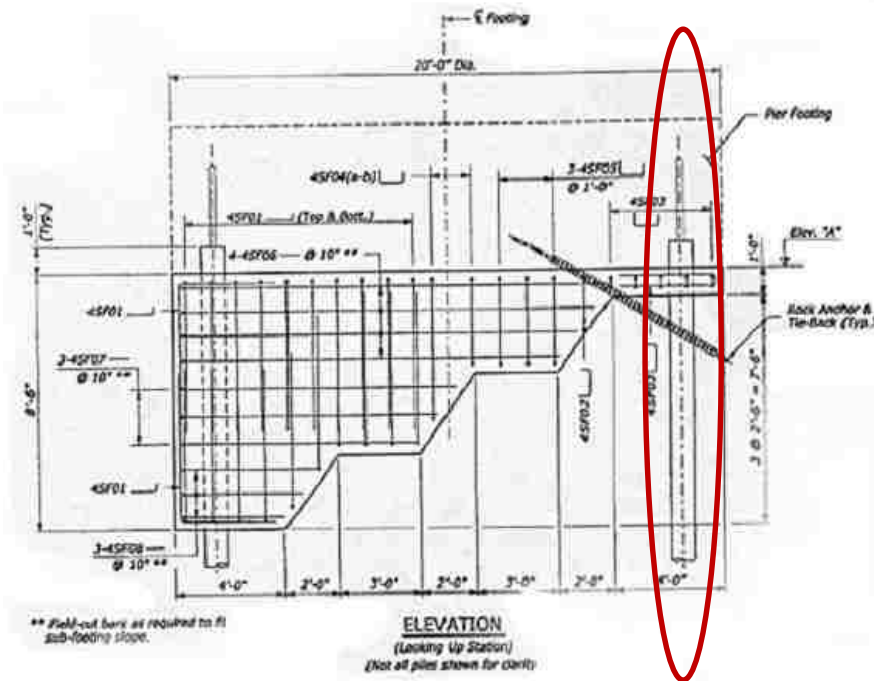
Figure 5.3. Micropile No.1 as Located in the Drilled Platform.

5.1.2. Model Geometry and Material Parameters. The models of ground and micropiles, both, are selected to be 3D deformable bodies.

• Soil/Rock: The selected size of the model is 20'X20'X100' to minimize the boundary effect of the model on the results. The width is selected to be 30 times of diameter (30D) and the depth as 2 times of the piles' length (2L) as shown in Figure 5.4. 30D and 2L are conservative as reported by Helwany (2007). However, the boundary size depends on many factors such as loading conditions, mesh size, and study type (static, explicit). If no verification check is conducted, 30D and 2L are considered enough in most of the cases. In this study, a verification check is conducted by taking sections across the model to verify that boundaries have negligible effect on the results. The strain

around the micropile becomes relatively constant at a certain distance away from the
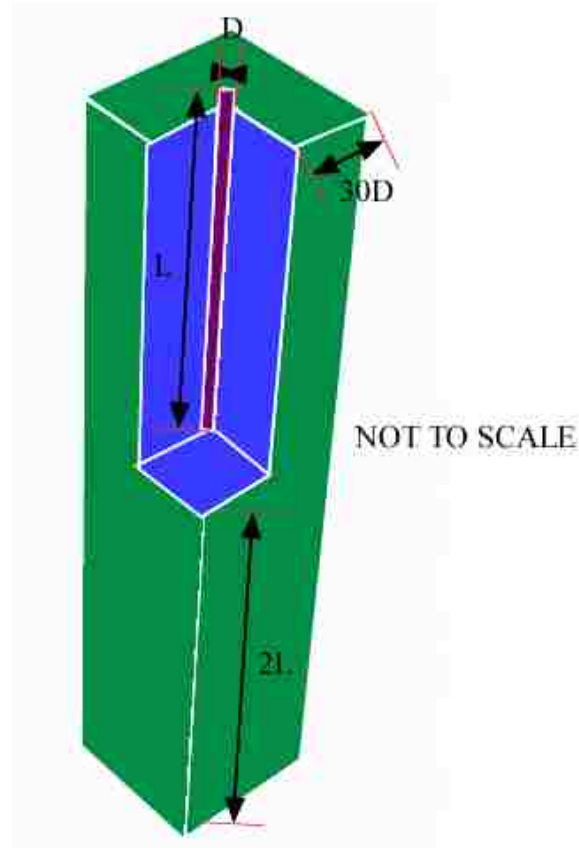
micropile.

Figure 5.4. Model Geometry of Micropile No.1.

Parameters of the Mohr coulomb constitutive model for Micropile No. 1 is shown

in Table 5.1. The parameters values were explained earlier in Section 4.1.

Table 5.1. Ground Parameters of Micropile No.1.

Depth (ft)	Soil/Rock	Elastic Modulus (ksf)	Poisson's Ratio	Mass Density pcf	Friction Angle (°)	Dilation Angle (°)	Cohesion (psf)
0-1	Concrete Platform	580,400	0.3	150	-	-	-
1-27	Overburden Soil I	3,000	0.3	130	35	5	100
27-55	Competent Rock I	104,450	0.3	162	30	5	2100
55-100	Competent Rock II	208,900	0.3	162	30	5	2100

• Micropile: The micropile diameter is 0.802' and it is constant along the micropile to reflect the real geometries of the micropile. The micropile was selected with two different axial stiffness (EA) as shown in Table 5.2 and Figure 5.5; bond zone area has lower axial stiffness because of the steel casing absence in that region. If the overburden soil stiffness of layer No.1 is assigned as the reference modulus, E_{cased} becomes 375E, where E is the elasticity modulus of layer No.1 shown in Table 5.2. The bond zone modulus (200E) is lower due to the stiffness reduction. The ratio between the stiffness in the cased zone and the bond zone of the micropile is 200/375.

Table 5.2. Micropile No.1's Bond and Cased Zones.

Micropile section	E (ksf)	v
Cased Zone	1,493,680	0.25
Bond Zone	822,960	0.25
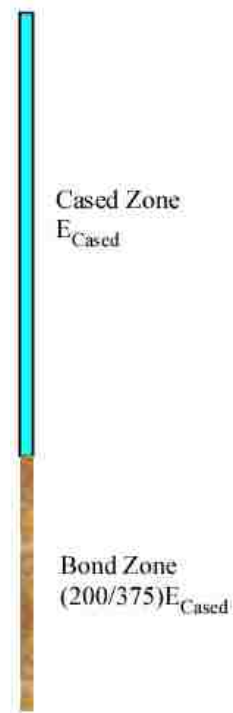
Figure 5.5. Micropile No.1's Section.

The cased zone extended one foot in the competent rock to reduce the stress concentration due to the stiffness reduction. This will be confirmed in the numerical modelling results. The extension is necessary in the design specifications of the micropiles.

5.1.3. Interaction Properties. Interaction at the interface between the micropile and the ground was studied earlier in Section 4.2.2. It appeared that the friction coefficient is the critical parameter which has influence on the amount of load transfer from the micropile to the ground. It was concluded that the contact and interaction mechanism are as follows:

- Cased Zone: A "Hard" normal contact and "Penalty" tangential contact. The friction coefficient assigned for the cased zone is 0.1 for overburden soil.

- Bond Zone: A "Hard" normal contact and "Penalty" tangential contact. 1.00 is interface friction coefficient.

- Pile tip zone: "Tie" Constraint is applied. The interaction properties as well as the friction coefficients are shown in Figure 5.6.

A "Tie" constraint is also used to connect different parts of the micropiles together. The different parts were necessary in order to assign different contact algorithms. The micropile consists of three parts;

One part that is connected with the drilled platform, this contact was deactivated as discussed earlier in single analysis. The second part is connected with the overburden soil and the third part with the rock. "Tie" connects the three different parts to compose the micropile. Tie ensures continuity condition at the interface.
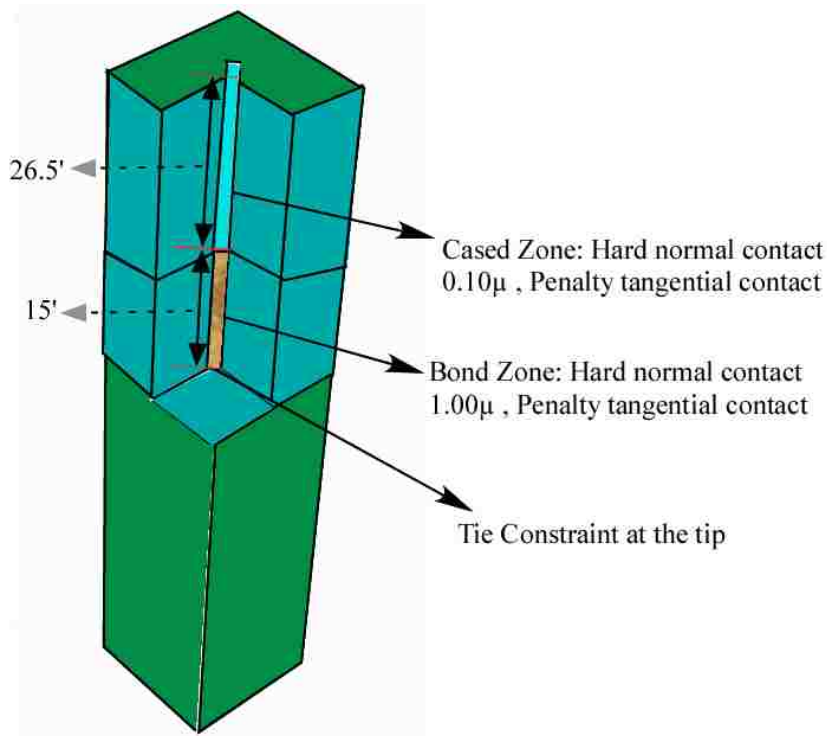
Figure 5.6. Interaction Components of Micropile No.1.

5.1.4. Loading Conditions and Boundary Constraints. In this section, the boundary and loading conditions are discussed. The loading includes the own weight of the ground/ geostatic stresses and the load of the structure.

5.1.4.1 Boundary conditions. Boundary at each side of the model was constrained to translate in the normal direction. This condition can be simulated by applying Rollers at the sides and the bottom of the model. The boundary was extended to eliminate any effect on the results as presented earlier in the Model Geometry.

5.1.4.2 Loading conditions. The load consists of two steps:

1. Geostatic step: to ensure initial equilibrium under initial stresses, the geostatic step should be simulated first. Abaqus standard has many options to define the stresses of the ground, some of them are:

▪ Gravity: use the assigned density of the materials multiplied by the gravity acceleration. If the layer is below ground water table, a reduction in the density by water density is necessary.

▪ Body force: needs the input as unit weight.

▪ Predefined field: to predefine the stresses by users.

All the displacement should read displacement and strains approaching zero at the end of this step.

All the three options were conducted in separate analysis. The Gravity option was found to be the most accurate and convenient option.

2. Static step: where the structural load is applied. It was chosen instead of transient step due to the deep ground water table; i.e. below the overburden soil. "Transient step accounts for soil dissipation and consolidation". Therefore, there will be no build up in the pore water and coupling the pore water pressure with stresses is meaningless (Helwany, 2011).

To study the performance of micropiles under different loading conditions, a wide range of load will be applied on the micropile. This will be beneficial in studying the mechanism under different load increments. Hence, applied loads are ranging from 200 kips and 500 kips. Table 5.3 shows the strain readings after bridge completion stage. The

load can be applied by either concentrated load or by inducing a pressure over the equivalent diameter area, results have no big difference in either case.

Table 5.3. Strain Gauges Readings of Micropile No.1 at Bridge Completion Stage.

Depth (ft)	Strain (Micros)	Load (kips)
5	-559.58	-422.32762
10	-476.868	-359.90301
30	-298.9	-225.58656
36	-205.506	-66.823187
42	-40.376	-13.128828

5.1.5. Mesh Convergence Study. Mesh size has great importance on the results. Not enough refined mesh will lead to some inaccuracy and may be divergence. However, time computation increases with continuous refinement. Accuracy of the results and the time of computation need to be optimized. The mesh of the model was refined until the results were within few percent difference as shown in the Figure 5.7. Mesh No.1 is the coarsest with 1' in major areas. Some areas with stress concentration were kept finer such as the pile cap, drilled platform area at the cased/bond zone boundary. The mesh element size was reduced by half each time. Mesh No.2 is 0.5'X0.5'X0.5' and Mesh No.3 is 0.25'X0.25'X0.25'.
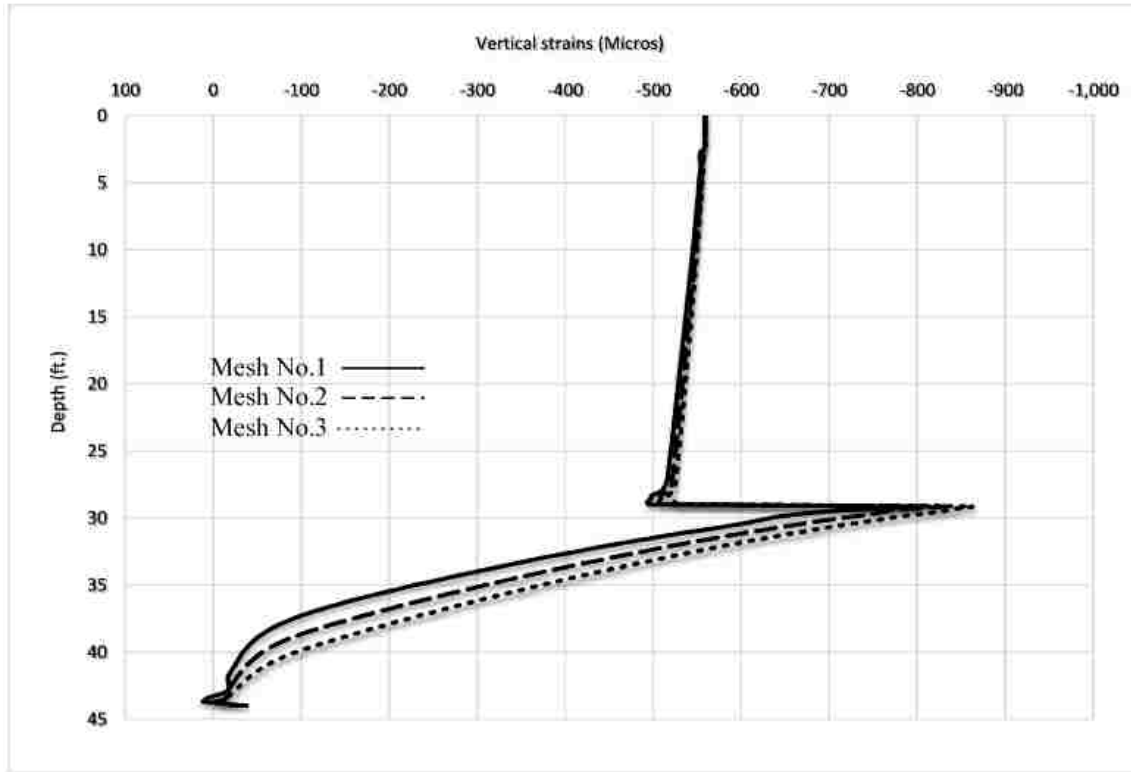
Figure 5.7. Strain with Different Mesh Sizes of Micropile No.1's Model.

5.1.6. Numerical Analysis of Micropile No.1. The numerical analysis of Micropile No.1 is conducted according to the steps mentioned earlier. The numerical analysis results are presented in this section. Results include the vertical load, stress, and strain at the interface between the micropile and the ground. Also the same results are shown at distance 1d and 2d away from the micropiles surface as well as for several transverse cross sections taken across the ground and the micropile. Thereby, the results cover all the model.

5.1.6.1 Behavior at the interface. The interface between the ground and the micropile is important since the load is transferred within this area. Understanding the load transfer in this area implies the understanding most of the load transfer mechanism from the micropile to the ground and vice versa. The micropile, ground and the interface are shown in Figure 5.8.
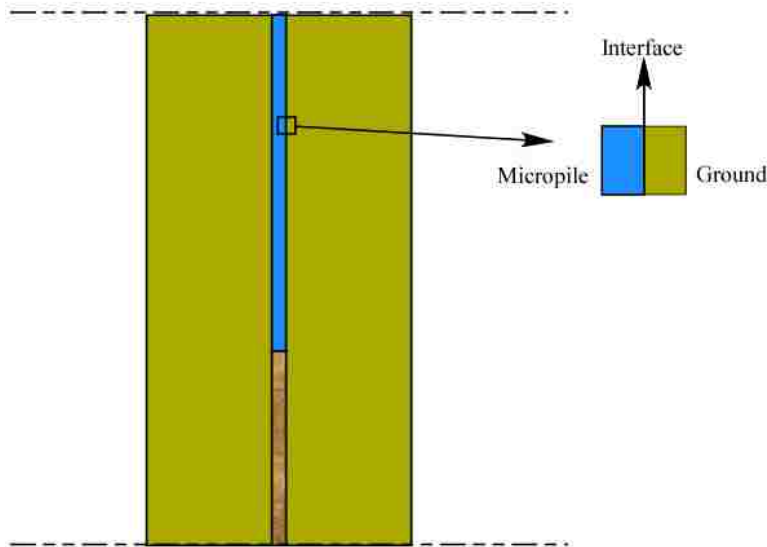
Figure 5.8. Micropile No.1's Interface.

5.1.6.1.1 Micropile performance at the interface. Figure 5.9 presents the load transfer distribution of Micropile No. 1 along the depth.

At all loading conditions shown in Figure 5.9, the micropile transfer some load in the overburden soil i.e., for 420 kips loading condition, the applied load was 420 kips and then decreases to 350 kips at the bottom of the cased zone, therefore, 70 kips was

transferred in the soil region. The behavior is the same for other loading conditions. Generally, 15% of the load is transferred in the cased zone.
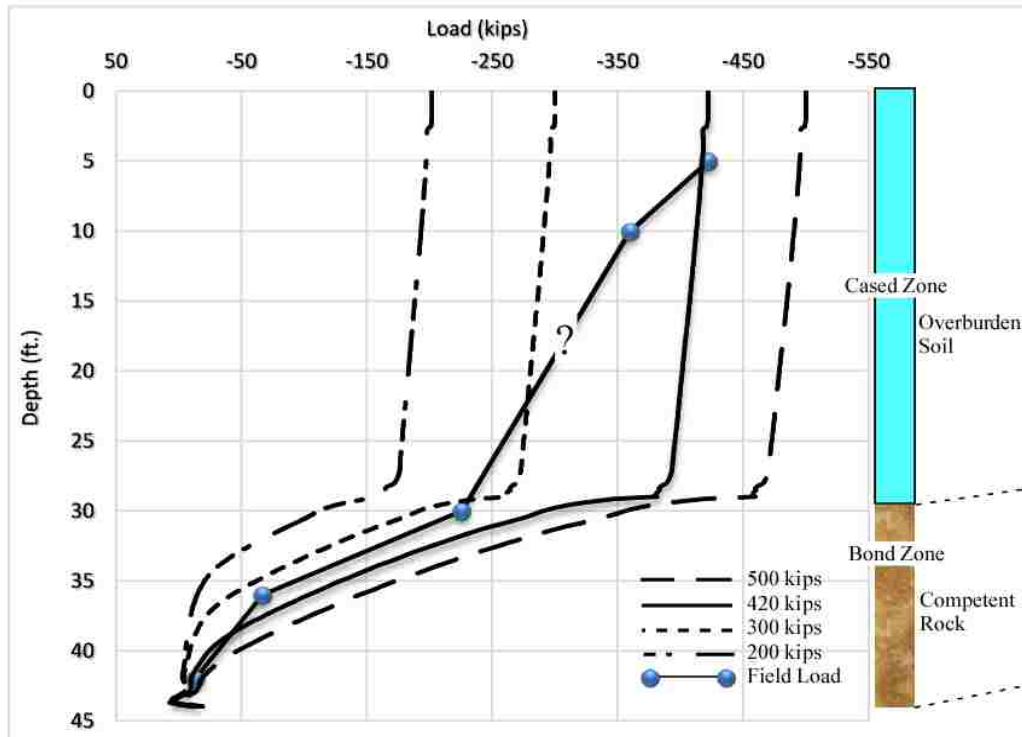
Figure 5.9. Micropile No.1's Load Transfer.

All the remaining 85% load is transferred in the competent rock region. The load measured in the field appears to match a 300 kips to 420 kips loading condition. However, connecting a straight line between the calculated loads of the field is not a good fit of the data. Therefore, it is shown with question mark. Since the behavior is predicted using FEM, the line between the second and the third reading can now be changed to represent a different fit that match the behavior of FEM as shown in Figure 5.10.
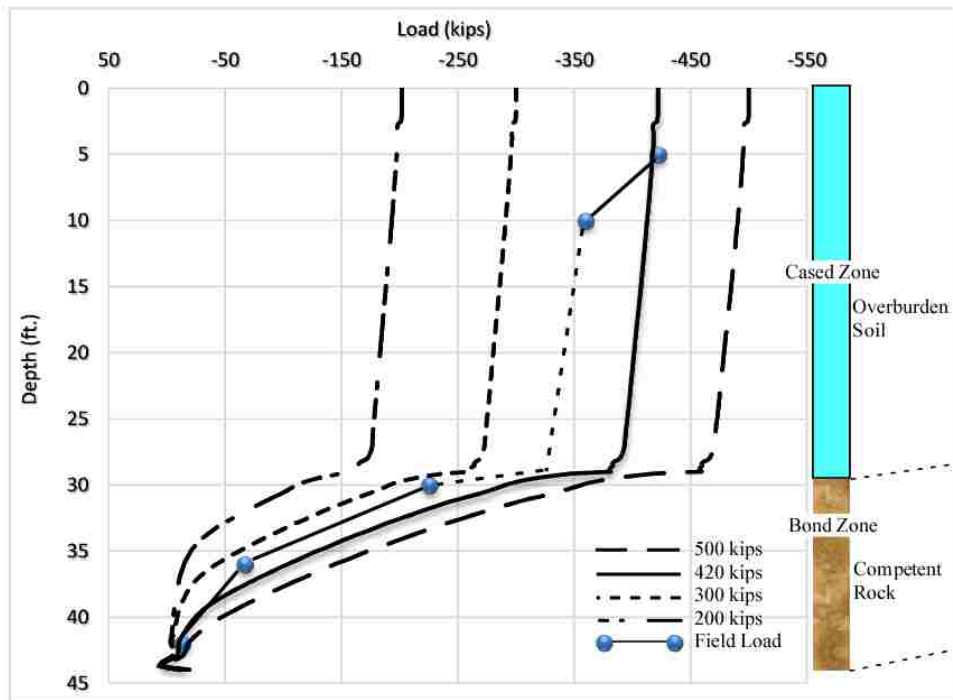
Figure 5.10. Micropile No.1's Load Transfer-Different Curve Fit of Field Data.

Connecting the second and the third loadings in similar behavior as the FEM makes the FEM results matches well with the field along the length of the micropile. The load that best match the field is around 400 kips. The big difference of the first and the second readings of the field are somewhat far from the predicted behavior.

The strain plots of the same loading conditions are shown in Fig. 5.11. It is obvious that at the regions where the steel casing is absent, the stress/strain concentration increases 50% within 0.5'. At 420 kips, the strain was 500 μs and when the steel is absent, the strain becomes 750 μs and it comes again to 500 μs within the next 5'.
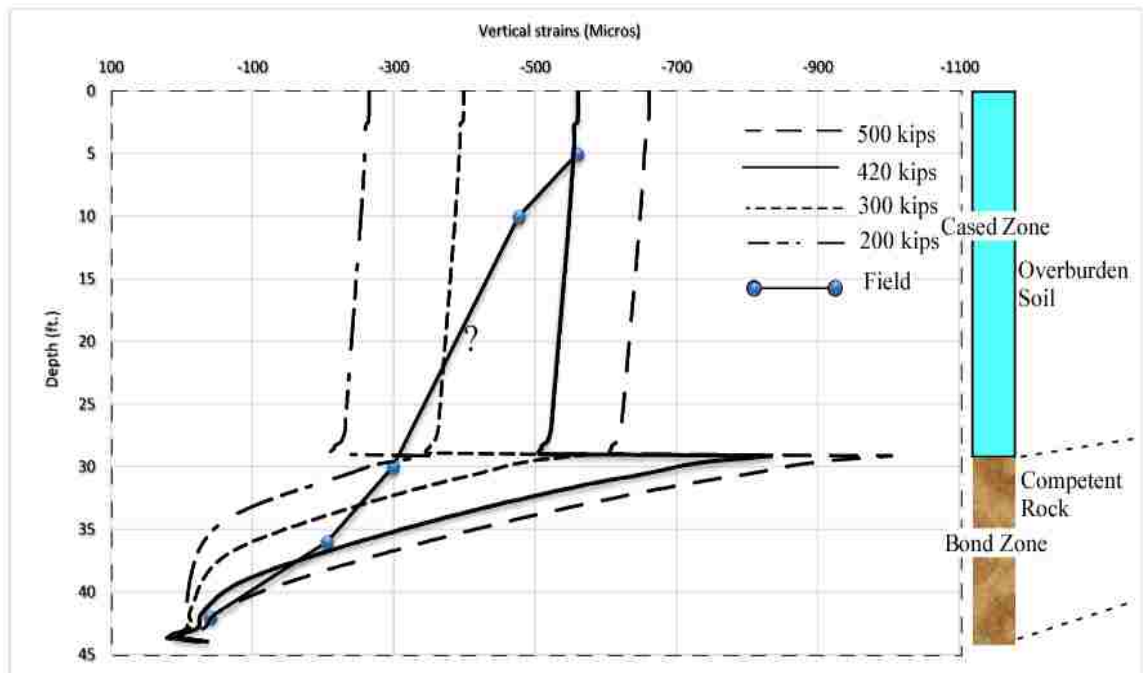
Figure 5.11. Vertical Strain at Micropile No.1's Interface-Micropile Side.

The strain at the tip of the pile comes to small values and reads a positive range of 2-5 µs. These values are small and it implies that all the load was transferred to the ground.

Figure 5.12 presents the stresses at the surface of Micropile No.1. It is also shown that most of the stresses carried by the micropiles are transferred in the bond zone.
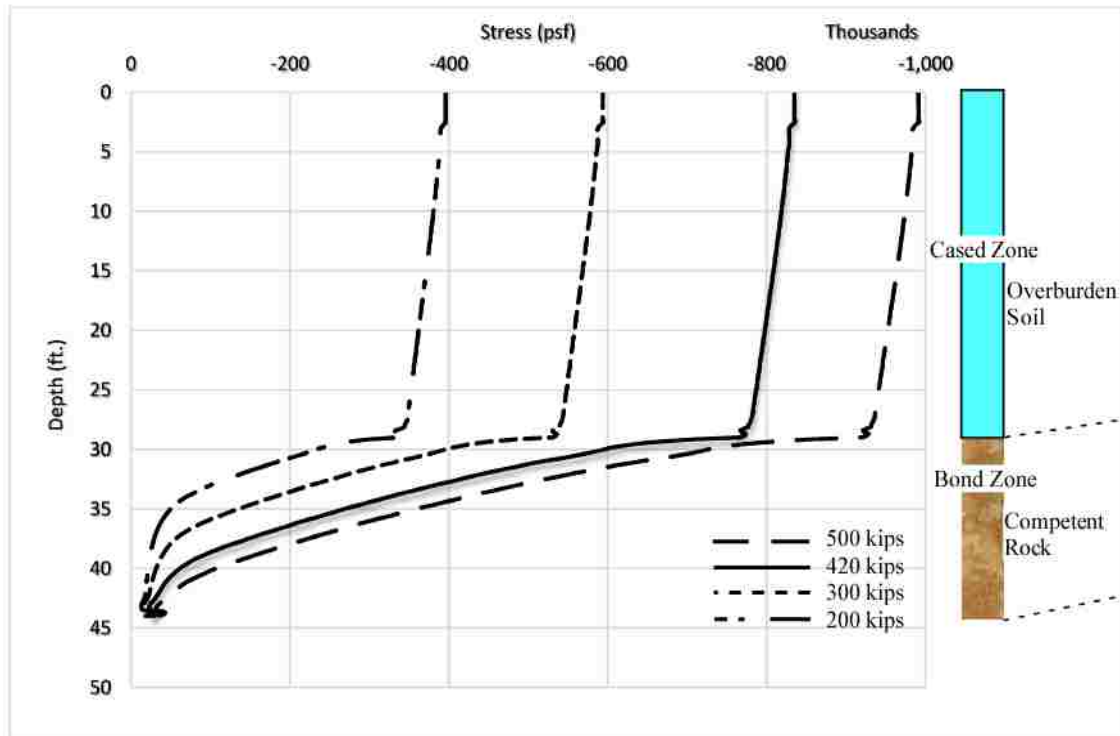
Figure 5.12. Vertical Stress at Micropile No.1's Interface-Micropile Side.

For 420 kips, the stress is 835 kips/ft^2, it is decreasing linearly until it becomes

710 kips/ft^2. So, around 15 % of the stress is transferred in the cased zone. The bond zone

stress starts with 710 kips and it reads 20 kips/ft^2. The stresses are not reading zero at the

pile tip because it still reads the vertical stress of the ground at any location. The load

transfer does not show jump as in the strains and this is because of the reduction in the

axial stiffness. The load is calculated using the following formula,

$$P=\varepsilon EA$$ Eq 5.1

Eq 5.1 implies that the force is equal to the strain multiplied by the axial stiffness,

EA. The axial stiffness reduction in the bond zone multiplied by the sharp increase of the

strain reduced the sharp change of the calculated load at the boundary. If the axial stiffness remains the same, the axial load will increase sharply to reflect same pattern of the strain.

5.1.6.1.2 <u>Soil & rock performance at the interface.</u> The ground surface of the interface consists of the overburden soil and the competent rock. The ground surface performance at the interface will be presented in this section.

Figure 5.13 shows the response of the ground due to loading of the micropile. As shown, the ground does not feel significant strain for most of the interaction length. It reads 7 µs at a depth 23' before feeling the changes of both, starting of the bond zone and the steel casing absence.

The performance shows that the ground feels positive strains at 23-29' i.e., 6' before the bond zone (last 20% of the cased zone length). This means that the ground is in tension. On the contrary, the micropile feels additional negative strain in this area as shown previously in Figure 5.11.

Figure 5.14 compares the strains of the ground and the micropile strains using field data performance and FEM. Generally, the strain felt by the ground is very small relative to the micropile. The maximum strain felt by the soil is 300 microstrains. However, the micropile reads 950 microstrains at the same location which is three times of the ground. This is because of the high modulus of the material around. However, overburden soil has low modulus but does not read a large values of strains and this is due to poor interaction of the materials between steel casing and the ground.
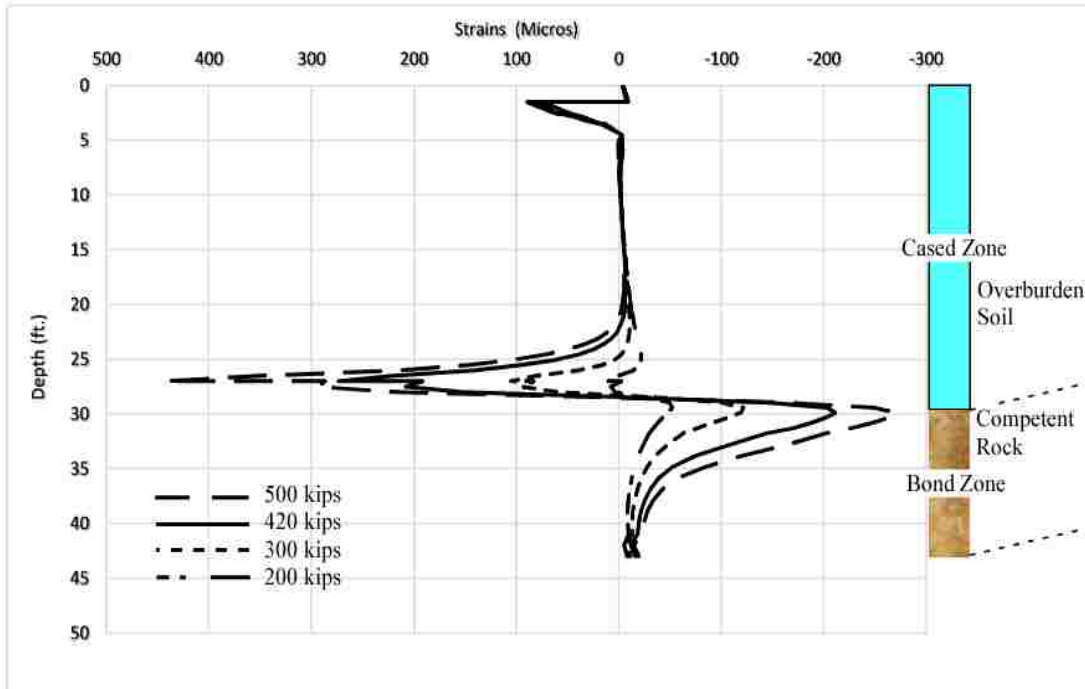
Figure 5.13. Vertical Strain of at Micropile No.1 Interface-Ground Side.
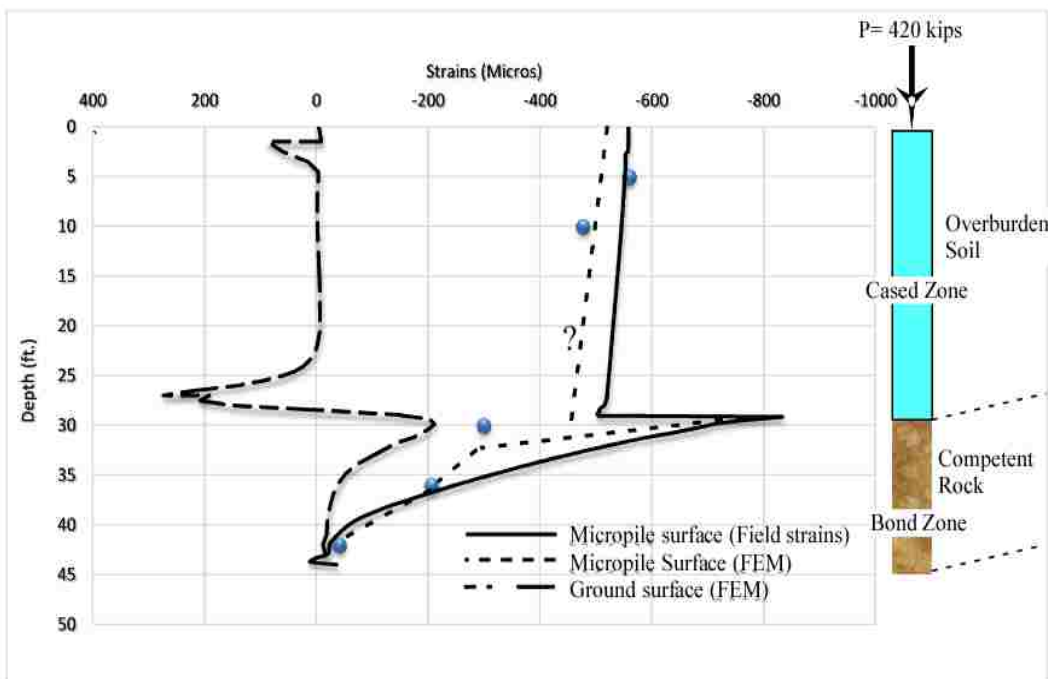
Figure 5.14. Vertical Strain at Micropile No.1's Interface-All Sections.

Therefore, in order for the ground to feel more strain; two important factors must be met;

1. The modulus of elasticity. If the modulus of elasticity is very high like this case study, the strain values will be small. For a completely rigid material will be zero. According to Hooke's law,

$\varepsilon = \sigma / E$ Eq 5.2

When increasing the modulus of elasticity, the strain becomes small.

2. Friction between ground and the micropile. If there is poor interaction due to the low friction between the micropile and ground, i.e. overburden soil, the strain will be very small even though the modulus of elasticity is very high.

The strain felt by the ground is very small. Ground feels the absence of the steel casing and respond by giving the micropile additional stresses. It starts then, transferring the load effectively in the bond zone. This also can be verified by the stress curve in Figure 5.15 which shows the amount of stresses felt by the soil.

Stresses values of the ground are negligible compared to the micropile due to the reason stated earlier in items 1 and 2 of the previous page. The stress read by the ground in the cased zone is close to the vertical geostatic stress due to the poor interaction of the micropile and the ground at that location. Thereafter, stress increases sharply and it stats to transfer the load to the ground. The stress will not be zero at the pile tip because it will read the vertical geostatic stress.
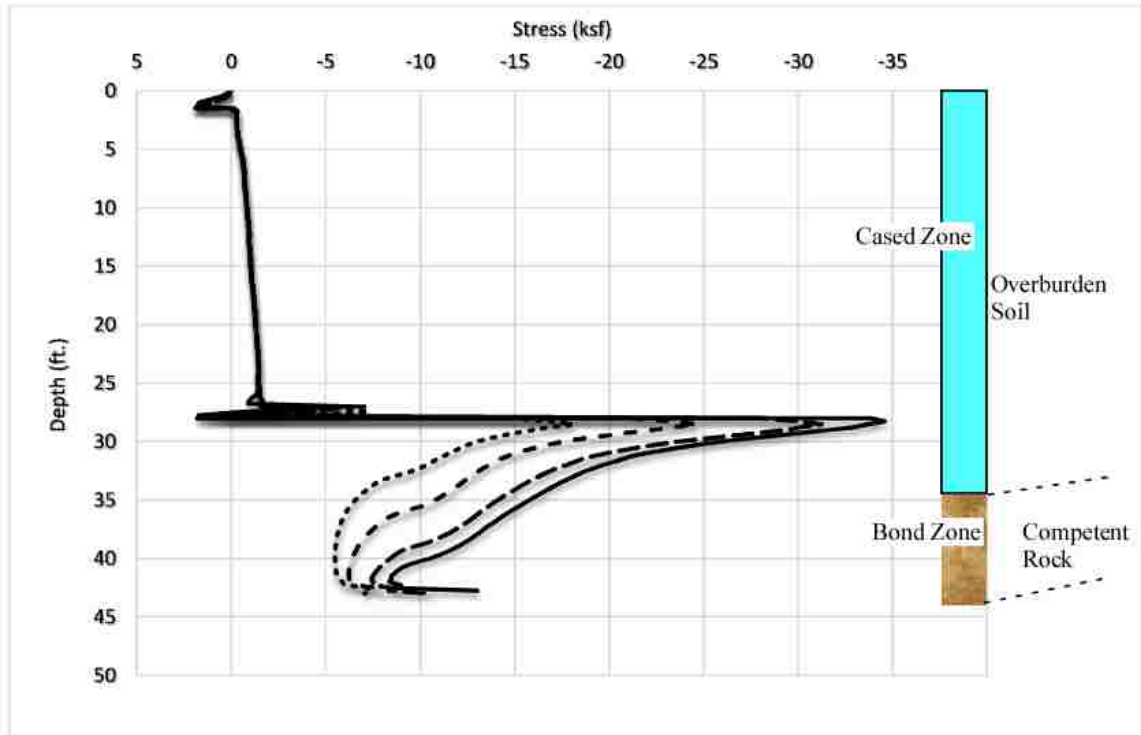
Figure 5.15. Vertical Stress of the Micropile No.1's Interface-Ground Side.

5.1.6.2 Ground performance at all locations. So far, the response of the ground and micropile at the interface was introduced in the two earlier sections. However, the performance of the ground at all other locations does have an equal importance. Therefore, the response of the ground at all other locations will be discussed here. Sections at distance of one diameter and two diameters from the interface are studied. Transverse sections across both, the micropile and the ground at different and critical locations will be presented as well.

5.1.6.2.1 <u>Performance along 1d and 2d from the interface.</u> Sections along 1d

and 2d are taken away from the interface as shown in Figure 5.16.
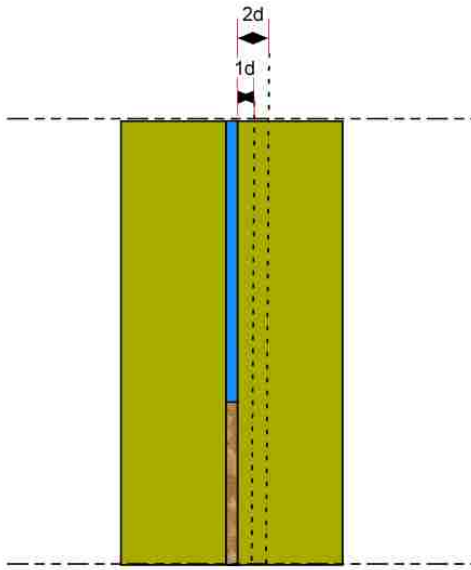
Figure 5.16. 1d and 2d Sections.

Figure 5.17 presents the strain in micros along 1d and 2d from the interface. As

shown, the strain at 1d from the interface is higher than 2d. At 2d, the ground strains is

almost negligible. To compare the strain at all locations, Figure 5.18 shows strains of the

interface including the micropile surface and ground surface. It also presents the strains at

1d and 2d away from the interface.
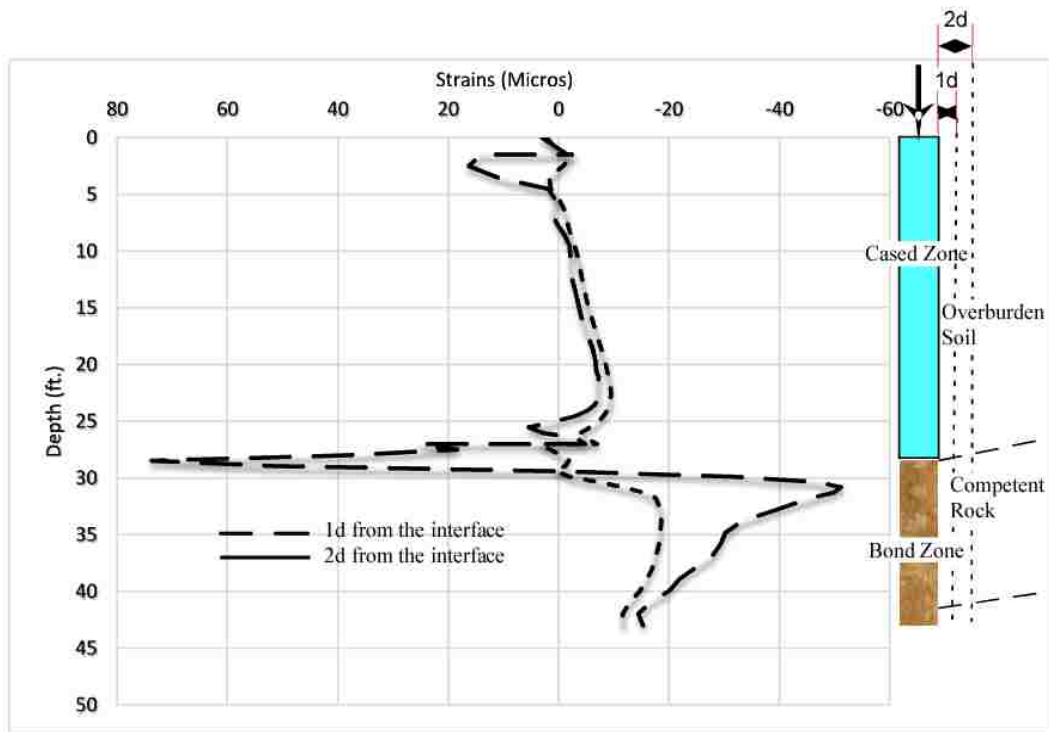
Figure 5.17. Vertical Strain along 1d and 2d of Micropile No.1.

As shown in Figure 5.18, The strain of the micropile surface along the interface is the highest among all others.

The gorund strain is 25% of the micropile strain at the interface. At 1d from the interface, the behavior is the same as the ground surface at the interface but with smaller amplitude. Therefore, it can be concluded that at distance greater than 2d from the interface, the strain becomes the ground geostatic strain.
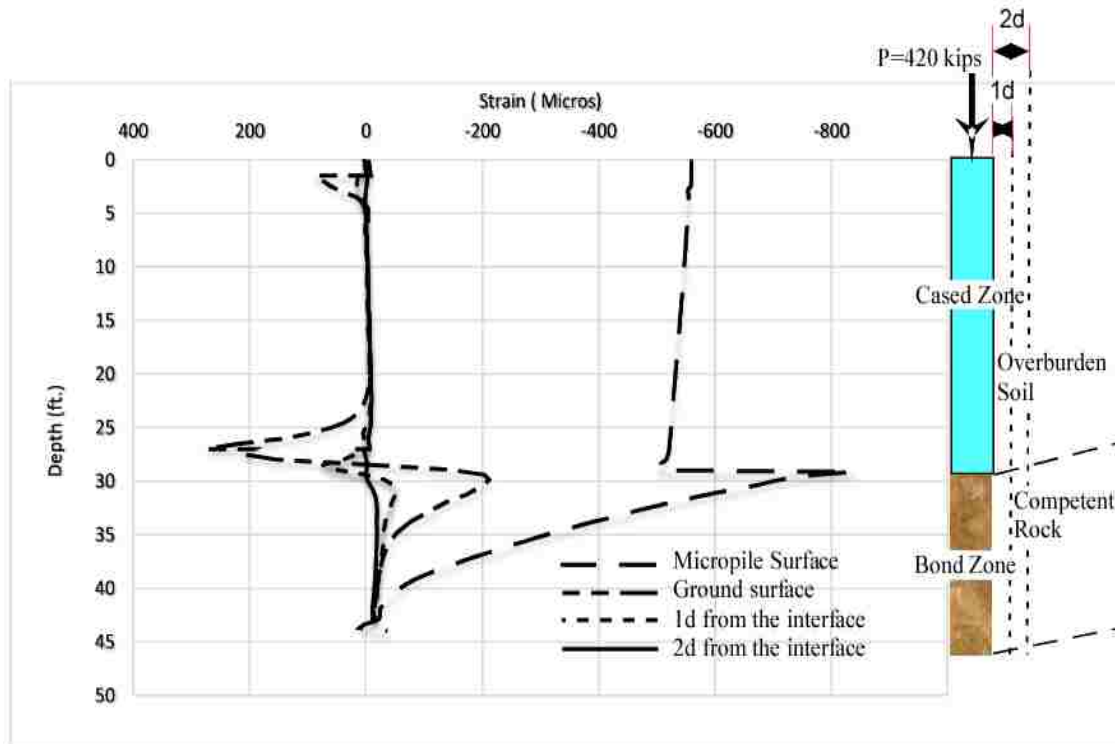
Figure 5.18. Vertical Strain of the Interface, 1d and 2d of Micropile No.1.

The stresse plot is also shown in Figure 5.19, 5.20. The ground vertical stress is considered to have small value at 1d away from the interface and it is negligable at 2d.

Since the interaction is weak at the cased zone, the stresses are the same as the geostatic stresses and the micropiles have negligible effect on the stresses. However, in the bond zone, the stresses transferred from the micropiles are added to the geostatic stress. At 2d, the vertical stress is very close to the geostatic stress.
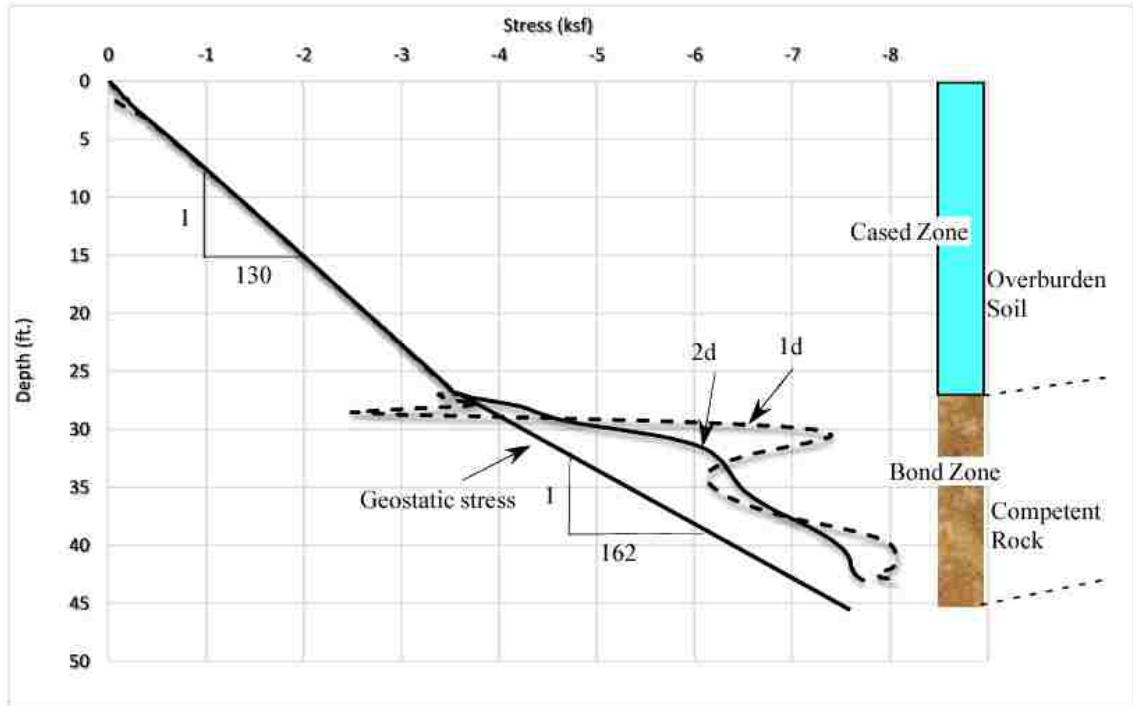
Figure 5.19. Stress at 1d, and 2d from the Interface.

The unit weight of the soil and rock are 130 and 162 psf, respectively. The slope of FEM solution matches the overburden soil unit weight. In the competent rock area, it is very close and converges to the geostatic stress.

Therefore, as the distance increases from the interface, the stresses becomes equal to the vertical effective stress as clearly shown at distance 2d from the micropile.

As shown in Figure 5.19 and Figure 5.20, all the stresses at 1d, 2d and ground surface of the interface do not exceed 6 ksf. However, they can be over 800 ksf at the micropile surface at the head of the micropile. They keep transferring stresses until it becomes equal the geostatic vertical stress.
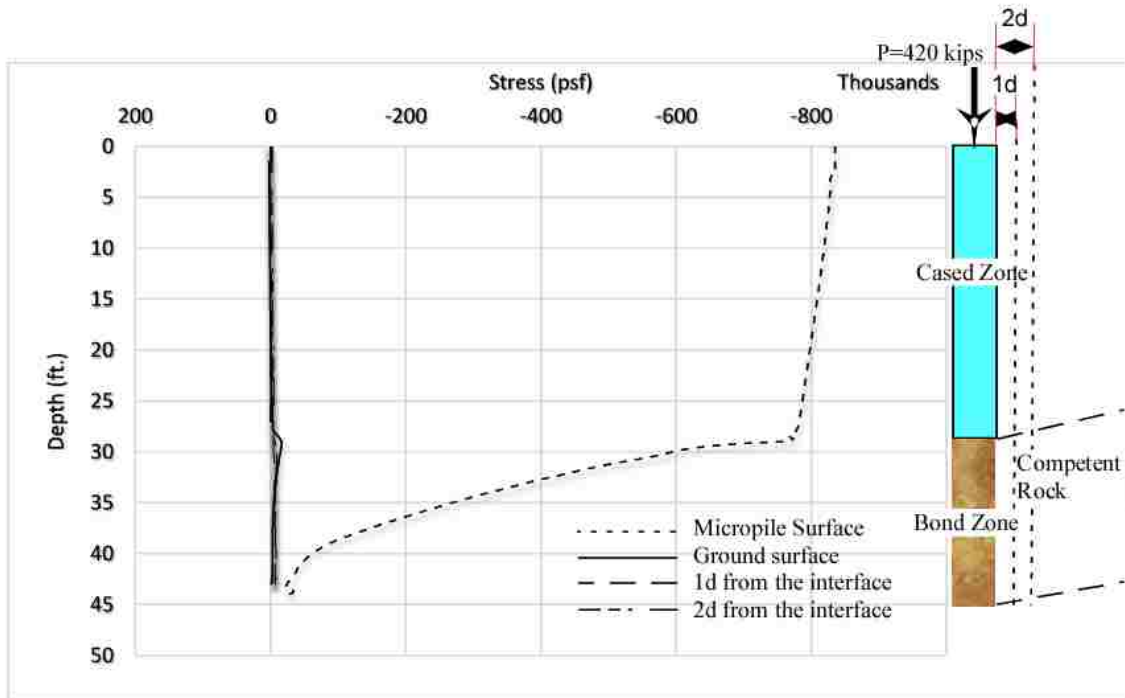
Figure 5.20.Vertical Strain at the Interface, 1d and 2d of Micropile No.1.

5.1.6.2.2 Performance at all other locations. In order to capture all the behavior

at all locations of the ground and the micropile; several transverse cross sections were

taken across the ground and the micropile as in shown in Table 5.4 and Figure 5.21.

Sections include the critical transition zones where the jump in the strains occur i.e., near

the case zone-bond zone boundary and rock-soil.

Table 5.4. Sections across Micropile No.1 and the Ground.

Section	Distance from the Micropile head	Ground
Section A-A	6.53	Soil
Section B-B	28.93	Soil
Section C-C	36.86	Rock
Section D-D	41.98	Rock
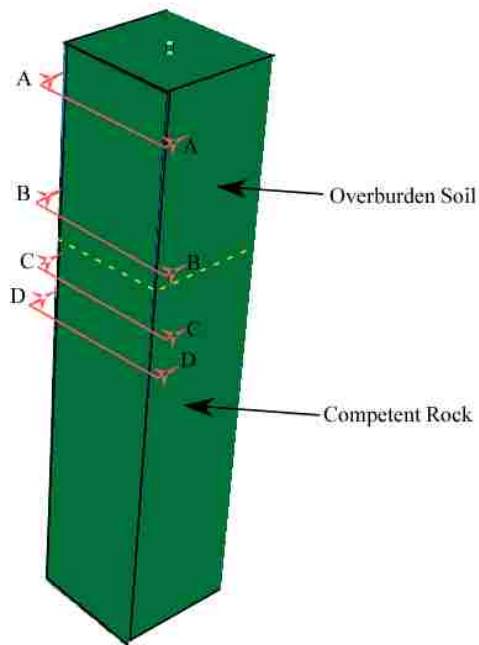
Figure 5.21. Sections across Micropile No.1's Model.

Figures 5.22 shows the vertical strain across the sections of Table 5.4 and Figure 5.22. The figure shows that section B-B has the largest strain which is expected, section B-B is located at the stress concentration area of the interaction where the transition between the cased and the bond zones occur.

Section A-A comes second because of the high load applied to the micropile. Section C-C and D-D have the least values of strains because they are located in the bond zone after significant load transfer was occurred.
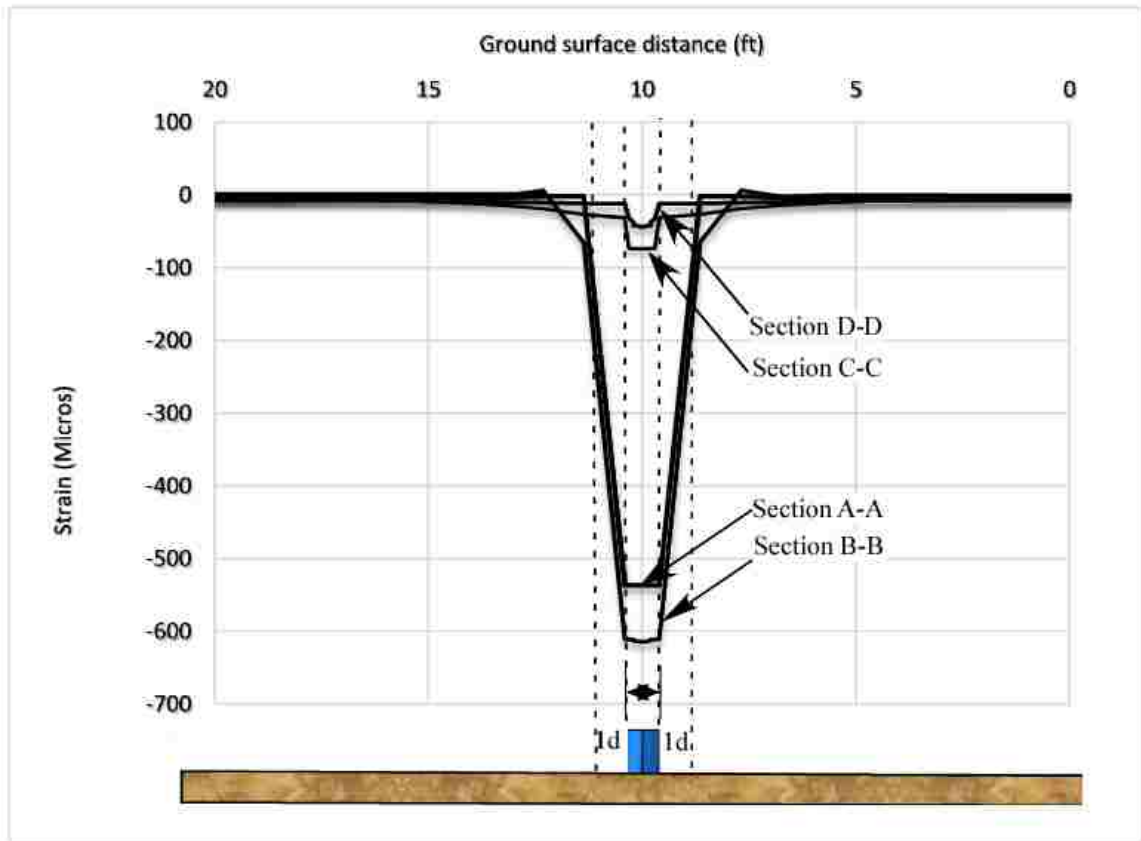
Figure 5.22. Vertical Strain across Sections of Micropile No.1's Model.

In addition, figures emphasize that the strains are negligible at distance 1d-2d from the interface. Small diameter of the micropile and the embedment in a high material modulus cause the deformations to be small. If there are Material A, B and C. Material, A, that is subjected to a load, P, and should transfer the load to materials B and C in separate situations. Material, B, has high modulus, but Material C has low modulus. Strain on material A will be transferred to material B according to the degree of bonding. The net strain developed on material, B, will be the amount of strain transferred from material A divided by the ratio of the relative modulus between the A and B. Since B

material has high modulus, the strain will be smaller by relative modulus, n, factor. The ratio, n, will be higher in the contact between A and B than A and C.

Overburden soil modulus relative to the micropile is 375/1 in the cased zone and 200/1 in the bond zone. But rock has a relative modulus of 375/25 in the cased zone and 200/25 in the bond zone. Therefore, if the strain received by overburden soil and the rock are equal, the strain in the competent rock will be (375/25)/ (375/1) i.e., lower 25 times, the relative modulus between soil and rock.

Figure 5.23 shows the stresses with depth for the same cross sections. The stresses are ordered according to their location which is unlike the strain. Therefore, section A-A has the highest stress due to its location as the closest to the load source, followed by section B-B , section C-C section and finally section D-D. Stress, load and displacement will always be ordered, in this particular example, according to their location and distance to the load source. However, the strain is different because of the transition in the stiffness that increases the strain of the micropile sharply at a certain location.

However, for load, stresses, and displacement, they will decrease as the distance increases from the load source.
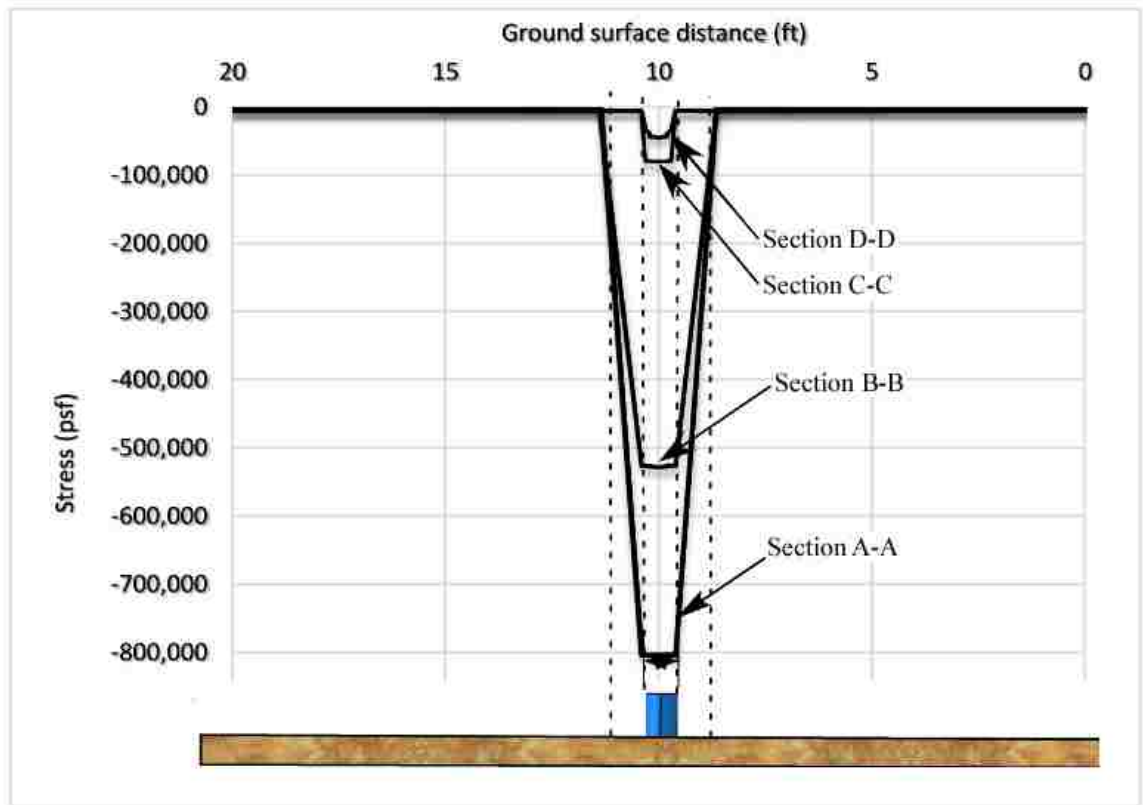
Figure 5.23. Vertical Strain across Sections of Micropile No.1's Model.

5.2. NUMERICAL MODELLING OF MICROPILE NO.16

Micropile No.16 is representative of the long micropiles in Pier No.1 and Pier No.2. Long micropiles have an intermediate layer with intermediate stiffness values. Micropile No.16 has weathered rock consisted of weathered Metaconglomerate and Metasandstone. Micropile No. 16 carries lower load than Micropile No.1 due to long distance to the competent rock down in the ground. Micropile No.1 is closer to the load source and therefore carries higher load. In this section, numerical modelling of micropile No.16 will be presented as well as the modelling techniques and assumptions.

5.2.1. Subsurface Conditions and Location. Micropile No.16 is mounted in different topography including overburden soil, weathered rock and competent rock. The stratigraphy shown in Figure 5.24 of Micropile No.16 is characterized as follows:

1. 0'- 6' is the concrete platform which had provided level topography for the constructed pier.

2. 6'-50' is the overburden soil layer which has 50% gravel, sand and silt.

3. 50'-70' is the weathered rock which has intermediate stiffness value.

4. Lower than 70' is the competent rock layer which has very high RQD with high recovery.
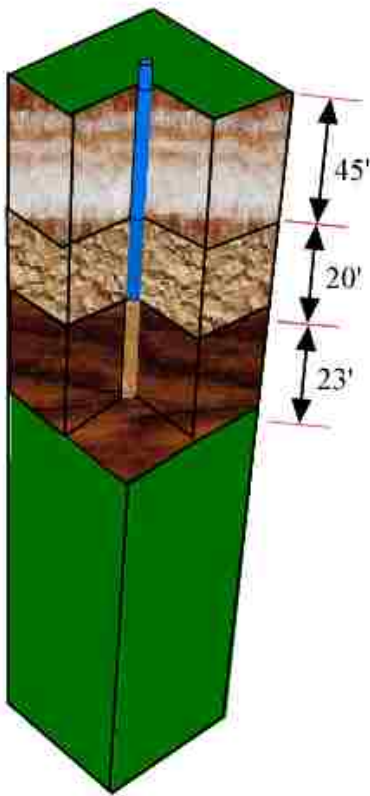
Figure 5.24. Micropile No.16's Subsurface Characterization.

The location of Micropile No.16 within other micropiles is shown in Figure 5.25.

Location of the micropile in the embedment length is also shown in Figure 5.26.

Legend
Red: Rock, Yellow: Weathered Rock, Green: Overburden Soil, Brown: Concrete, Blue: Water Table
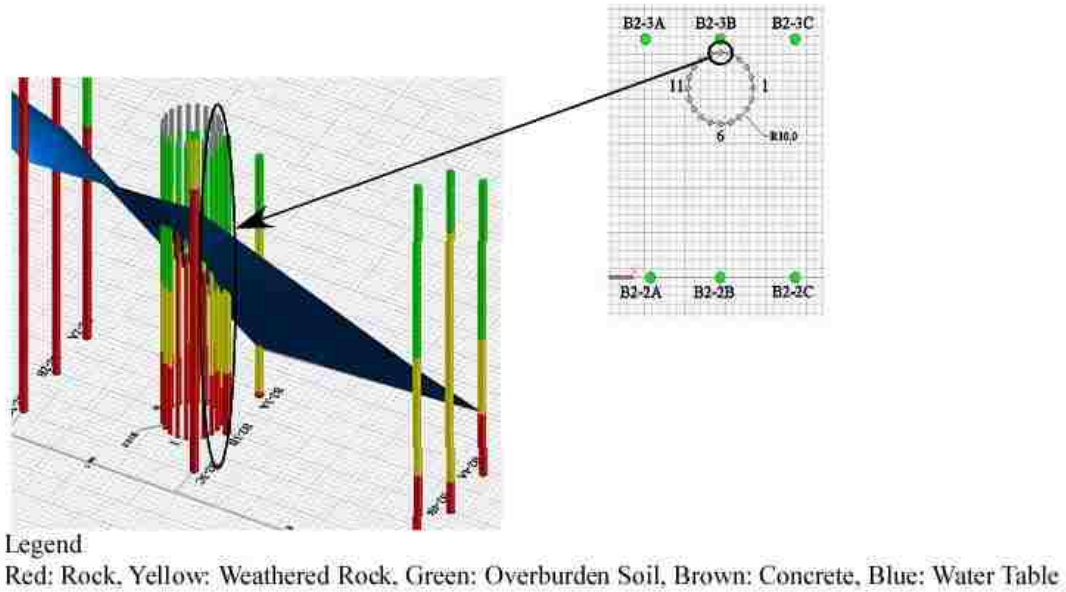
Figure 5.25. Subsurface Conditions of Pier No.1.
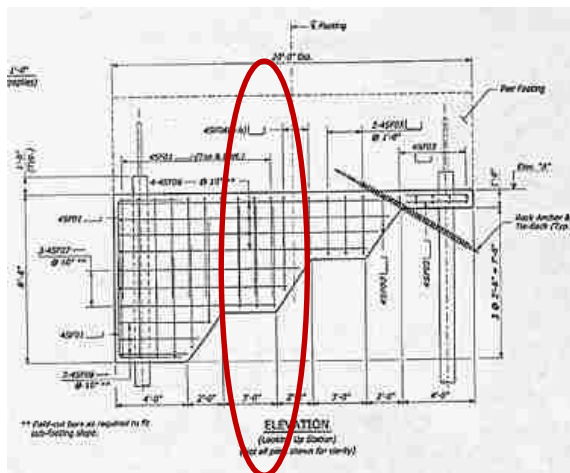
Figure 5.26. Micropile No.16 as Located in the Drilled Platform.

5.2.2. Model Definition. The modelling approach is similar to Micropile No.1. Therefore, a general and short definition of the model numerical approach will be provided.

1. Model Geometry: size of the model is 20'X20'X200' which is larger than Micropile No.1 because Micropile No. 16 is longer. Parameters of the Mohr coulomb constitutive model for micropile No. 16 are shown in Table 5.5. The parameters were explained earlier in Section 4.2.

Table 5.5. Ground Parameters of Micropile No.16.

Depth (ft)	Soil/Rock	E (psf)	γ	P (psf)	ϕ (°)	ψ (°)	C (psf)
0-6	Concrete Platform	580,393	0.3	150	-	-	-
6-30	Overburden Soil I	3,000	0.3	130	35	5	50
30-50	Overburden Soil II	5,000	0.3	130	35	5	50
50-70	Weathered Rock	52,225	0.3	155	30	5	2100
71-100	Competent Rock I	104,450	0.3	162	30	5	2100
100-200	Competent Rock II	208,900	0.3	162	30	5	2100

The micropile diameter is 0.802', two different axial stiffness were defined to account for discontinuity of the material properties as discussed earlier.

2. Interaction Properties: Contact mechanism for this micropile is shown in Figure 5.27. The contact algorithm was explained earlier in Section 4.3. A "Hard" normal contact and "Penalty" tangential coulomb friction. Separation was not allowed after contact in the bond zone.
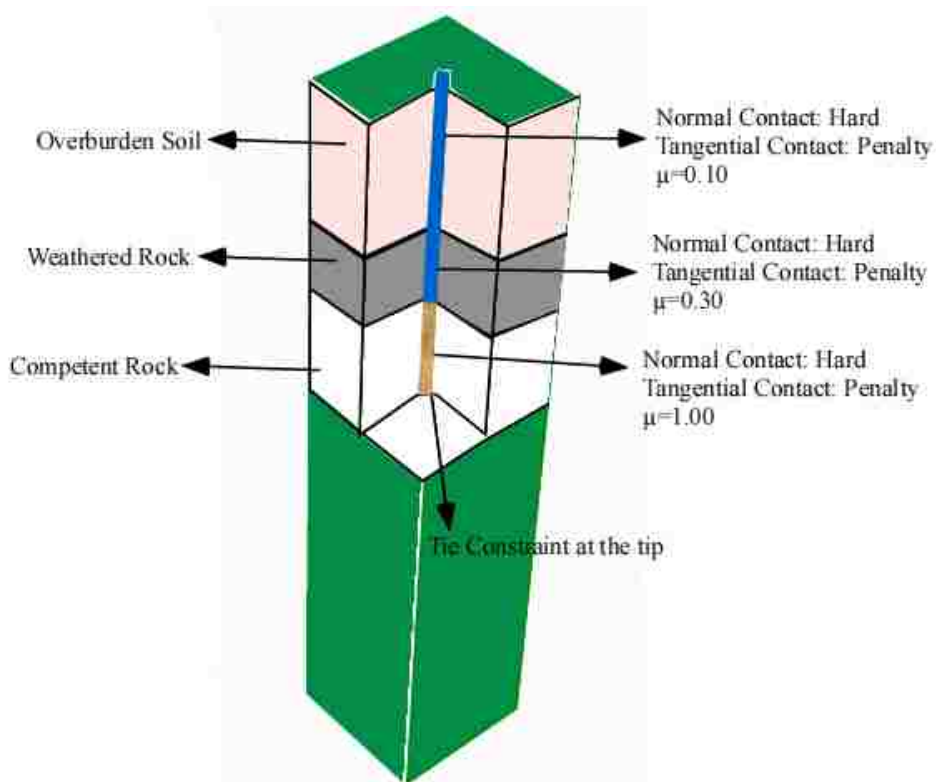
Figure 5.27. Interaction Components of Micropile No.16.

3. Loading conditions and boundary constraints: The load was applied in two step; geostatic step to eliminate the initial displacement of the initial stresses applied by the body force or gravity. This step ensures the initial equilibrium of the model. The second step applies the structure load of the bridge using a static step. Transient step was not used due to quick dissipation of water. This also implies the couple analysis of pore water pressure with stress is not needed.   The load calculated by the first strain reading of the strain gauge is 187 kips as shown in Table 5.6. Therefore, 100 kips to 250 kips loading conditions will be applied to study the performance of Micropile No.16.

Table 5.6. Strain Gages Reading of Micropile No.16.

Depth (ft)	Strain (Micros)	Load (kips)
8	-248.038	-187.19986
13	-201.782	-152.28942
58	-132.888	-100.29356
80	-17.052	-5.5446994
90	19.698	6.40508374

4. Element type and Mesh design: C3D8 elements with reduced integration were used. Mesh convergence study was conducted to ensure the accuracy of the results. The mesh is sensitive in certain locations only. The analysis and the location may need refinement as necessary. Mesh sensitivity analysis is shown at the end of this section.

5.2.3. Mesh Convergence Study. Similar to Micropile No.1, mesh was refined until the results were within few percent as shown in the Figure 5.28. The mesh element size was reduced by half each time, Mesh 1 is the coarsest; 1'X1'X1'. Mesh No.2 is 0.5'X0.5'X0.5' and Mesh No.3 is 0.25'X0.25'X0.25'. Some areas were kept finer more than others areas of the model because of the relative sensitivity to mesh size.
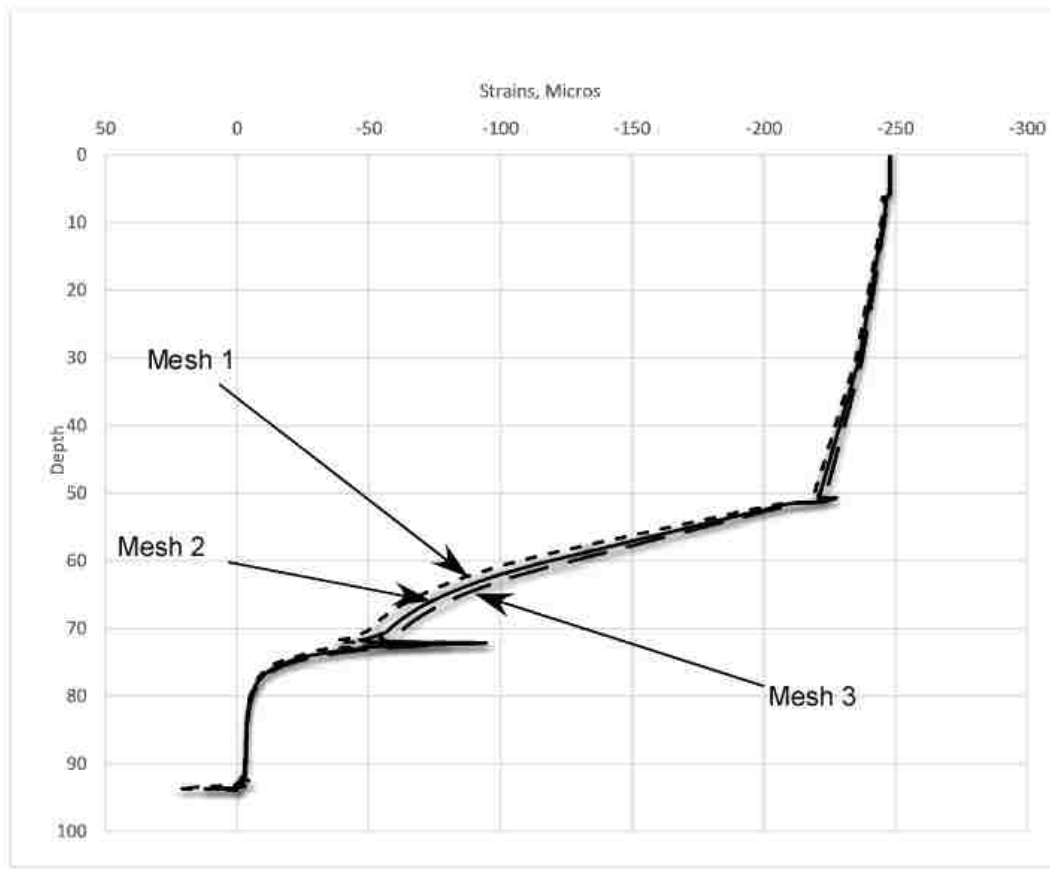
Figure 5.28. Strain with Different Mesh Sizes of Micropile No.16's Model.

5.2.4. Numerical Analysis of Micropile No.16. After building the numerical model of Micropile No.16, all jobs of the models were submitted. Each job needed many hours of computation for single pile analyses. In this section, numerical modelling results and analysis of Micropile No.16 will be presented including the ground and the micropile at the interface as well as the rest of the ground at all locations of the model.

5.2.4.1 Behavior at the interface. In this section, the results along the interface that connects the micropile with the ground will be presented. The interface is not fully understood and it was always an issue. This numerical model attempts to explain the load transfer mechanism at the interface. The results will be supported by field results that verify the performance obtained by FEM.

5.2.4.1.1 <u>Micropile performance at the interface.</u> The interface comprises the exterior surface of the micropile and the interior surface of the soil. In this section, the response of the micropile due to different loading conditions will be explained.

Figure 5.29 shows that the overburden soil transfers a little load, but the weathered rock transfers a considerable amount of load even with low assigned friction of 0.3. It is also clear that the stress/strain concentration is lower than Micropile No.1 due to the lower relative modulus between competent and weathered rock. The estimated load to match the field is 160-180 kips.

It can be concluded that the micropile with intermediate layer that has relatively some stiffness can carry most of the load with small friction. The longer the layer, the more efficient it would be. The competent rock has insignificant impact in the load transfer mechanism, but it will serve as additional caution if higher load is applied over the structure.
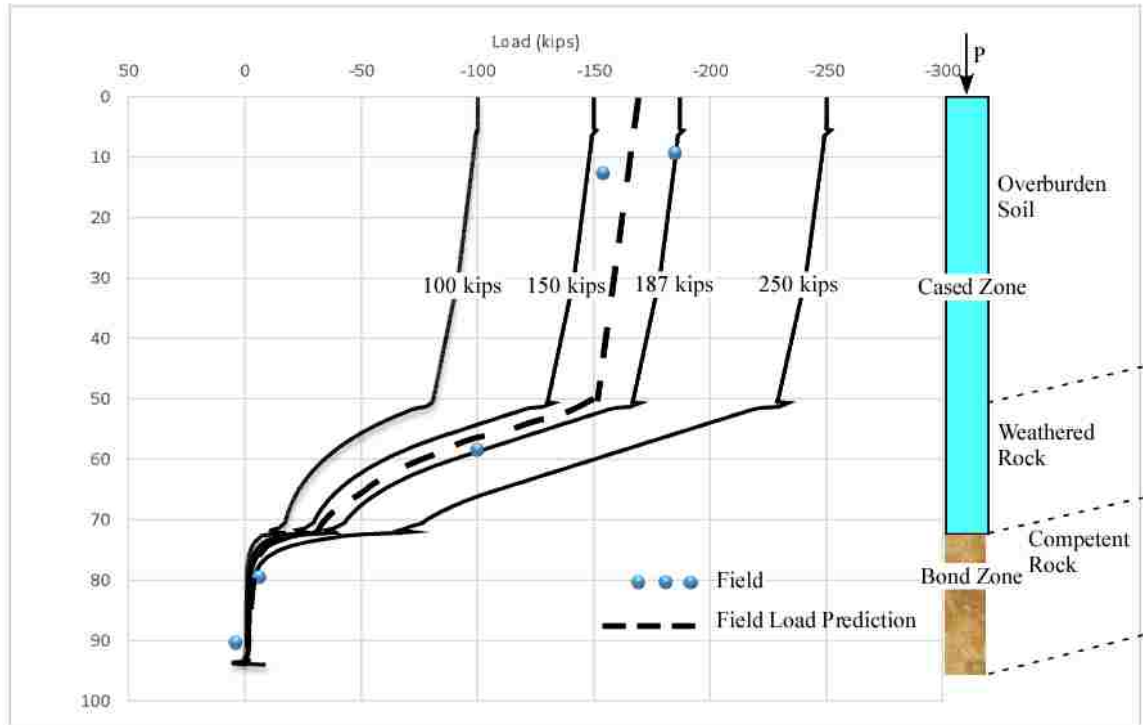
Figure 5.29. Micropile No.16's Load Transfer.

Figure 5.30 shows the strain readings along the micropile at the interface. Positive readings were observed at the very end of the micropile, this suggests that when complete transfer happen to the load, then the micropile is no longer carry axial load and therefor the confined stresses tend to push the micropile causing some positive readings. This happens at the last few feet because it is close to the end of the micropile. This issue will be addressed well in the next section since more positive readings occurs in the parametric study.
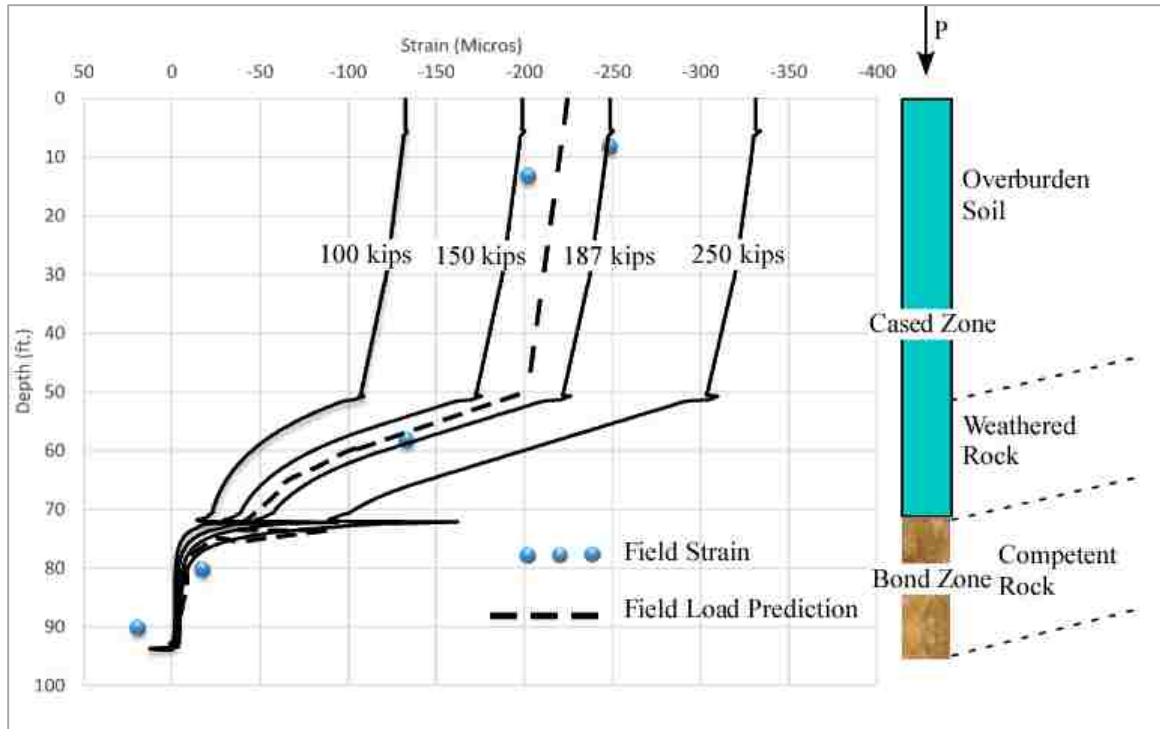
Figure 5.30. Vertical Strain at Micropile No. 16's Interface-Micropile Side.

Figure 5.31 presents the stresses of the micropiles. Most of the stresses carried by the micropiles are transferred in the weathered rock.
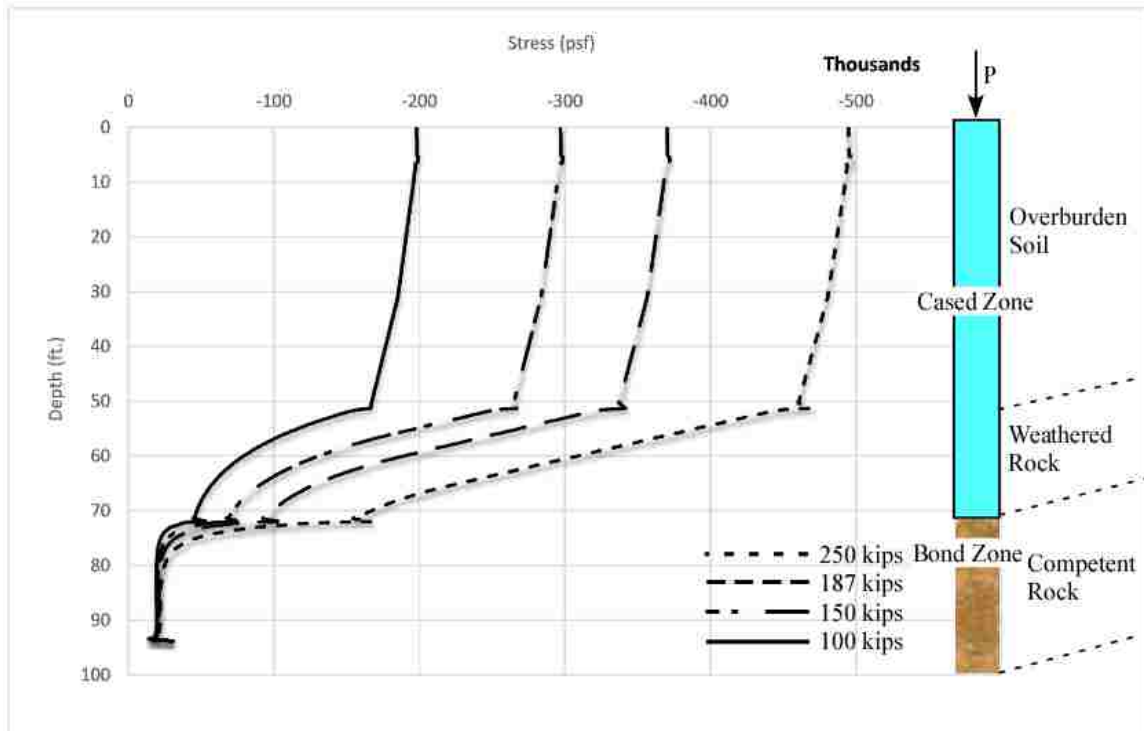
Figure 5.31. Vertical Stress at Micropile No.16 Interface-Ground Side.

5.2.4.1.2 Soil & rock performance at the interface. Figure 5.32 presents the

strains of the ground at the interface due to different loading conditions. Mesh refinement

of the model did not have significant impact on the strain values at these locations.
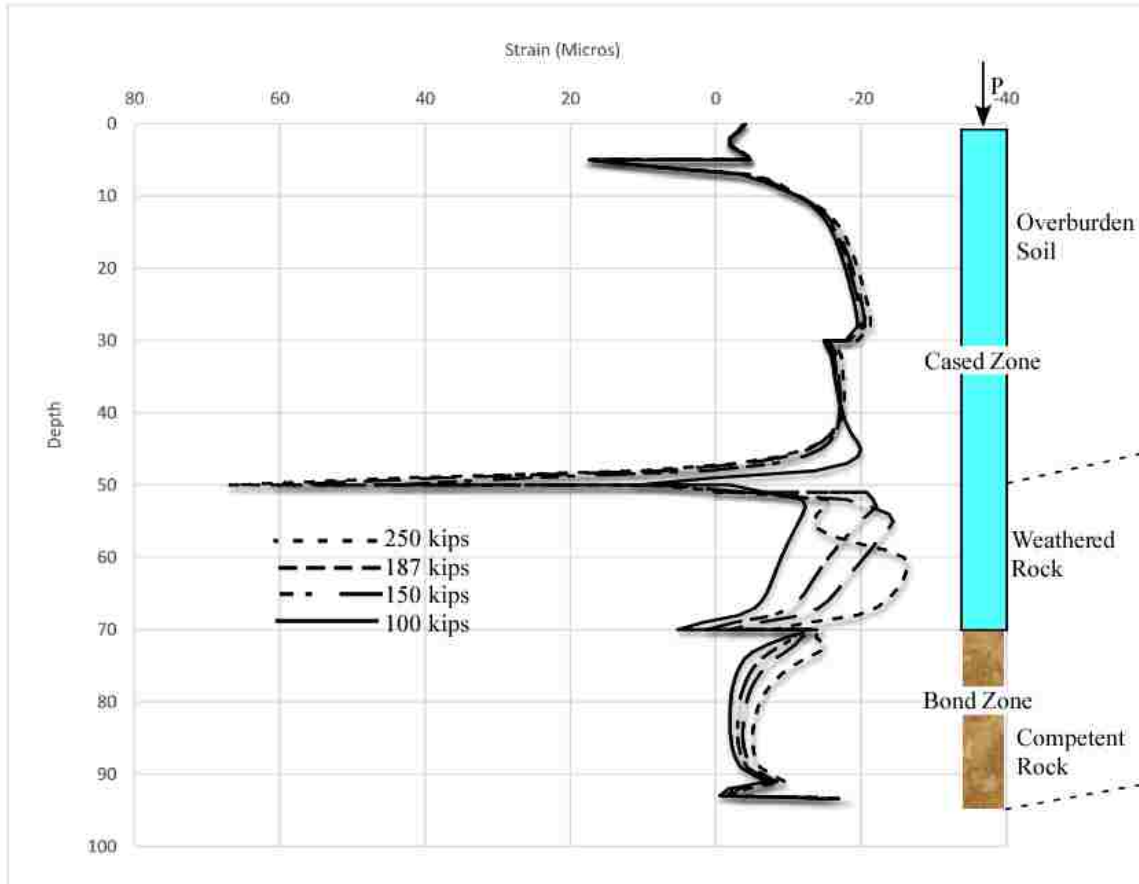
Figure 5.32. Vertical Strain at Micropile No.16's Interface-Ground Side.

The stresses of the ground are shown in Figure 5.33. At the overburden soil, the figure shows the vertical stress of the ground is close to the geostatic stress at that location. It gets additional stress in the weathered rock since most of the load transfer occurs at that location. In the bond zone, vertical stress increases due to the geostatic stress.
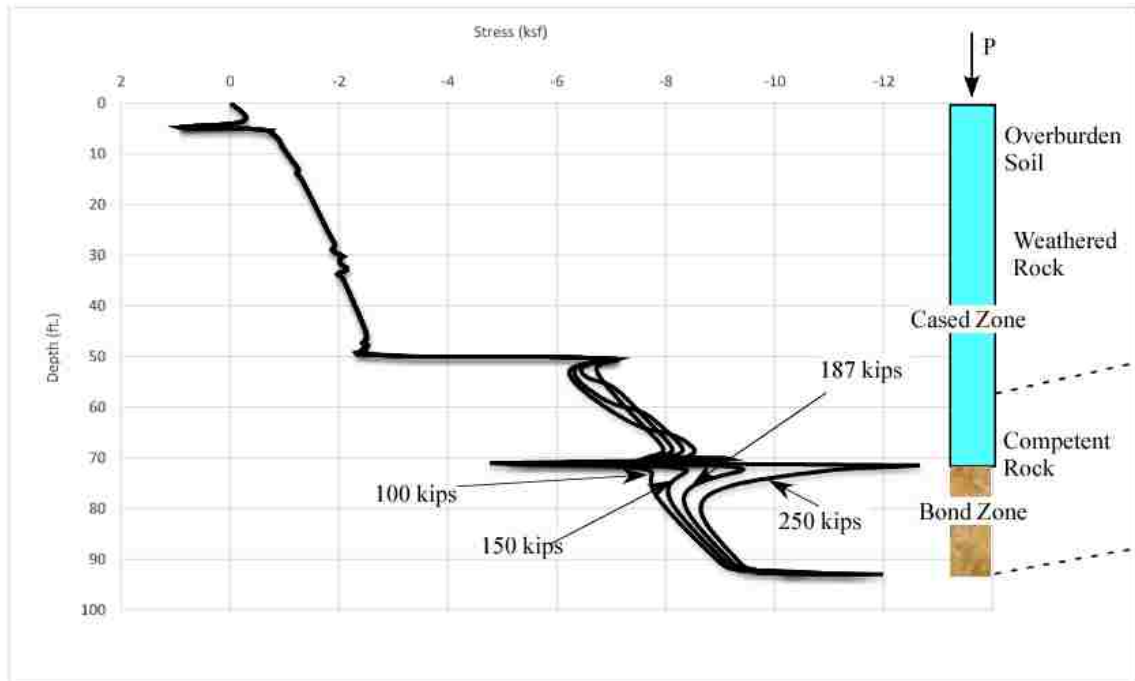
Figure 5.33. Vertical Stress at Micropile No.16's Surface-Ground Side.

The comparison of the strains at the interface between the micropile surface and the ground is shown in Figure 5.34. The arrows length indicates the amount of load needs to be transferred. As shown in the figure, the strains of the ground is small relative to the micropile.

The strains of both, the ground and the micropile, are negligible in the bond zones which indicates that all load was transferred in previous layers. The line with question mark indicates a closer estimate for the strains of the micropile using field data based on the same behavior of the FEM. Additional strain gage in the middle would have helped to ensure the accuracy of this fit.
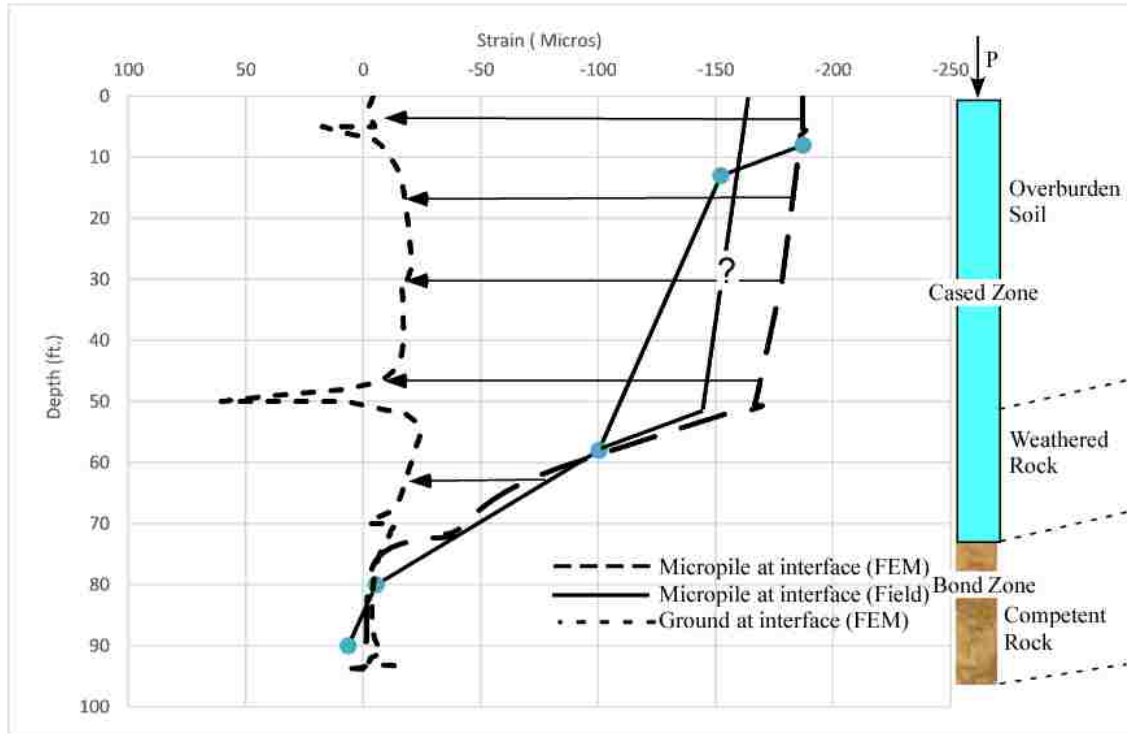
Figure 5.34. Vertical Strain at Micropile No.16's Interface-All Sections.

5.2.4.2 Ground performance at all locations. This section discusses the response of the ground of the entire model. Sections at distance of one diameter and two diameters from the interface are studied. Transverse sections across both, the micropile and the ground at different and critical locations will be presented as well.

5.2.4.2.1 <u>Performance along 1d & 2d from the interface.</u> The strain along the micropile and the ground at the interface, 1d and 2d from away from the interface are shown in Figure 5.35.
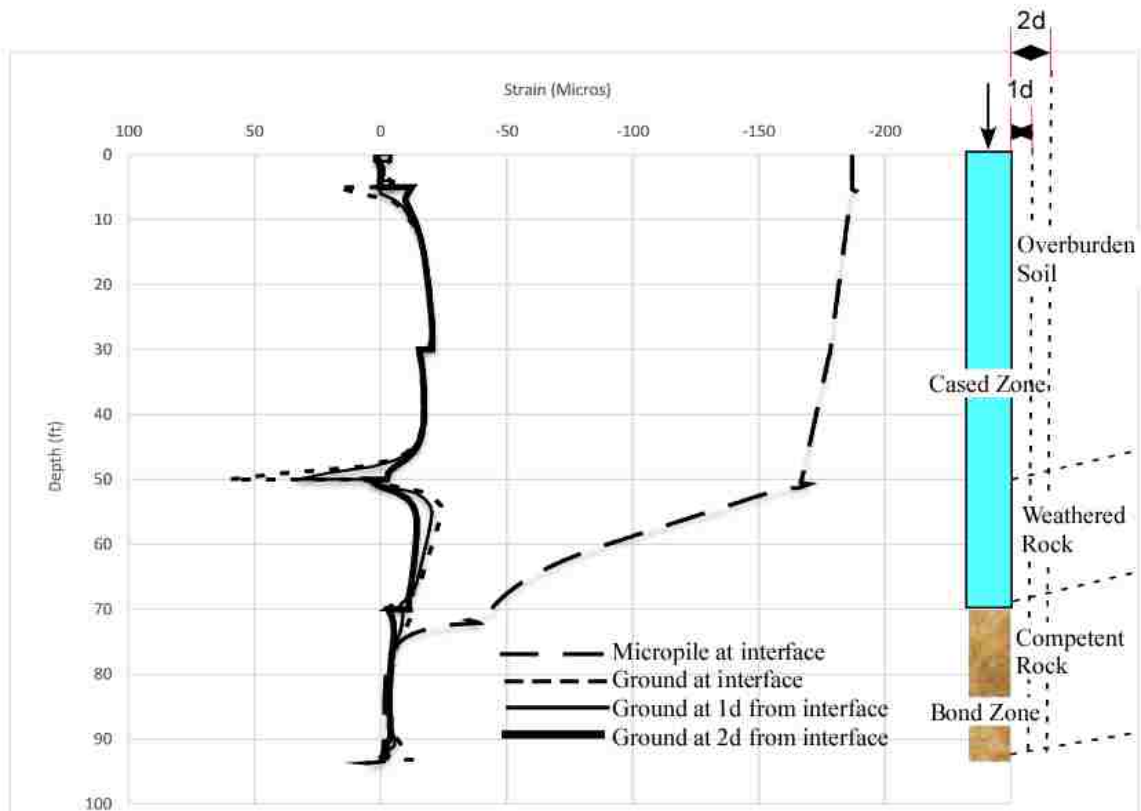
Figure 5.35. Vertical Strain of the Interface, 1d and 2d of Micropile No.16.

As shown in Figure 5.35, the strain of the ground at all locations including the interface is very small. This is because of the low friction in the cased zone as well as the high modulus in the bond zone as was explained earlier in Micropile No.1 analysis.

Figure 5.36 show the stresses of the ground at the interface, 1d and 2d. The stresses initially show increase due to the geostatic vertical stress. In the weathered rock, the micropile gives an additional stress to the ground as most of the load is transferred in that region.
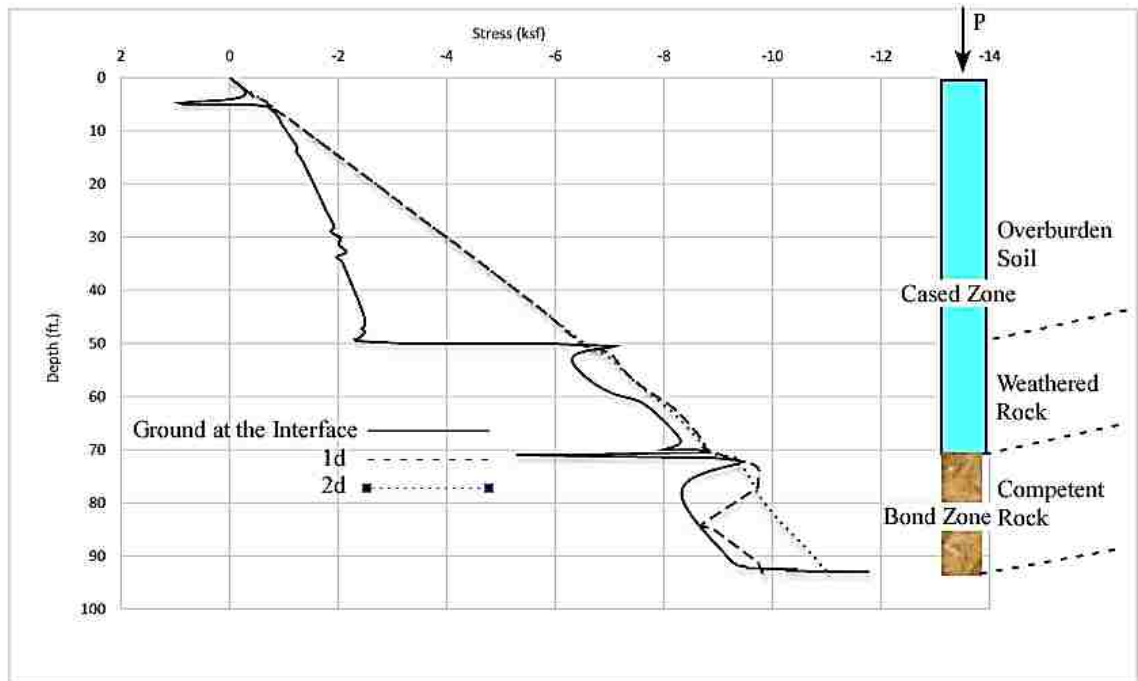
Figure 5.36. Vertical Stress of the Interface, 1d and 2d of Micropile No.16.

The stress at 2d is the closest to the vertical geostatic stress. However, all the ground stresses at all locations are negligible relative to the micropile as shown in Figure 5.37. This indicates that the transfer of the stresses has small effect on the ground stresses.

The three lines at the ground interface, 1d and 2d sections are appointed by the left arrow. They are shown on the curve as one line due to their negligible difference relative each other and to micropile stresses.
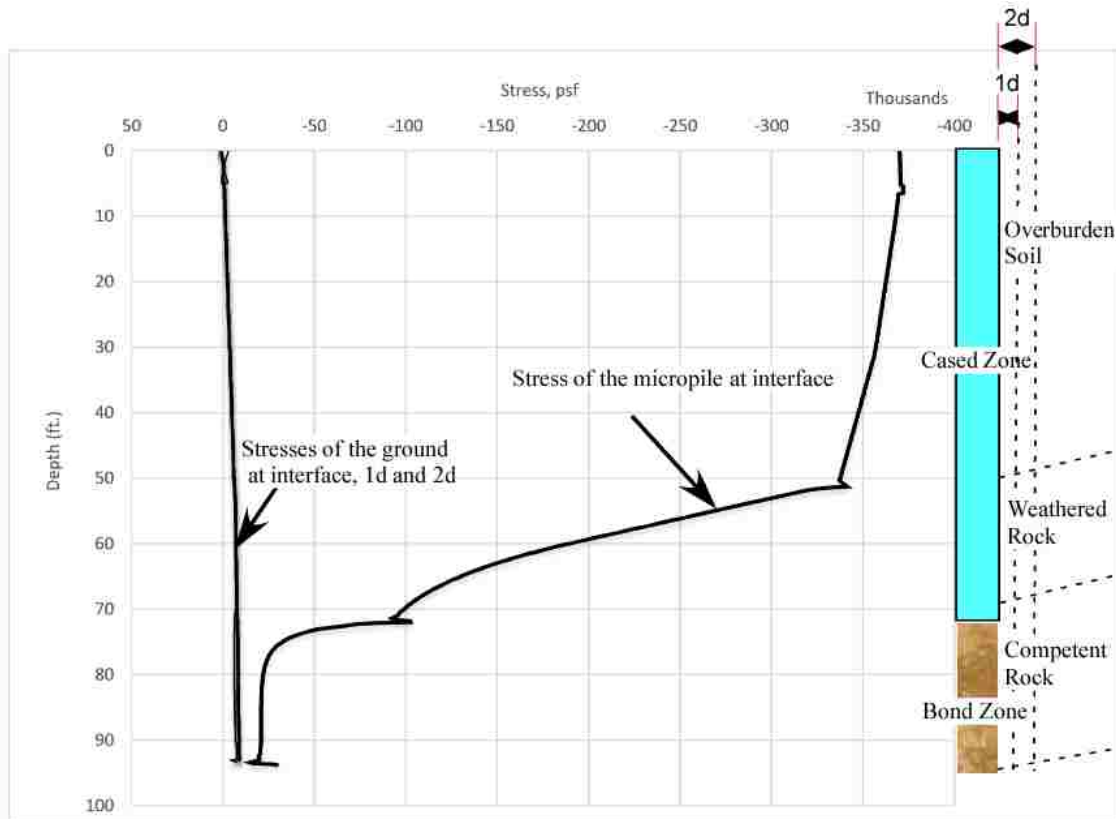
Figure 5.37. Vertical Stress of the Interface, 1d and 2d of Micropile No.16.

5.2.4.2.2 Ground performance at all locations. In order to capture all the

behavior at all locations of the ground and the micropile; seven traverse sections were

taken across the ground and the micropile as listed in Table 5.7 and shown in Figure 5.38.

Table 5.7. Sections across the Micropile and Ground.

Section	Distance from the Micropile head	Ground
Section A-A	35'	Overburden Soil
Section B-B	49'	Overburden Soil
Section C-C	70'	Weathered Rock
Section D-D	82'	Competent Rock
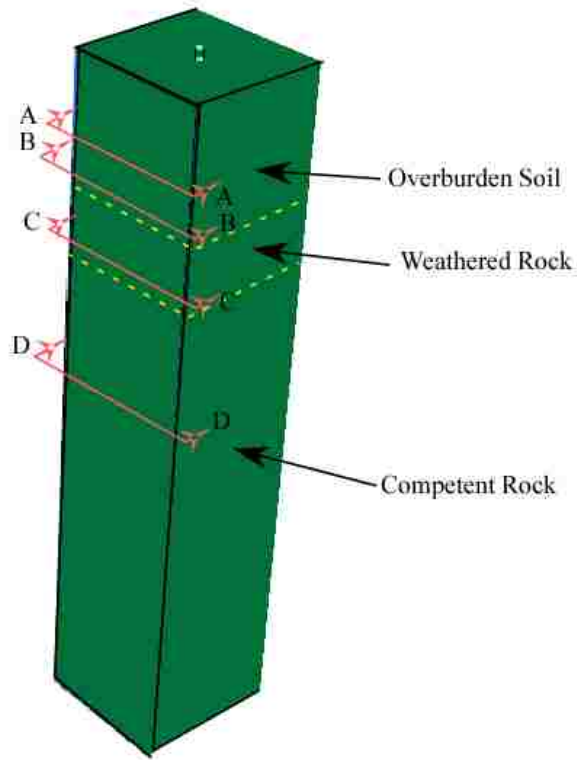
Figure 5.38. Sections across Micropile No.16's Model.

Section B-B and C-C are taken 1' before the dramatic change in the strains due to change in the ground characterization. Vertical strain and stress at Sections A-A through D-D are shown in Figures 5.39 and 5.40.
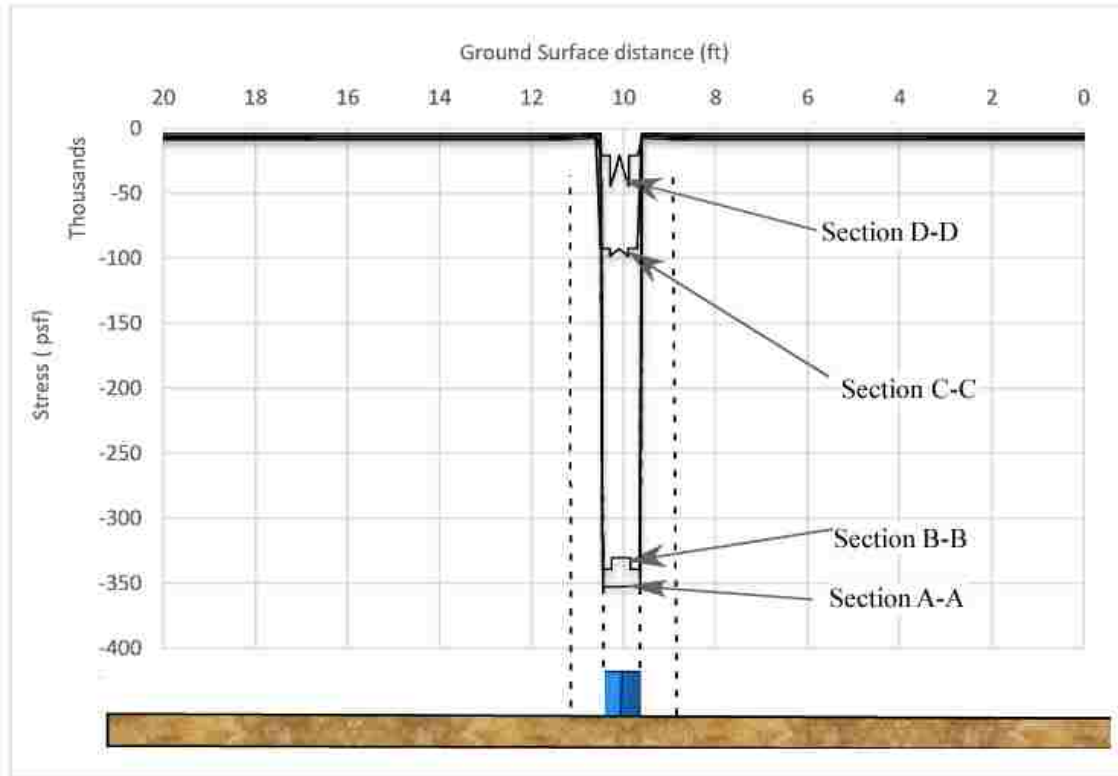
Figure 5.39. Vertical Stress across Sections of Micropile No.16's Model.

The vertical stress of the ground is considered as negligible relative to the micropile. The maximum stresses are the micropile stresses. However, the ground reads small stresses due to the geostatic stresses.
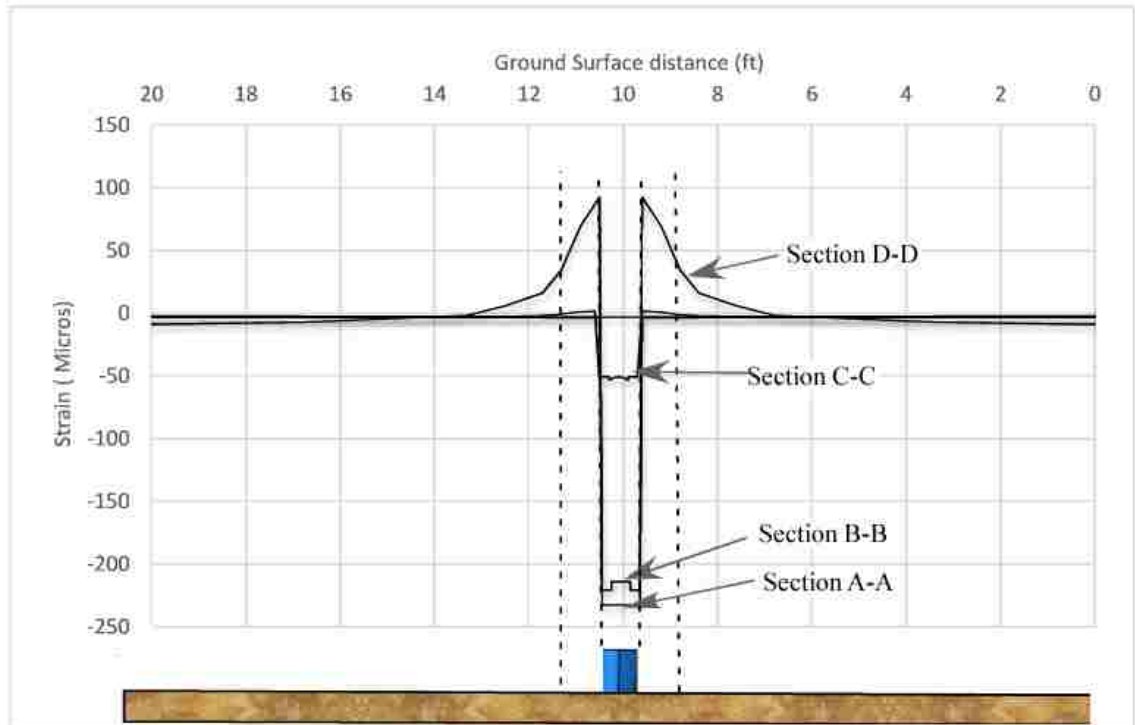
Figure 5.40. Vertical Strain across Sections of Micropile No.16's Model.

The strains across the model shows that the maximum strains belong to the micropile and they are constant along its section. The ground strains show small strains in most of the sections except at D-D. Section D-D reads positive strain because of the change in the stiffness from the weathered to competent rock, 8E to 25E, where E is the modulus of the overburden soil.

6. GROUP ANALYSIS OF BRIDGE NO.2's MICROPILES

Deep foundations with group effect may lower the capacity of the micropile relative its single behavior. This is due to interaction of the micropiles' stresses together. Exceeding a certain distance between any two micropiles, the group effect is no longer existed and the micropile will behave as a single pile.

The single behavior of the micropiles located in Pier No.1 and Pier No.2 was presented. Micropile No.1 and Micropile No.16 were taken as case studies for a short and long micropile, respectively.

Pier No.1 and No.2 consist of 20 micropiles with a 5' depth pile cap. The 20 micropiles are arranged circularly within the cap as shown in Figure 6.1.
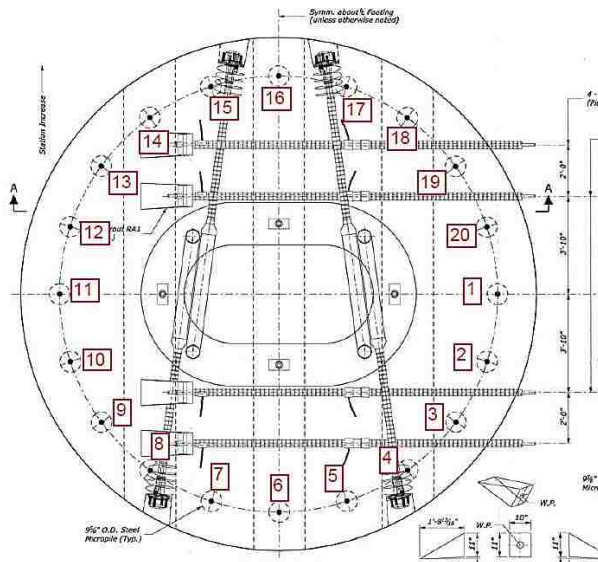
Figure 6.1. Cross Section of Pier No.1.

The distance is circumference of 17' diameter divided by 20 micropiles, this gives a value of 3.15. S/D is, therefore, equals to 3.90.

If Micropile No.16 is taken as an example as shown in Figure 6.2, it will be effected by the adjacent two; Micropiles No.16 and No.17 which they are the closest. It's so unlikely that Micropile No.16 will be affected by any other micropile. This assumption can be verified with the analysis of three micropiles; No.15, No. 16 and No.17. If there is no/little group effect by the adjacent two then, there is no group effect by the others.
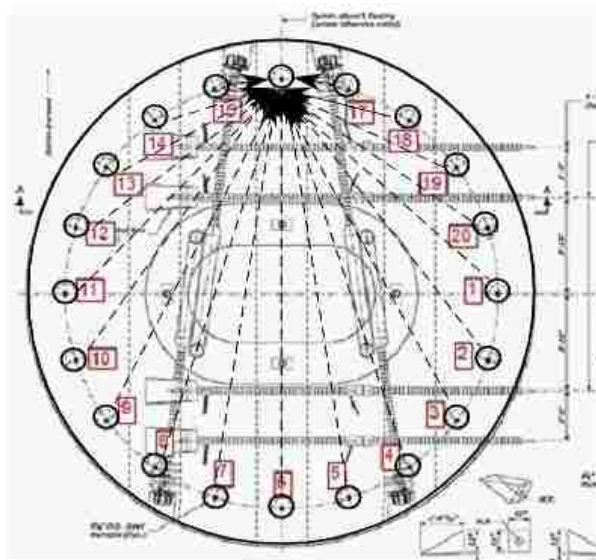
Figure 6.2. Micropile No.16's Group Effect.

In this section, Micropile No.1 and Micropile No.16 will be modelled within a group of the other two adjacent Micropiles without a pile cap. Next, Micropile No.16 will

modelled within the adjacent two micropiles with a pile cap. Lastly, Pier No.2 will be modelled with all micropiles.

6.1. INTERACTION OF MICROPILES (WITHOUT PILE CAP)

The model consists of three micropiles placed within S/D of 3.9.The material was assigned as indicated in the previous sections. Model width and depth were selected to be 30D and 2L of the micropiles, D is the micropile's diameter and L is the length. Analysis consists of two steps, geostatic step to establish the initial stresses equilibrium, and static step that include the load applied over the micropile surface. Model was meshed using C3D8R element type to account for the continuum soil nature. Ground layers were modelled using Mohr coulomb failure criterion and the pile as elastic model.

6.1.1. Analysis of Micropile No.16. Micropile No.16 was placed within the two adjacent micropiles No.15 and No.17. All three micropiles - have similar characteristics which is unlike Micropile No.1 and its two adjacent micropiles i.e. No.20 and No.2. Therefore, there will be three identical micropiles. The model definition was explained for the multi-micropiles interaction in the previous section.

The results of the analysis showed that all the three adjacent micropile have the response as appears from the strain values shown in Figure 6.3. Since all micropile reads same values that means the group effect is negligible. If the micropiles at the sides; Micropile No.15 and No.17 are different than No.16, that means there is group effect because it is supposed that the middle one should be affected most by the group behavior.

This leads to a conclusion that, the small difference which is negligible is due to the change in the mesh configuration at that location. Thus, strains and stresses will be identical.
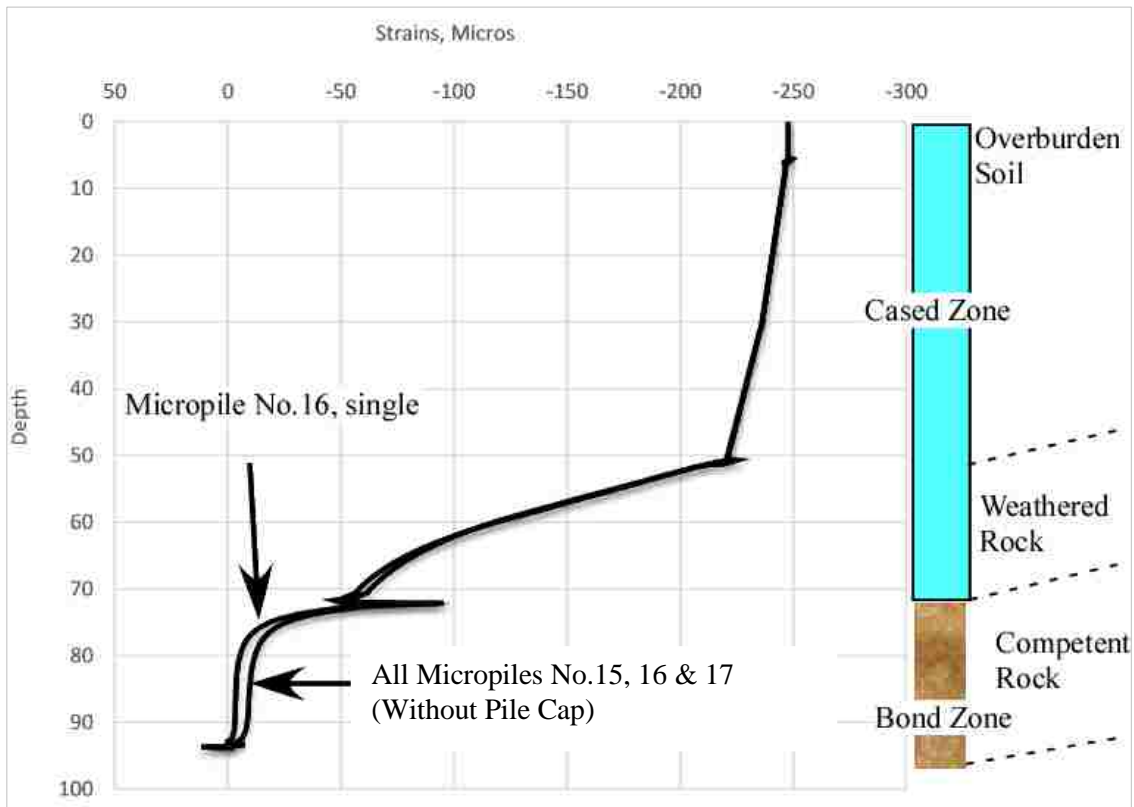
Figure 6.3. Single and Group Performance of Micropile No.16 (Without Pile Cap).

Sections across the micropile and ground is taken at different locations as listed in Table 6.1.

Table 6.1. Sections across the Piles (No.15, No.15 & No.17) and the Ground.

Section	Distance from the Micropile head	Ground
Section A-A	44'	Overburden Soil
Section B-B	72'	Competent Rock

Strain and stresses across sections A-A and B-B of the ground and micropile are shown in Figures 6.4, 6.5, respectively. It appears that the three micropile have similar response.

Figures 6.4 and 6.5 show that the maximum strains and stresses occur at the micropile. The ground readings are negligible. This indicated that there is poor interaction between micropiles and they behave like single micropiles.
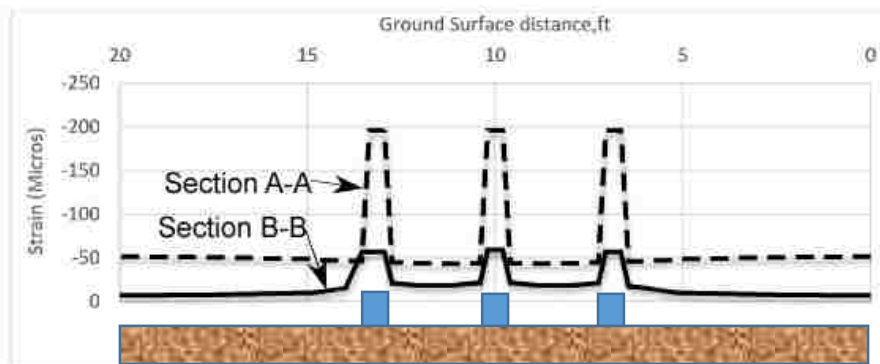
Figure 6.4. Vertical Strain at Different Sections across Micropiles and Ground.
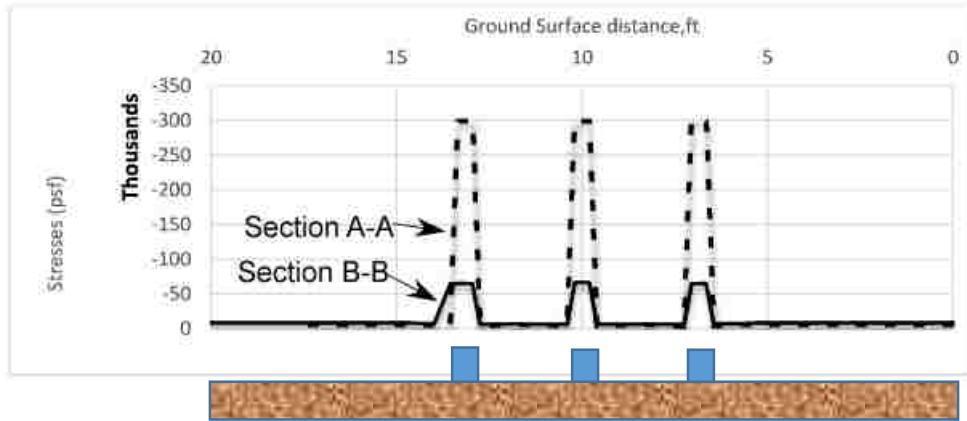
Figure 6.5. Vertical Stress at Different Sections across Micropiles and Ground.

6.1.2. Analysis of Micropile No.1. Micropile No.1 was placed within the two adjacent micropiles No.2 and No.20. All three micropiles seems to have dissimilar lengths of bond and cased zones which is unlike Micropile No.16 and its two adjacent micropiles. Micropiles section and lengths are shown in Table 6.2.

Table 6.2. Micropile's Characterization.

Micropiles' Characterization							
Micropile	Diameter	Concrete Depth	Overburden Cased Depth	Wea. Rock Cased Depth	Total Cased Depth	Bond Depth	Total Depth
No.1	0.802	1.5	25.5	0	27	16	43
No.2	0.802	2	48	25	75	17	92
No.20	0.802	2	38	0	40	16	56

Similar to Micropile No.16, the group effect is negligible as shown in Figure 6.6.
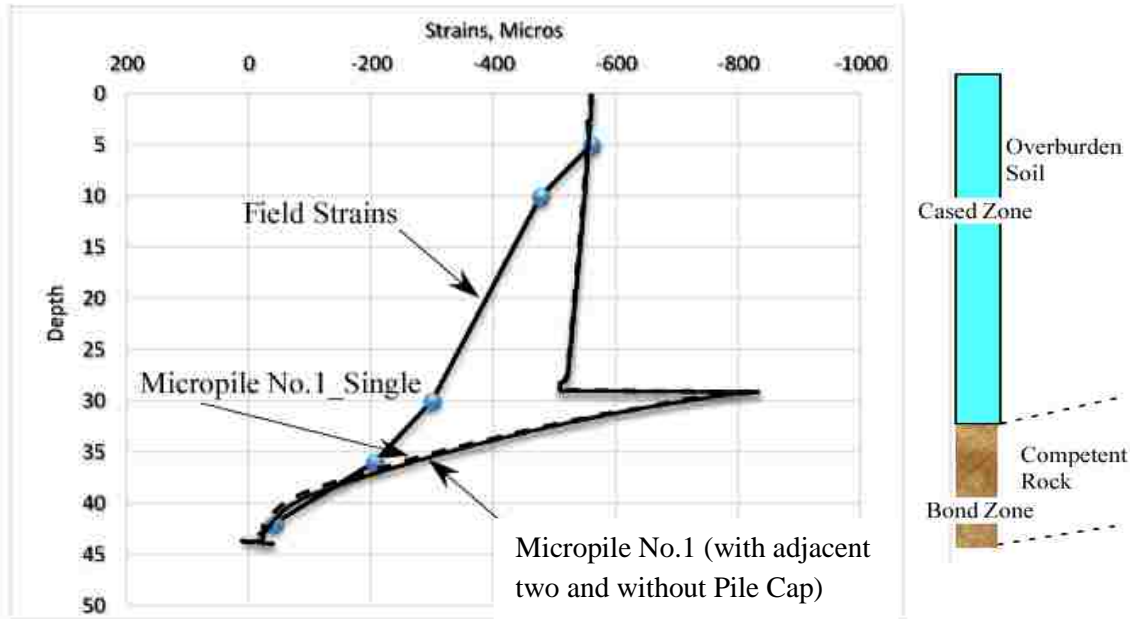
Figure 6.6. Strain of Micropile No.1 in Single and Group Analyses.

Some sections also were taken across the micropile and the ground at different depths to observe the change in the strain and stress along the micropile to the boundary. Sections are shown in Table 6.3.

Table 6.3. Sections across the Piles (No.1, No.2 & No.20) and the Ground.

Section	Distance from the Micropile head	Ground
Section A-A	3'	Overburden Soil
Section B-B	26'	Overburden Soil
Section C-C	30'	Competent Rock

The micropiles do not have similar lengths, therefore, the stresses (shown in Figures 6.7 and 6.8) will be different across sections paths which is unlike micropile No.16. The stresses, strains shows that after small distance away from the micropile surface, all values come back to the stresses, and strains of the ground.
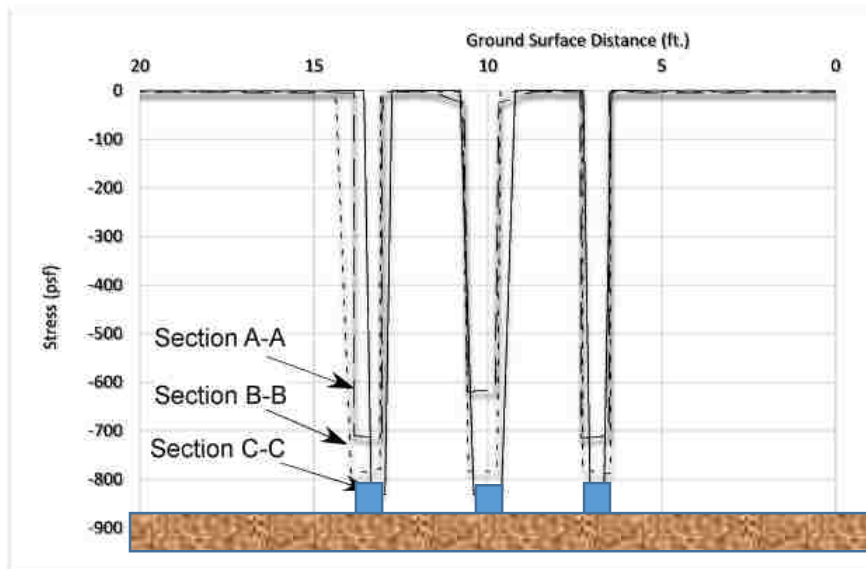
Figure 6.7. Vertical Stress at Different Sections across Micropiles and Ground.
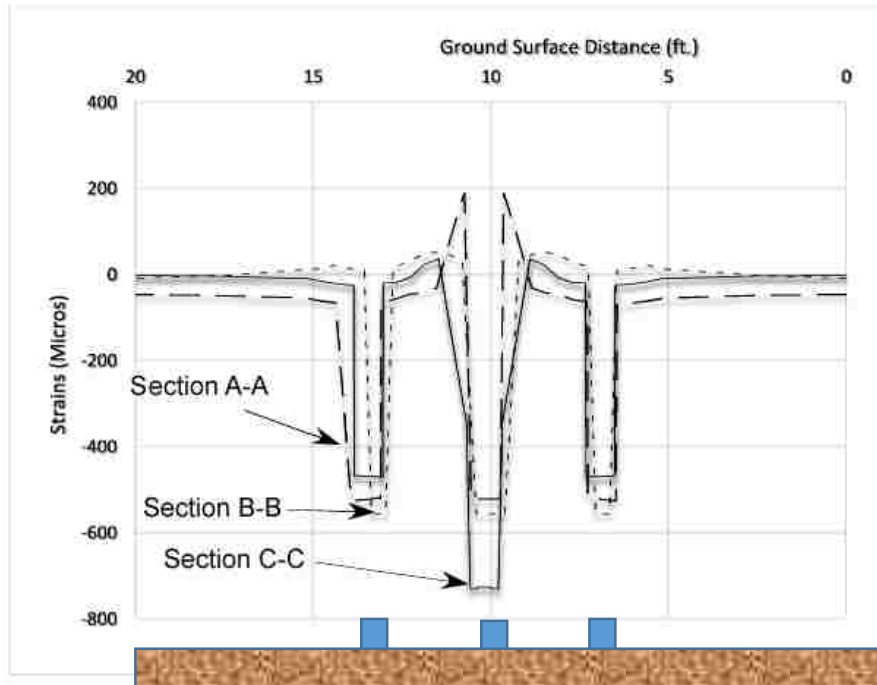
Figure 6.8. Vertical Stress at Different Sections across Micropiles and Ground.

6.2. MICROPILES' GROUP BEHAVIOUR (WITH PILE CAP)

Pile cap connects the micropiles together, reduces the differential settlement and distribute the load to the micropiles. The load is applied as pressure over the whole area of the cap not directly over the micropiles as shown in Figure 6.9. This raises an additional questions on the load transfer mechanism of the micropiles. Will this load goes completely to the micropiles? Will part of this load be carried by the ground? If so, how much? Will there be any group effect?
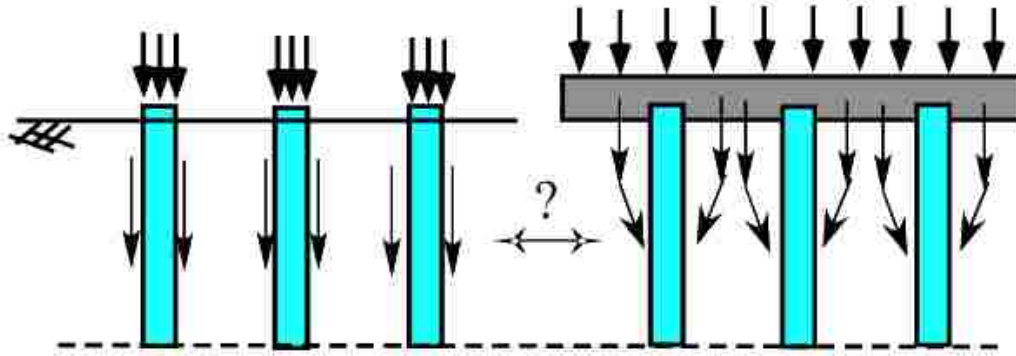
Figure 6.9. Loading and Load Transfer Mechanism Scenarios of Multi-Micropiles.

In General, the pile cap will have effect on the load quantity due to the load that is carried by the cap. It also may cause effect on the load transfer mechanism that occur due to the overlapping of the micropiles together.

6.2.1. Load Quantity Effect. When the pile cap is included in the analysis of single micropile, the applied load distribute itself to the cap, soil and to the micropile. The cap in this analysis is 5' thick and 5' diameter. Therefore, it will take some load before it starts transferring the load to the micropile as well as to the soil. However, regardless of the load, the behavior is always the same and the difference is only about the load quantity.

6.2.2. Group Effect. Analysis of the single micropiles showed that stresses and strains read the geostatic stress roughly after 2d from the interface. This indicates that group effect of the micropiles are negligible upon exceeding this distance. However, a group behavior analysis is conducted to check this assumption.

In this section, Micropile No.16 will be modelled within a group of the other two adjacent Micropiles with a pile cap. Pier No.2 will then be modelled with all micropiles.

6.2.3. Group's Numerical Analysis. Three micropiles analysis is implemented followed by all the micropiles in the pier.

6.2.3.1 Micropile No.16' group analysis. The properties of the model and the layers are similar to Table 5.5. The pile cap represents the tributary area of three micropiles as shown in Figure 6.10.

The load was applied over the three micropiles as range of the expected load that should be carried by three micropiles. Micropile No.16 is expected to carry 187 kips based on the strain gages readings. Therefore, load between 300 kips and 750 kips is applied over the pile cap.

Micropile No.16

Micropile No.15

Micropile No.17

45'

20'

23'
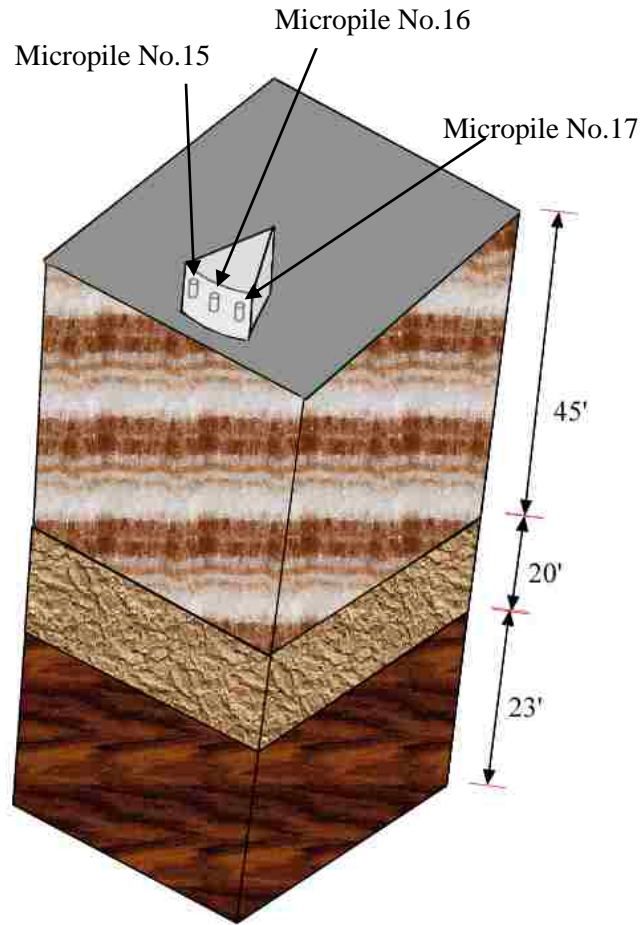
Figure 6.10. Micropiles No.15, No.16 and No.17 with Pile Cap.

Figure 6.11 shows that the strain is similar to the single behavior. This is obviously starts at the overburden soil when the interaction becomes small between the ground and the micropile. The load of the micropile starts to accumulate and increases in the pile cap and the drilled platform regions. Then, it starts transferring the load as the single behavior of the micropile.
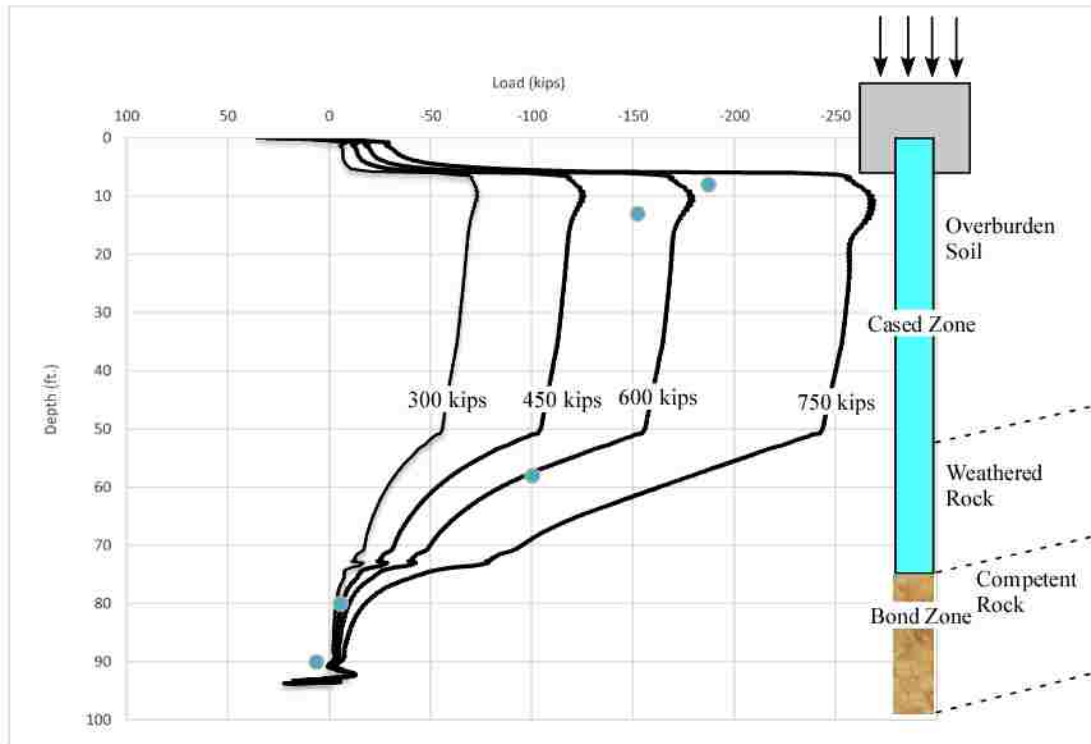
Figure 6.11. Micropile No.16's Group Behavior.

6.2.3.1 All micropiles in Pier No.2. After conducting the group analysis of three micropiles, all micropiles are modelled as shown in Figure 6.12.

Model's layers are shown in Table 6.4. The loading conditions including the geostatic loading as well as the static load of the Pier. The estimated load of Pier No.2 is 2500 kips based on Dixon (2013). Therefore, to study the load transfer mechanism of Pier No.2, a load that is between 1500 and 4000 kips will be applied over the cap.

All micropiles of pier No.2 are relatively of equal length of 100'. Therefore, the model consists of 20 micropiles of 100' long. This length includes 59' in the overburden soil as well as 13' in the weathered rock. The bond zone/competent rock length is 23'.
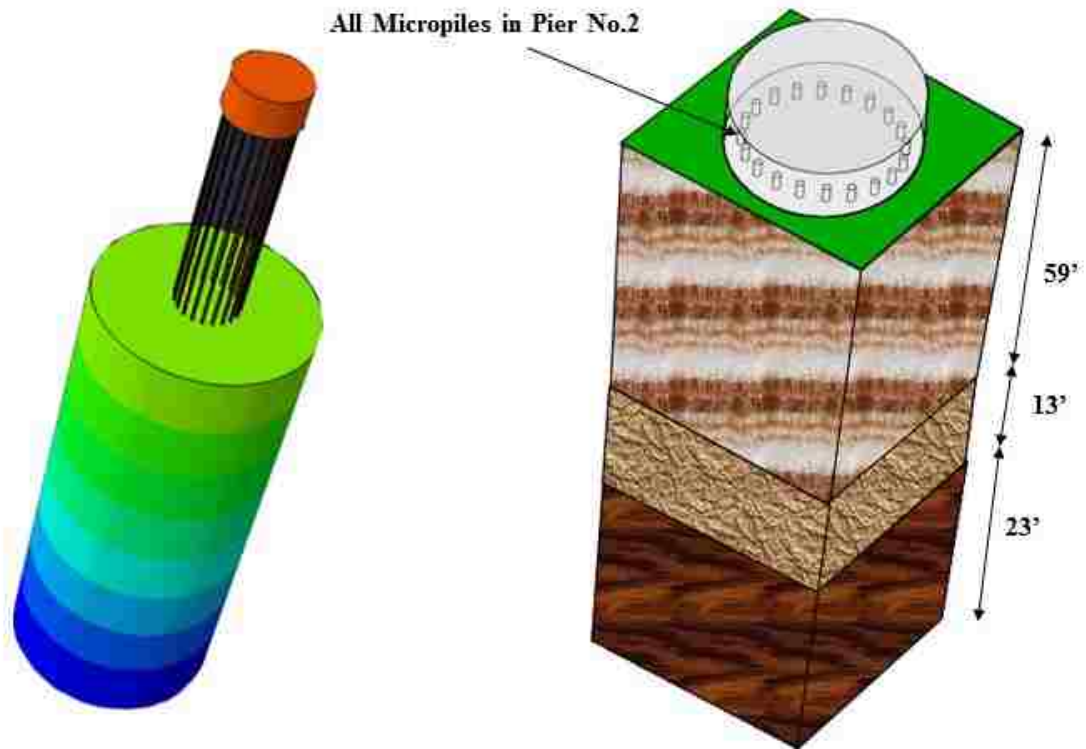
Figure 6.12. Pier No.2's Model.

Table 6.4. Pier No.2's Model Characterization.

Depth (ft)	Ground Char.	E (psf)	ν	γ (psf)	φ (°)	ψ (°)	C (psf)
0-5	Concrete Platform	580,393	0.30	150	-	-	-
530	Overburden Soil I	3,134	0.30	130	35	5	100
30-64	Overburden Soil II	5,226	0.30	130	35	5	100
64-76	Weathered Rock	31,335	0.30	155*	30	5	2100
76-100	Competent Rock I	104,450	0.30	162*	30	5	2100
100-200	Competent Rock II	208,900	0.30	162*	30	5	2100

*Water level at 60' below ground surface, unit weight is
reduced in simulation

Pier No.2's analysis is conducted to confirm that the group behavior of micropiles is similar to the single behavior at depth below the pile cap. This was also concluded from the group behavior of three micropiles. Pier No.2's adds further understanding on the quantity of the load transferred to the micropile and the ground.

Pier No.2's analysis is closer to simulate the actual loading and boundary conditions. However, it is somehow redundant in terms of interpreting the group behavior of micropiles since it was explained when modelling three micropiles together.

To understand the load transfer of the micropile into the ground, many cross sections will be taken as shown in Figure 6.13. They include sections along the interface at both sides; the ground side and the micropile side; Section A-A and Section B-B, respectively. This explains the interface behavior of the micropiles. Section C-C will be taken under the cap to understand and see the behavior under the pile cap.

Section D-D which is taken along two micropiles will show if there is any overlap in the stresses/strains of the micropiles.
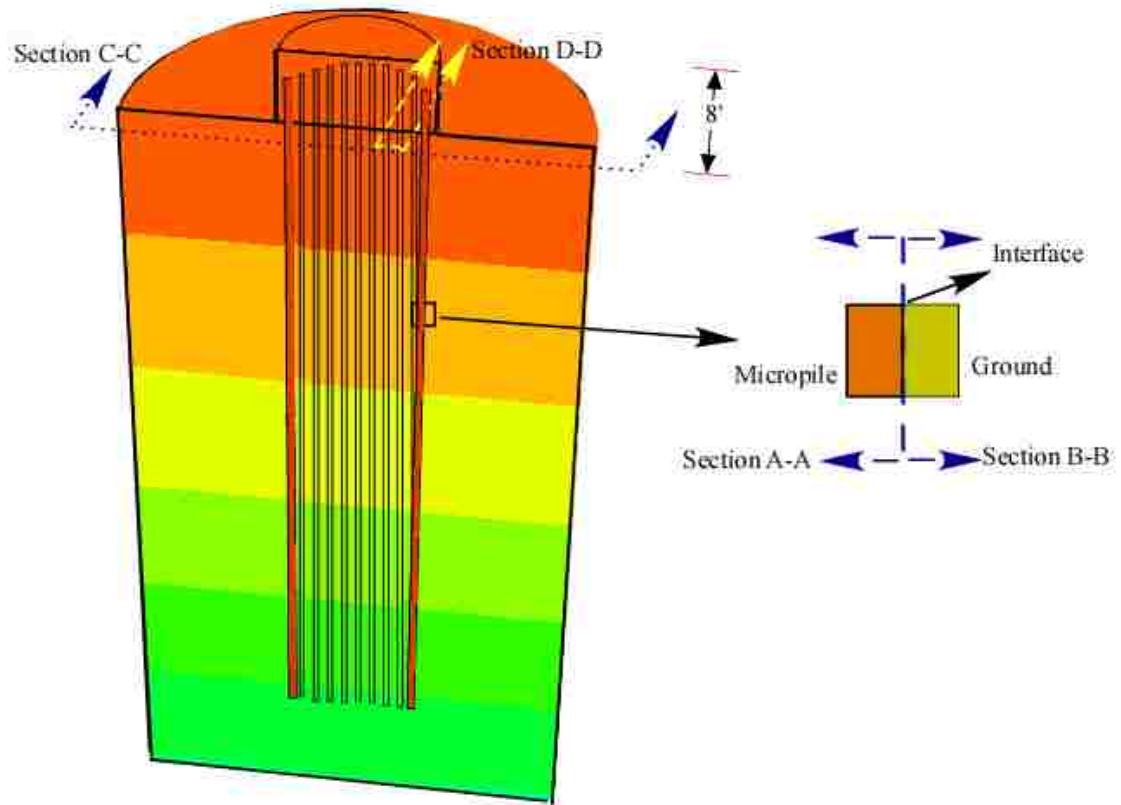
Figure 6.13. Pier No.2' Model Cross Sections.

The behavior of the Micropile's side at the interface (Section A-A) is shown in Figure 6.14.

The load transfer of all micropiles are similar and they show that the behavior is similar to single micropile starting from elevation under the pile cap and to the Micropiles' tip. The difference in the behavior is within the pile cap and the concrete platform.

The load at both regions is collected and transferred from the cap/concrete platform and is transferred to the pile. Therefore, the load is increasing at these regions. Strain gages in the concrete showed the load increased and this confirms this conclusion.
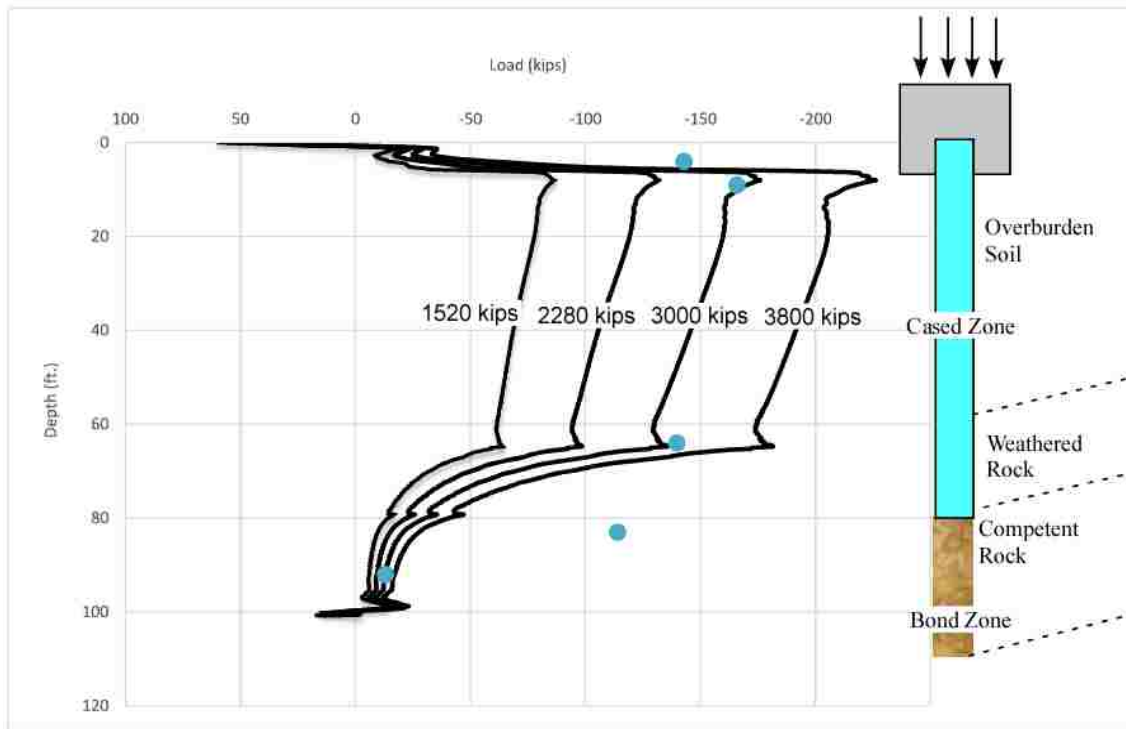
Figure 6.14. Load Transfer of Micropile No.16 (Section A-A).

The strain gages readings' belongs to Micropile No.16 of Pier No.2. Micropile No.16 was selected because it best closely to the 5' depth of the platform which was assumed to uniform in the model.

The best load that match the micropiles (20 micropiles, 100') is between 2500 kips and 3000 kips which is somehow close to load estimated above the pier.

The vertical stress along Section B-B is shown in Figure 6.15. The stress keep increasing until and it converges to a geostatic stress slope. The stress is larger than the stresses of single micropiles or group of micropiles without a cap.
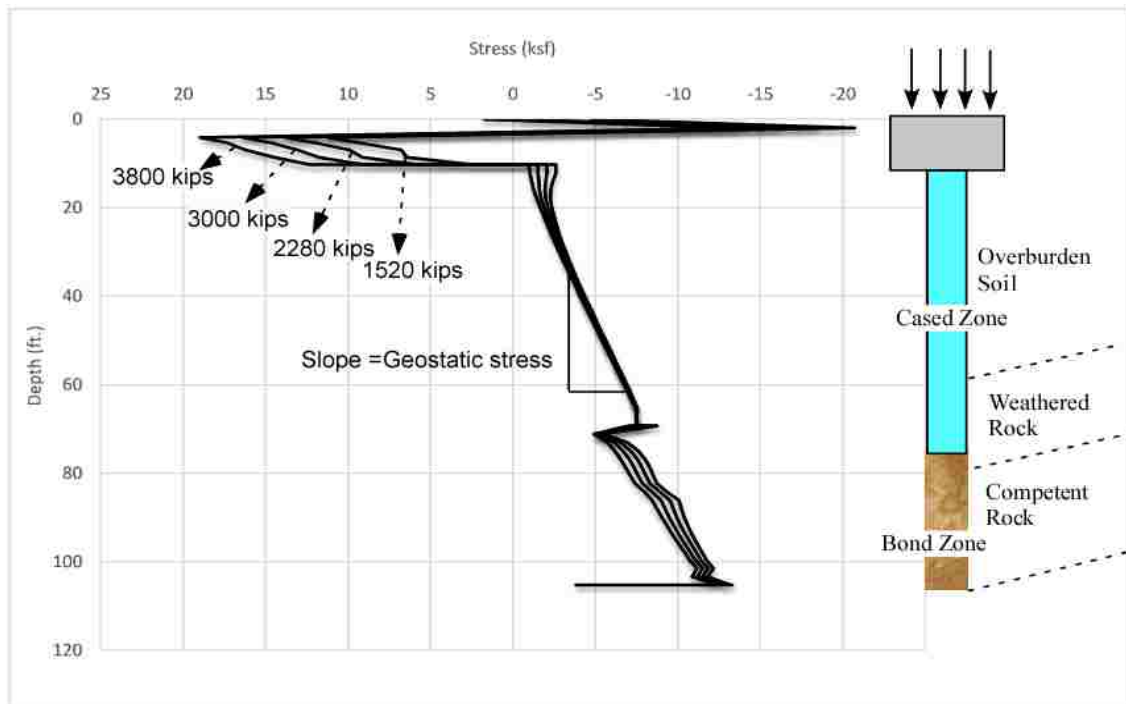
Figure 6.15. Vertical Stress along Section B-B.

Vertical strain of the ground is shown in Figure 6.16. The strain can be explained in terms of Hooke's Law. The strain in the concrete is small due to the high stiffness. It increases with concrete depth due to self-weight of the cap. The strain sharply increases at the overburden soil which is due to the low stiffness. It decreases again in the rock. So, strain values are effected by the amount of the load transfer/friction and the layer stiffness.
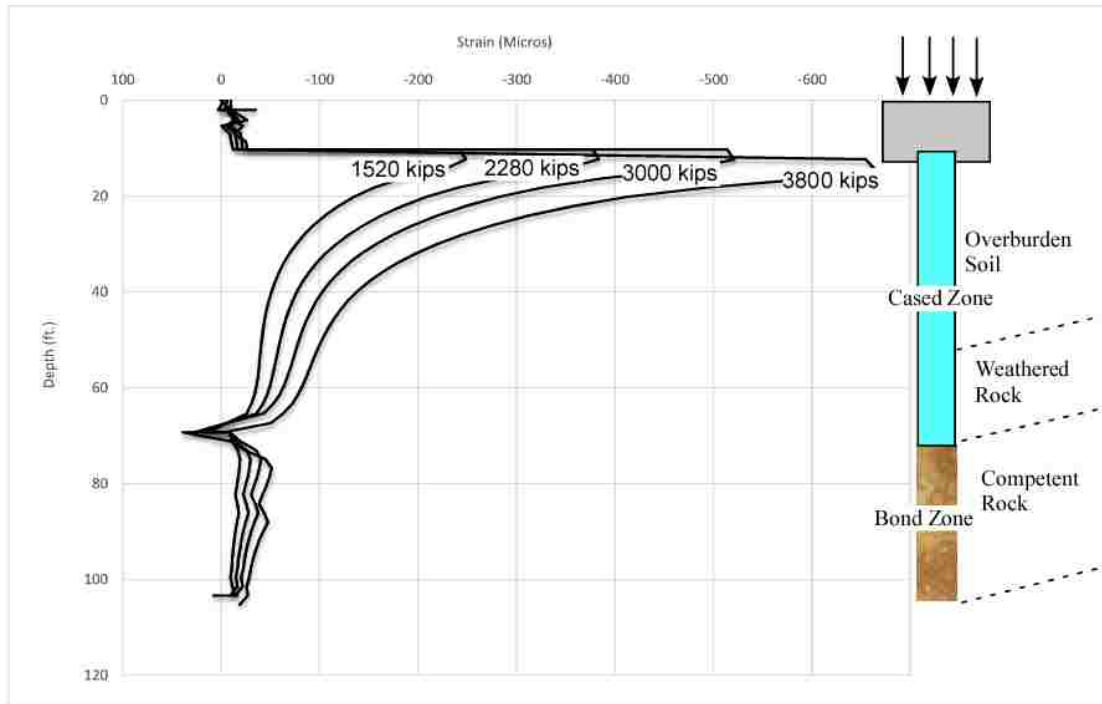
Figure 6.16. Vertical Strain along Section B-B.

The behavior of Section C-C located under the pile cap is shown in Figure 6.17. Section C-C is 2' below the concrete platform and 8' below the pile head. As shown, the strain is maximum in the pile cap and it decreases as the distance increases in the model.

The micropiles strains are smaller since the micropiles have higher stiffness. The strain is maximum at the areas around the micropiles and decreases away from the piles.
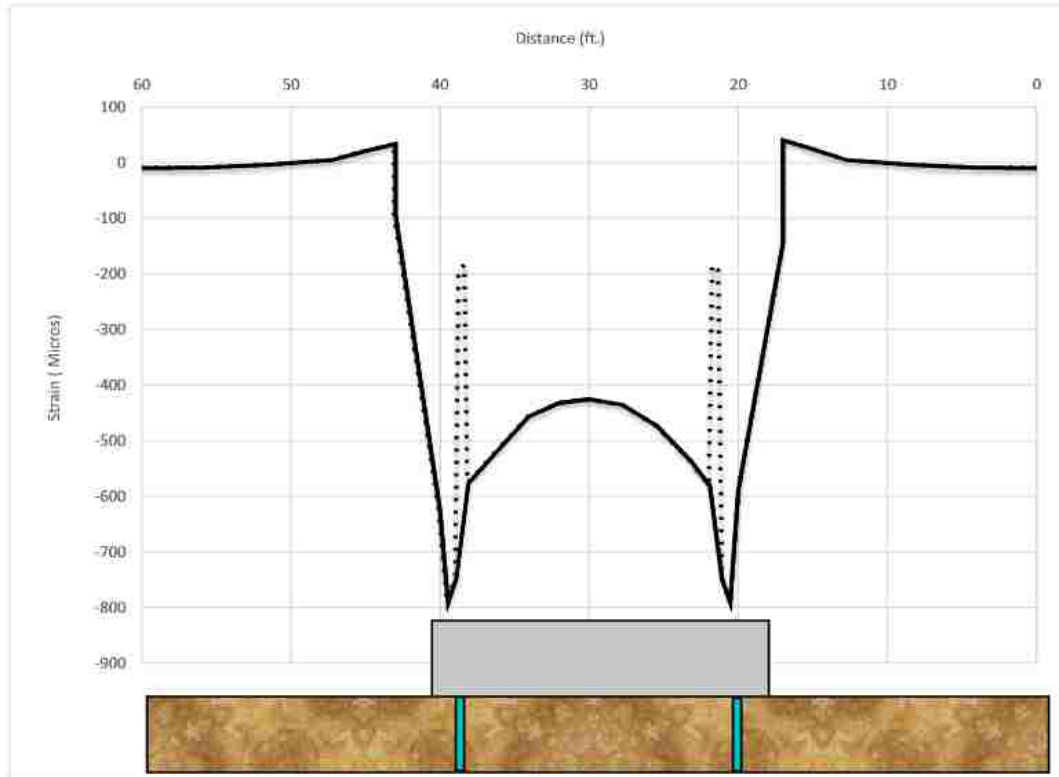
Figure 6.17. Vertical Strain along Section C-C.

The stresses are shown in Figure 6.18. This graph was plotted without including the micropiles, because the micropiles have much higher stresses and the ground will have flat stresses and variation in the ground stresses cannot be seen.
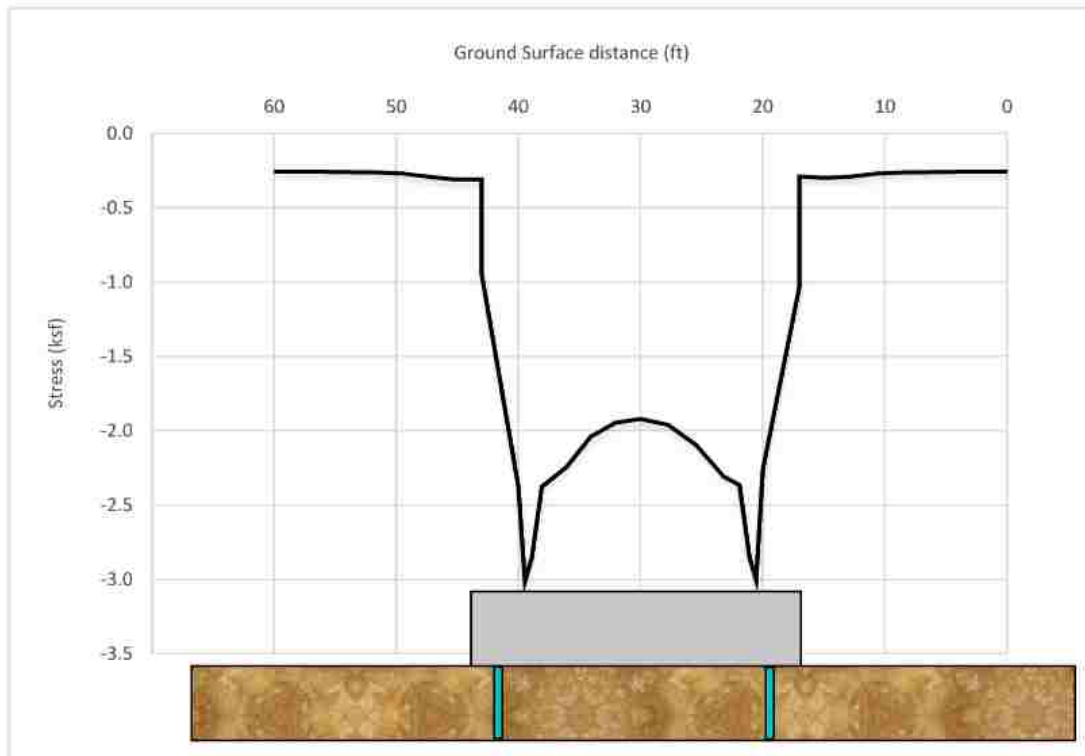
Figure 6.18. Vertical Stress along Section C-C.

Last section, D-D, is located 8' below the pile head (2' below concrete) and it is taken across two micropiles to study the overlap in stresses/strains. The strains are shown in Figure 6.19 which obviously shows that is no overlap between the micropiles. The other reason that indicates that there is no overlap between the micropiles; are the load transfer shown in Figures 6.14 and 6.15. These plots are identical in all micropiles (since they are modelled as equal length micropiles).
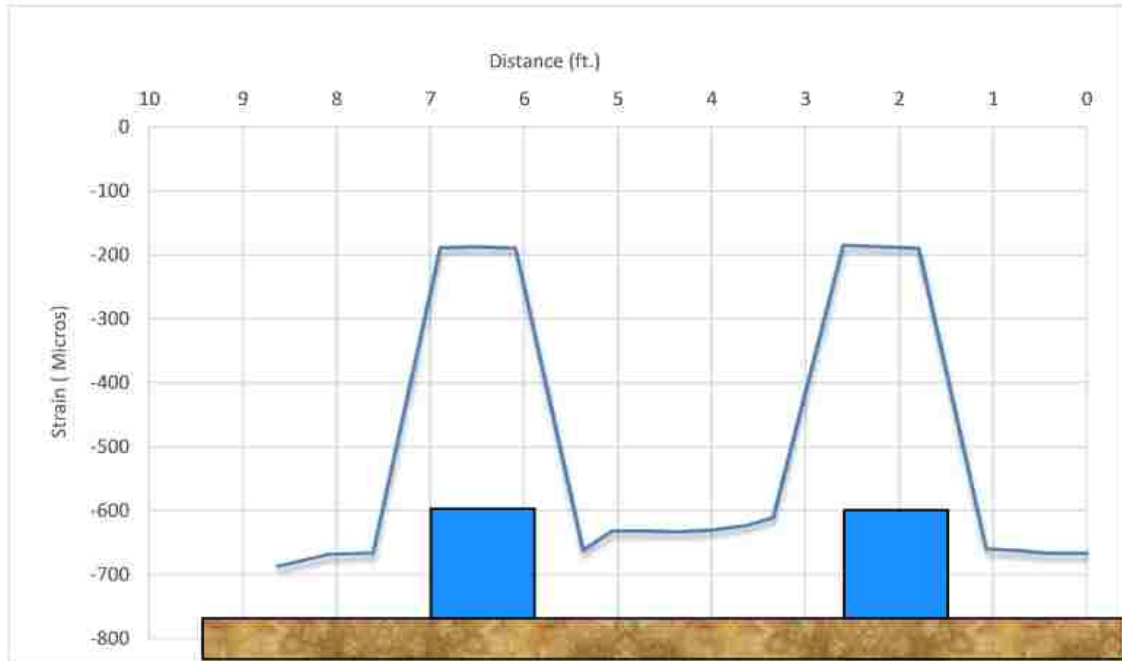
Figure 6.19. Vertical Strain along Section D-D.

To study the pile cap effect on the stresses of the ground, two longitudinal section were taken parallel to the micropiles, one section from the center of the pile cap down to the tip of the micropile, and another section outside the region of cap. The stress is shown in Figure 6.20.

As shown in Figure 6.20, the stress of the ground 5' away from the cap reads exactly the geostatic stress. However, the stress inside the cap region is different; the stress is maximum at the surface and then decreases because it is taken by the micropile.

Both stresses converge to the geostatic stress at the middle of the overburden soil, then the stress of the section inside the cap is greater in the rock zone because the load is carried most in the rock.
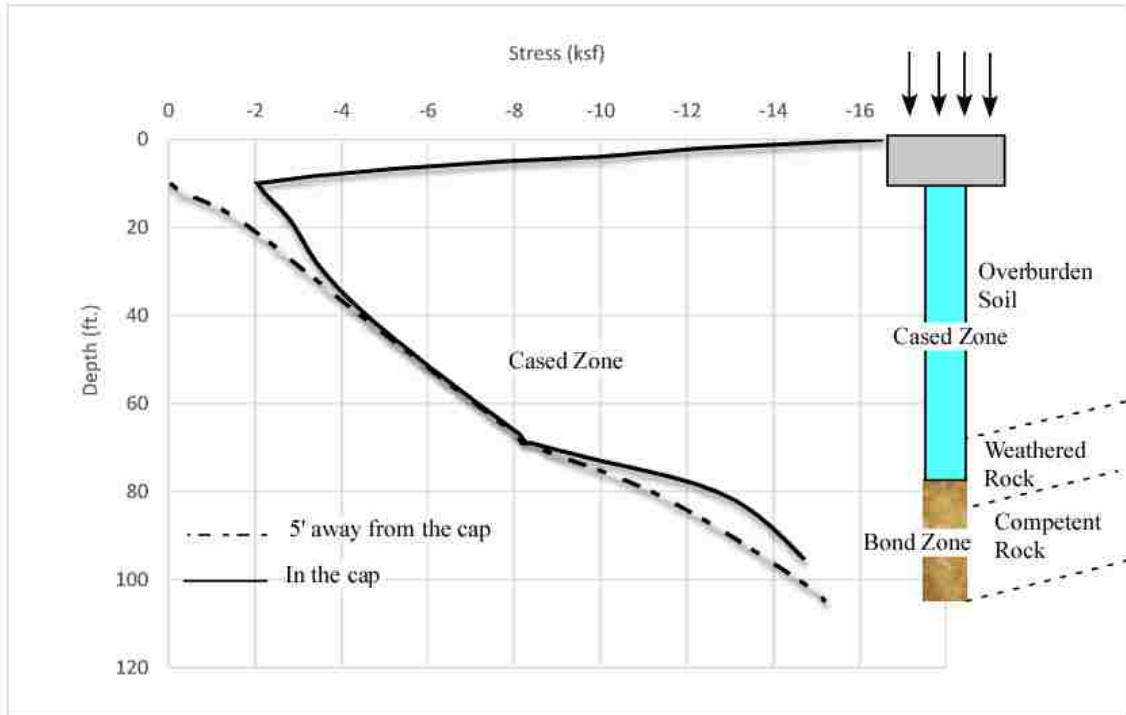
Figure 6.20. Vertical Stress of the Ground inside and outside the Pile Cap.

7. PARAMETRIC STUDY

A parametric study is conducted to evaluate the impact of parameters on the model and analyze the results of each parameter change on the load transfer mechanism of micropiles. This covers wide range of uncertainty on soil/rock properties presented in the constitutive model parameters in Section 4.2.1. It also includes all possible scenarios of the contact and the interaction mechanisms. Micropile No.16 in Pier No.1 was selected to show the effect of these variations and the constraints that these parameters might cause on the model.

This section studies the effect of elasticity parameters including the elasticity modulus and Poisson's ratio. It, also, studies failure parameters variations including cohesion, friction and dilation angles. In addition, friction coefficient sensitivity analysis is studied. The section is divided into two further sections according to the degree of noticeable change and effect on the load transfer mechanism; Section 1: Parameters that show significant change on the load transfer mechanism process upon variation of their values. This includes modulus of elasticity and coefficient of friction. However, Section 2 involves parameters that have no or small changes on the load transfer mechanism process upon variation. This includes Poisson's ratio, cohesion, friction and dilation angles.

The sensitivity analysis is conducted to show the effect of the parametric variations of Table 7.1.

Table 7.1. Parameters' Range of the Ground.

Soil/Rock	Elastic Modulus (ksf)	Poisson's Ratio	Mass Density pcf	Friction Angle (°)	Dilation Angle (°)	Cohesion (psf)
Soil	2,089-7,883	0.25-0.40	130	30-45	5.0-15.0	100
Weathered Rock	20,890-47,025	0.25-0.30	155	25-35	5.0-15.0	1044-3133
Competent Rock	104,450-313,350	0.25-0.30	162	25-35	5.0-15.0	1044-3133

The interaction mechanism between the micropile and the ground may have different scenarios as shown in the flowchart of Figure 7.1. The contact of the cased zone and the ground may be neglected and this implies that the bond zone friction is the most important as shown in the left side of the flow chart. The friction may vary from 0.4 to 1 in the bond zone. The effect of this variation is shown in this section.

The other scenario assumes that there is some friction in the cased zone region in addition to the bond zone. Therefore, the friction in the cased zone can also affect the load transfer mechanism. Thereby, the variation of the interface friction coefficient in the cased zone is studied within the realistic range shown in Figure 7.1.
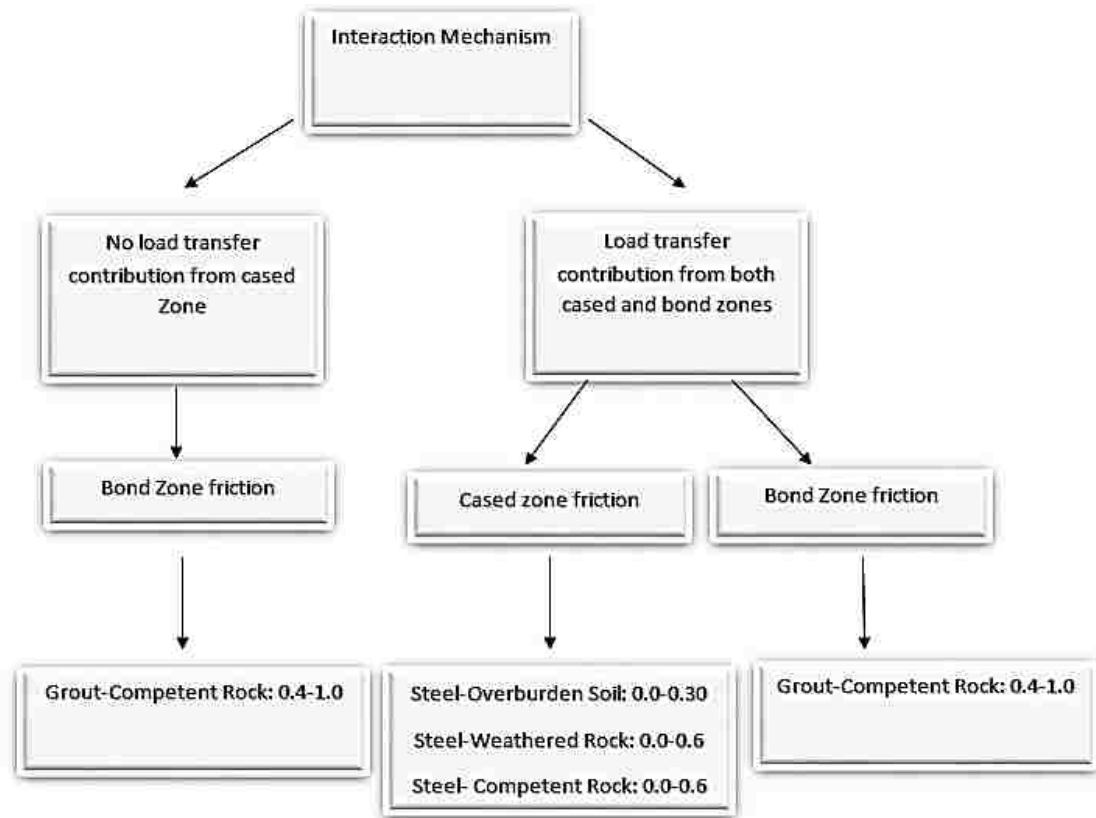
Figure 7.1. Possible Interaction Mechanism between Micropile and the Ground.

7.1. PARAMETERS WITH MOST INFLUENCE ON THE LOAD TRANSFER

This section discusses the parameters that have the most influence on the load transfer mechanism which they are the friction coefficient and elastic modulus. In this section, different contact scenarios are discussed as well as the effect of the ground stiffness.

Contact mechanism scenarios as shown in flowchart of Figure 7.1 have two approaches;

- The cased zone and the ground have no interaction. The drilling and construction method of replacement piles indicates that this interaction is neglected as was explained earlier in Section 2.

- The cased zone and the ground may have small friction. This is due to friction gain with time that might occur and triggers some load transfer mechanism.

The two approaches, ultimately, are controlled by one parameter which is the coefficient of friction. If the friction coefficient is zero, then there is no load transfer contribution from the cased zone. However, if there is a non-zero friction value, this implies a load transfer; the quantity depends on the friction quantity and the stiffness as shown next.

The elastic modulus expresses the amount of the stiffness in the material, the higher the stiffness, the lower the strain. Elastic modulus can be of great importance on the load transfer mechanism since it governs the amount of defamation of the ground.

The two factors; friction coefficient and the modulus of elasticity controls the behavior and the load transfer mechanism of micropiles. In order to relate them together, the springs-micropile/ground analogy illustration is developed. The analogy will be used to simplify the explanation of the results provided by the parametric study.

7.1.1. Springs-Micropile Analogy. Load transfer mechanism can be illustrated by springs connected in series with friction sliders on the sides of the interface as shown in Figure 7.2.
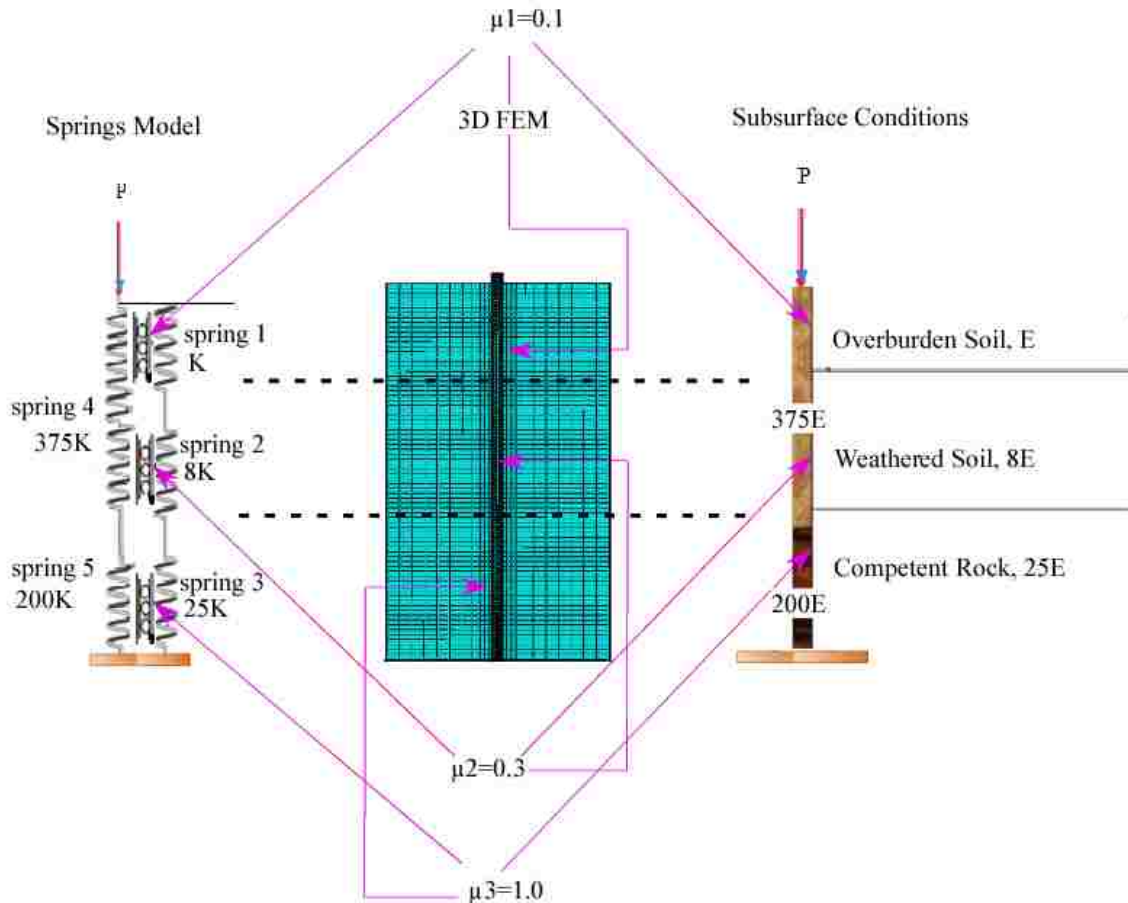
Figure 7.2. Springs-Micropile/Ground Analogy Model.

The analogy is realistic where the used constitutive model is Mohr Coulomb which assumes an elastic behavior by Hooks' law. In this model, each ground has a different stiffness which can be illustrated by spring with a stiffness k. The base stiffness is the smallest which is the overburden modulus of elasticity shown as spring 1.

Weathered rock and competent rock have modulus of 8k and 25k, respectively. The cased zone, bond zone are springs 4 and 5 and they have values of 375k and 200k. The mechanism can be explained as follows:

1. When the load is applied at the top of spring 4 having a stiffness K_4 of 375 K, the load compresses the spring according to the following formula,

$P = Kx$; K: stiffness and x: deformation   Eq 7.1

The energy stored which is the integration of the load over the distance.

$U = \frac{1}{2}Kx^2$; U: Potential energy (unit of energy)   Eq 7.2

2. The load starts to find its path to the surroundings. If no change in the deformation, x, the load remains constant, same applies to the potential energy. However, if there is a friction, µ1, µ2, or µ3 along the interface, this causes some reduction in the amount of deformation in x4 of spring 4 and ultimately P will be reduced according to Eq 5.1. However, this increases the amount of x_1, x_2 or x_3 and initiates loading on the adjacent springs given by p=Kx; p is a fraction of P; that means the load has been transferred.

3. The load, multiplication of Kx, transferred from spring 4 to springs 1 and 2. Deformation, x, of spring 2 will be lower than spring 1 under same load, p according to Eq. 5.1 because spring 2 has higher stiffness.

4. If the friction at any point along the interface of springs 1, 2 and 3 is negative (Negative Friction), this causes spring 4 to move upward, the load carried by spring 4 increases. Therefore, this friction is not desirable.

5. At a certain point of spring 4 or 5, the load will have been transferred effectively to springs 1, 2 and 3. The remaining length of springs 4 and 5 which they receive small load is a solid base and will be ready to take additional loads as needed.

6. As mentioned earlier, the efficiency of the load transfer mechanism depends on the friction and the stiffness. However, the load transfer process needs a minimum length to transfer the load. Therefore, shortage in the length of spring 5 may not allow efficient load transfer.

This analogy will be used frequently to illustrate and explain the sensitivity analysis results.

7.1.2. Interface Friction Coefficient. This section presents the observations noticed by friction coefficient sensitivity analysis for a series of cases that was shown and explained earlier in flow chart of Figure 7.1. Table 7.2 shows the cases studied on the friction of the interface.

Table 7.2. Coefficient of Friction Sensitivity Analysis.

Case No.	Interface	Interface Friction Coefficient Value			Figure No.
1	Overburden Soil-Micropile	0.1*	0.0	0.3	5.4
2	Weathered Rock- Micropile	0.3*	0.0	0.6	5.5
3	Competent Rock- Micropile	1.0*	0.4	0.7	5.6
4	Interaction is allowed only in the bond zone (μ=1.0) with no friction in the cased zone.				5.7

The values marked with star (*) are the initial values of Micropile No.16 model parameters which was presented in Section 4. The cases studied are labeled with numbers that refer to the figures presenting the results.

The parametric study observations can be summarized as follows:

Case No.1 and No.2: Interface friction coefficient at the overburden soil and weathered rock. When the friction was increased from 0.0-0.6 in the overburden soil and the weathered rock separately, the load transfer mechanism changed significantly as shown in Figures 7.3 and 7.4.
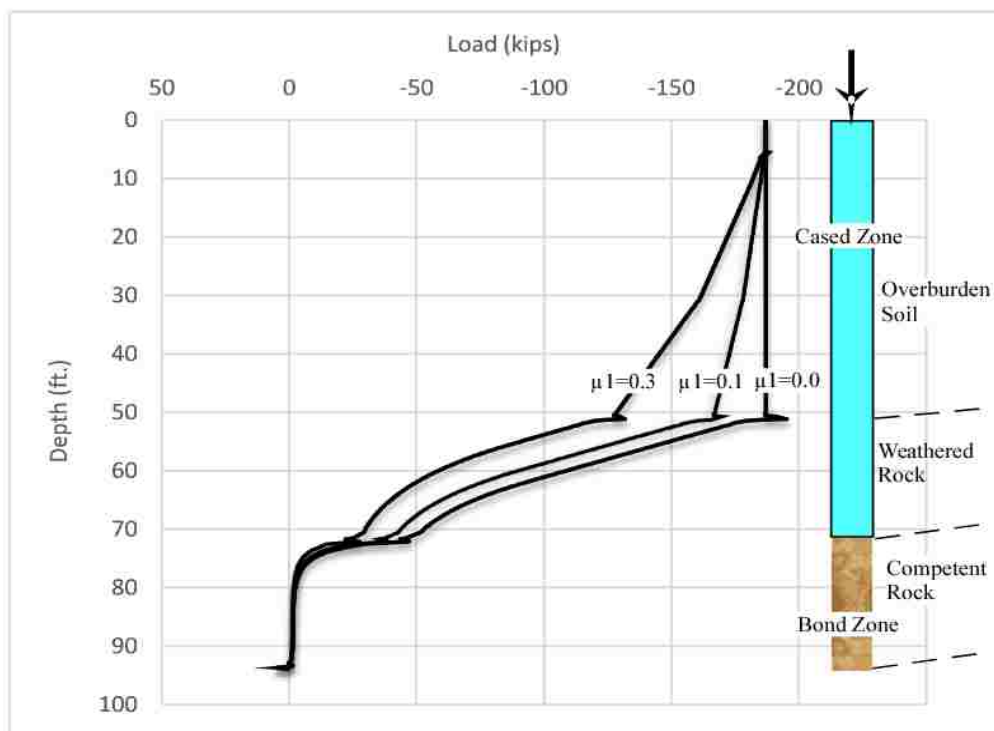
Figure 7.3. Load Transfer with Interface Friction Variation at the Overburden Soil.
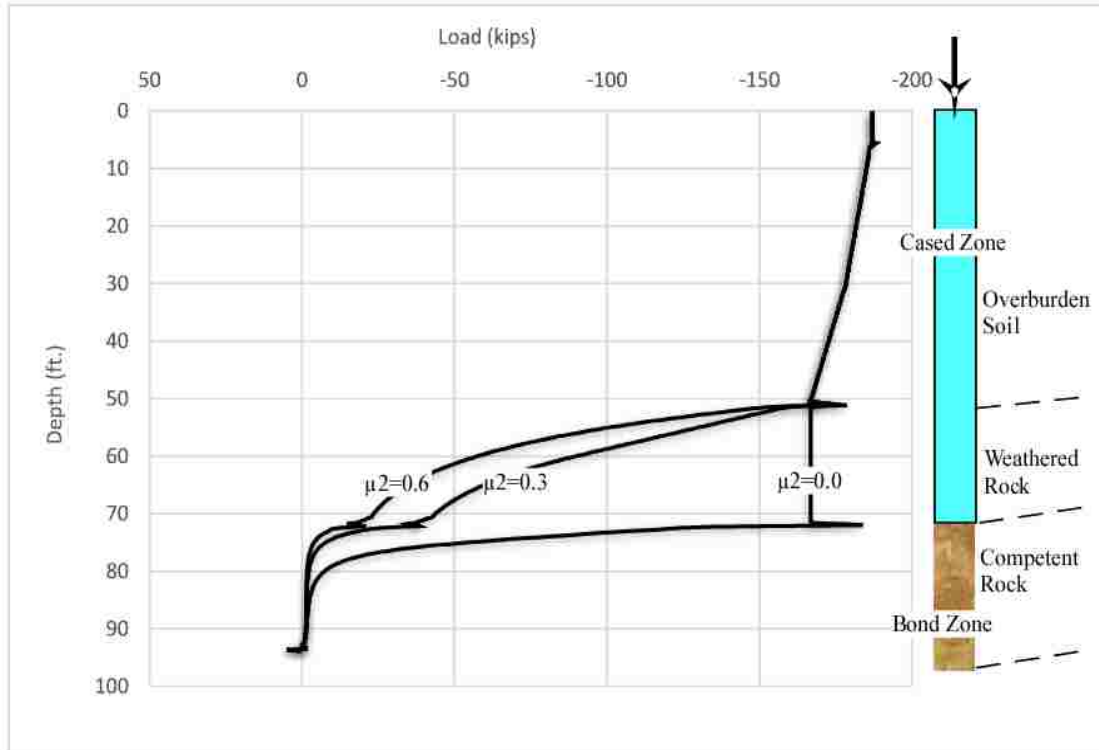
Figure 7.4. Load Transfer with Interface Friction Variation at the Weathered Rock.

Interface friction of the overburden soil and weathered rock has great influence on the transfer mechanism. They are closer to the load source than the competent rock. Therefore, parametric variations of the upper ground layers affect the load transfer mechanism more than the variation in the lower ground layers.

As shown in Figures 7.3 and 7.4, a zero friction implies that there is no load transfer in both, the overburden soil and the weathered rock layers. Increasing the friction from 0.0 to 0.1 and 0.3 in the overburden soil allows some load transfer. Overburden soil was divided into two layers; the second layer starts at 30' which is 1.67 times the modulus in the first layer. The load transfer starts to be more efficient at the beginning of

the second layer of the overburden soil because it has higher modulus. This will be discussed in the next section.

Increasing the interface friction in the weathered rock layer has a non-linear influence on the load transfer mechanism. Increasing the friction from 0.0 to 0.3 increases the amount of transferred load dramatically. On the other hand, increasing another 0.3 has a small effect on the transfer mechanism.

In addition, the load transfer mechanism maintains efficient with a zero friction in the weathered rock. The load can be transferred in the bond zone which verifies the the bond zone in this micropile/long micropiles can take further loads.

Drilling and construction methods of replacement piles break the bond and the friction along the interface. However, friction gain with time is possible. In case of low plasticity soil, if the bond breaks, it can regain friction, especially with high gravel fraction.

Case No.3: Interface friction coefficient at the competent rock. Interface friction variation effect on the competent rock is shown in Figure 7.5. Since most of the load is transferred without significant contribution from the bond zone, it's considered to be less sensitive to parametric variations.
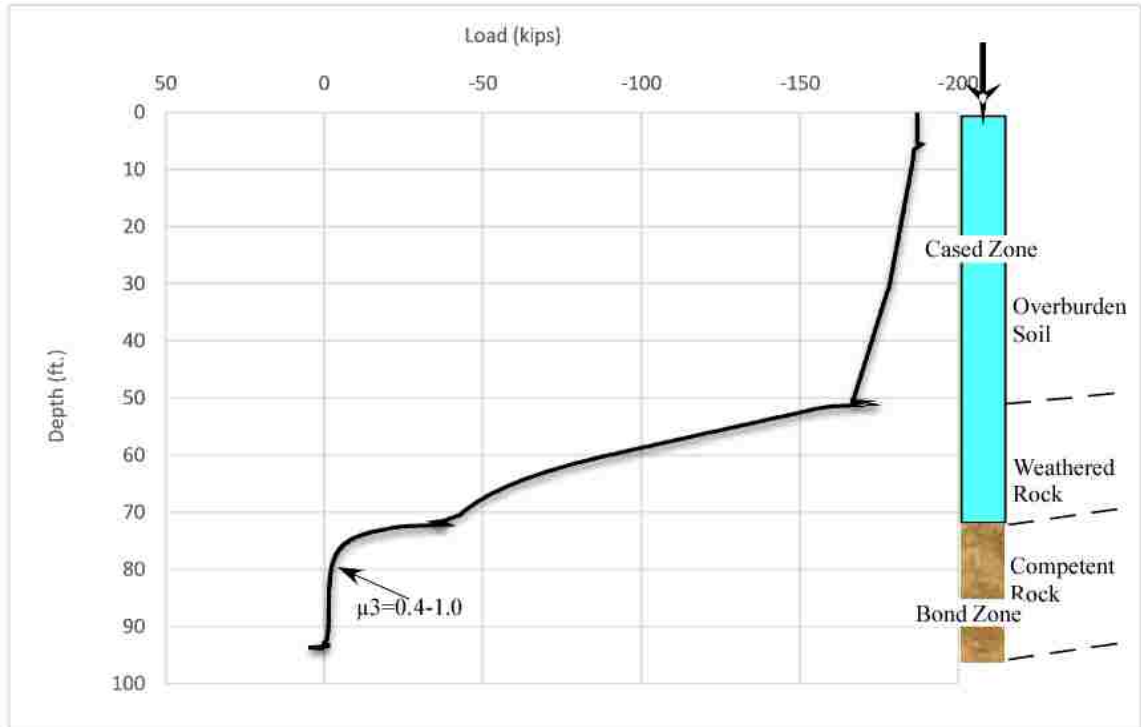
Figure 7.5. Load Transfer with Interface Friction Variation at the Competent Rock.

Tension is noticed at the end of the micropile as shown by the positive values in Figure 7.5. This matches with field observation. Tension occur since the micropile is no longer carrying any axial load and the neutral axis location of the micropile is reached before the pile tip.

Case No.4: No interface interaction at the cased zone. The load transfer triggered by the friction developed along the interface of these layers will be zero as shown in Figure 7.6; this assumes that the micropile is not restrained laterally along the total length of the cased zone. The load transfer starts to occur at the bond zone.
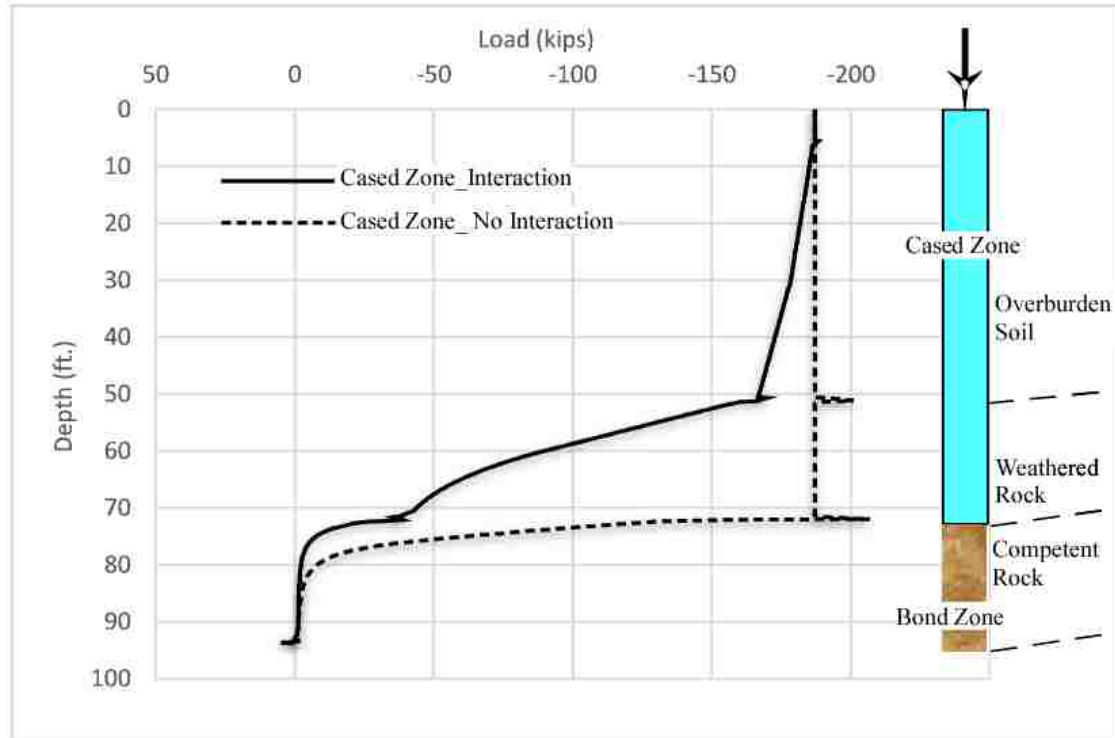
Figure 7.6. Load Transfer with no Interaction Contribution from the Cased Zone.

7.1.3. Elastic Modulus. Elasticity modulus variation will be conducted as shown

in Table 7.3. Each case was done with a separate analysis to see the effect of stiffness

variation of each ground characterization on the model.

Table 7.3. Modulus of Elasticity Sensitivity Analysis.

Case No.	Layer	E (ksf)	E/2 (ksf)	3E/2 (ksf)	Fig. No.
5	Overburden Soil No.1	3,134*	1,567	4,700	5.6
	Overburden Soil No.2	5,226*	2,613	7,839	
6	Weathered Rock	31,335*	15,675	47,025	5.7
7	Competent Rock No.1	104,450*	52,225	156,675	5.8
	Competent Rock No.2	208,900*	104,450	313,350	

The three cases are shown in Figures 7.7, 7.8 and 7.9. The elastic modulus variation at the weathered rock layer had the most effect on the load transfer mechanism as shown in Figure 7.7 because most of the load is transferred in that region. Generally, the higher the load transferred in a layer, the higher will be sensitive to parametric variation.
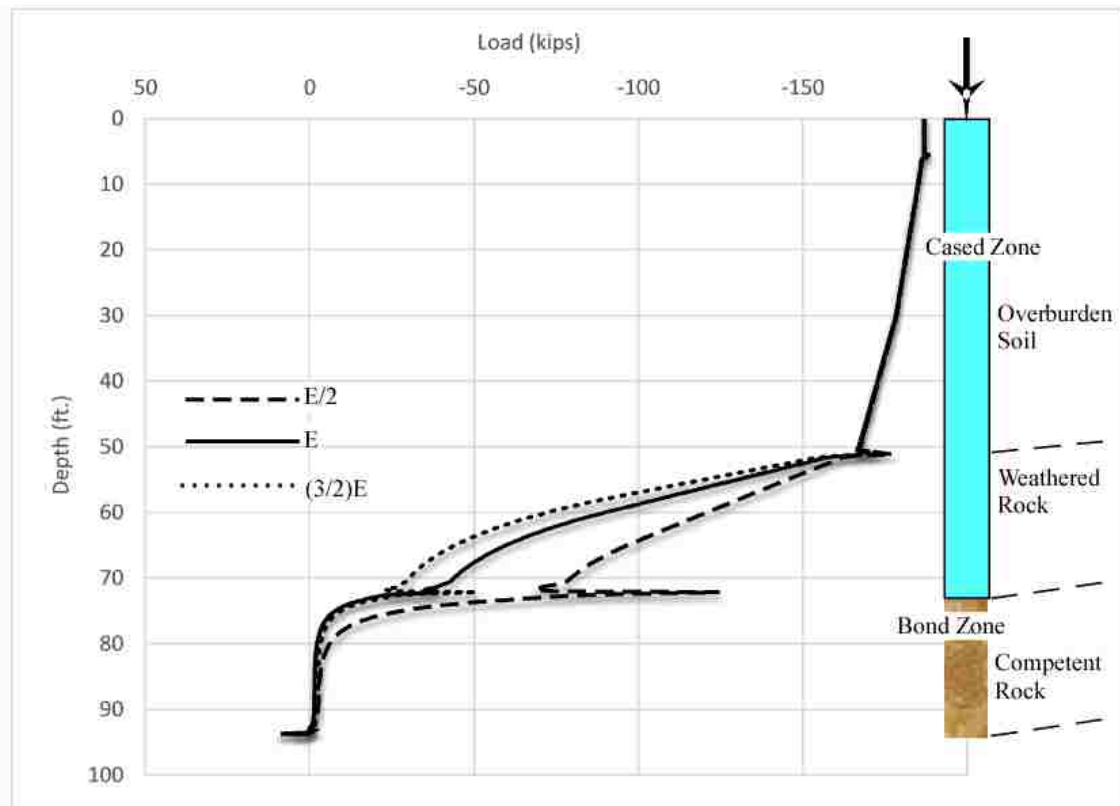
Figure 7.7. Strain Variation with Weathered Rock Elastic Modulus.

The increase of the stiffness in the overburden zone does not cause a significant change on the load transfer because of the low friction which causes a poor interaction between the micropile and the ground.
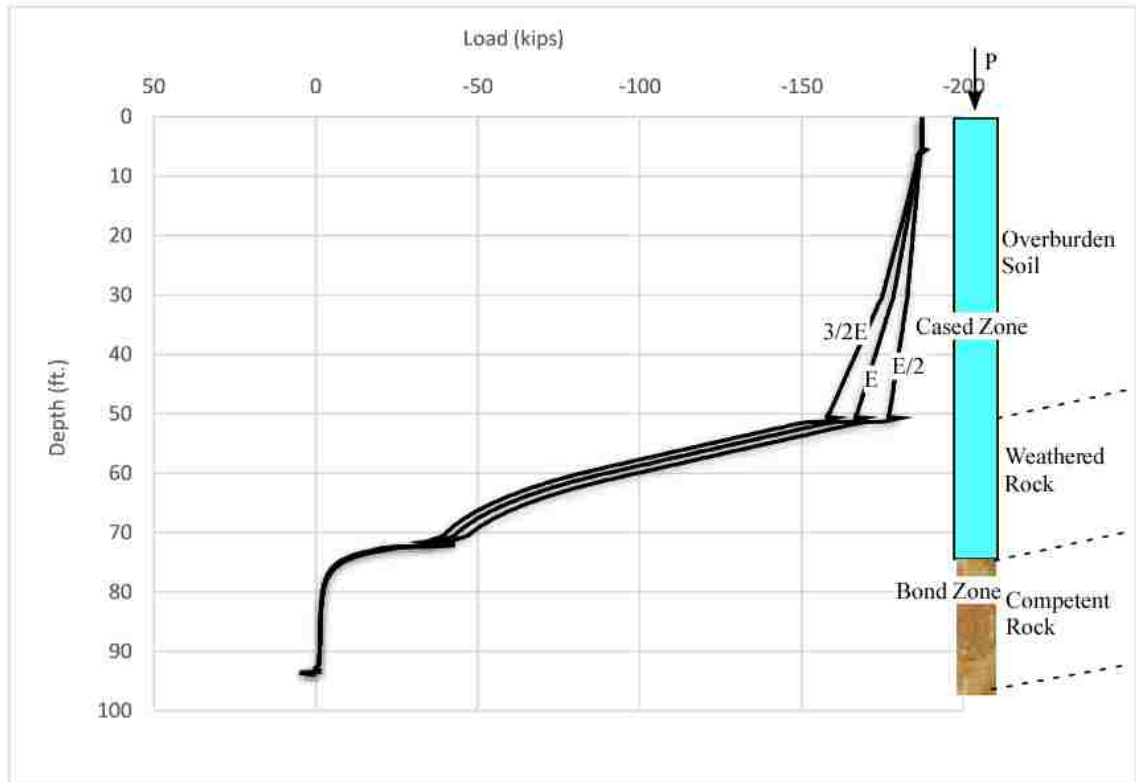
Figure 7.8. Strain Variation with Overburden Elastic Modulus.

Increasing the stiffness in the competent rock has no much effect on the load transfer mechanism since this variation comes after a significant load transfer in the weathered rock. However, this stores extra energy if additional load is added to the foundation from the structure. The extra energy can be given by the Eq. 7.2 in terms of springs-Micropiles/ground illustration. The weathered rock has low friction but it has a high modulus. Therefore, a minimum amount of friction can be enough to make a good load transfer.
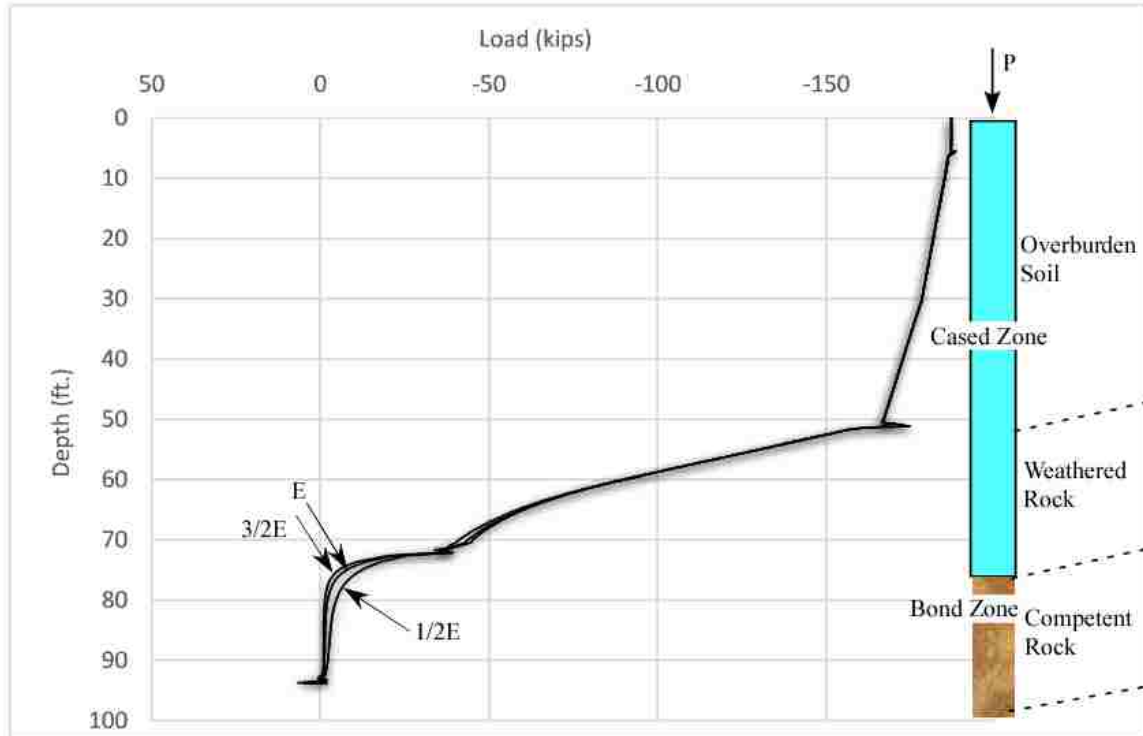
Figure 7.9. Strain Variation with Competent Rock Elastic Modulus.

The friction and the stiffness can be related together as shown in Table 7.4. If the friction and the stiffness are both small, the load transfer will be low. Increasing the friction with low stiffness will also make load transfer mechanism as shown in the soil with high friction. A low friction with high stiffness can make good load transfer, which is the same situation in the weathered rock layer. The competent rock has high load transfer because it has a high stiffness and friction.

Table 7.4. Effect of Stiffness and Friction on the Load Transfer Mechanism.

Ground Char.	Friction	Modulus	Load transfer
Overburden soil(low friction)	Low	Low	Low
Overburden soil (high friction)	High	Low	Low
Weathered Rock	Low	Medium-High	Medium-High
Competent Rock	High	High	High

7.2. PARAMETERS WITH LEAST INFLUENCE ON THE LOAD TRANSFER

In this section, the parameters that have less influence on the load transfer behavior will be discussed. This includes Poisson's ratio, cohesion, friction and dilation angles. Poisson's ratio is one of the elasticity parameters while cohesion, friction and dilation angles identify plasticity behavior.

7.2.1. Poisson's Ratio. Poisson's ratio is one of the parameters that identify the elasticity behavior of the Mohr coulomb model. It is the negative proportion of the lateral strain to the axial strain which is ranging 0 to 0.5 for most of materials.

Poisson's ratio sensitivity analysis range from 0.20 and 0.5 was conducted separately on the weathered and competent rock. The results are shown in Table 7.5 and Figures 7.10 and 7.11. The variation of Poisson's ratio on the weathered rock has insignificant effect on the load transfer mechanism as shown in Figure 7.10. The load transfer considered no change with variation of the Poisson's ratio in the competent rock, Figure 7.11.

Table 7.5. Poisson's Ratio Variation Effect on the Load Transfer.

Case No.	Parameter	Ground	Observation	Figure No.
8	Poisson' ratio	Weathered Rock	Insignificant	7.11
		Competent Rock	No change	7.12
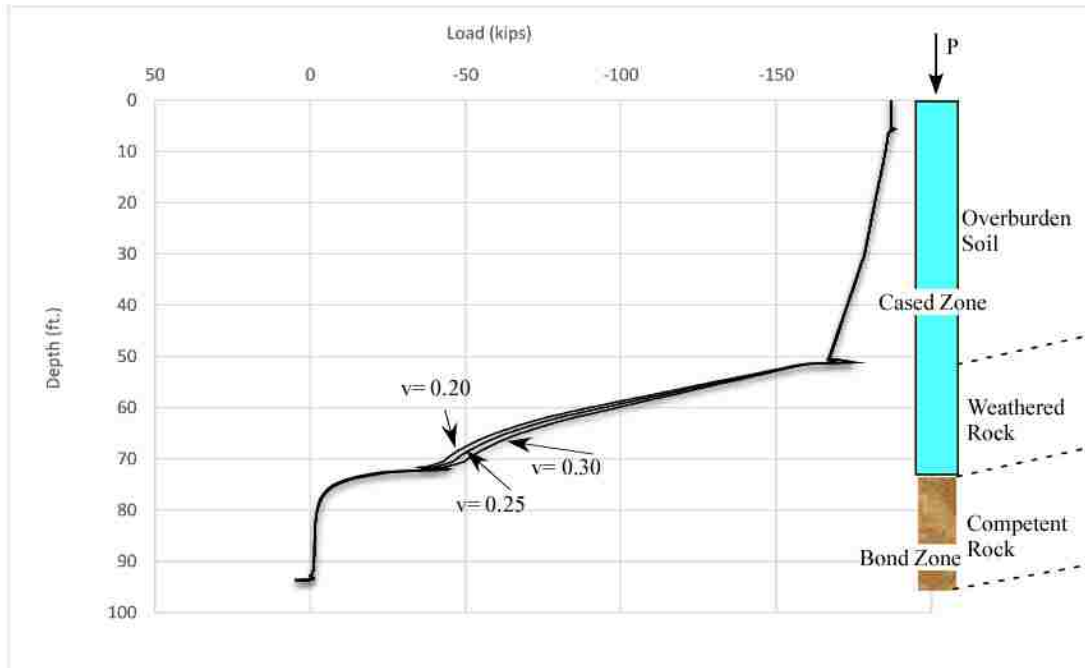
Figure 7.10. Strain Variation with Poisson's Ratio of the Weathered Rock.

Figure 7.11. Strain Variation with Poisson's Ratio of the Competent Rock.

7.2.2. Cohesion, Friction and Dilation Angles. Cohesion, friction, dilation angles are used to define the failure criterion of Mohr coulomb constitutive model. They control the behavior of soil after yielding. Sensitivity analysis of these parameters was conducted only in the weathered and competent rock zones.

Overburden soil sensitivity analysis were not conducted since only a small load transfer occur at that region.

Cohesion was studied on the weathered and the competent rock separately, cohesion was changed from 2100 psf to 1000 and 3000 psf. Cohesion of the weathered rock has an insignificant change on the transfer mechanism in the weathered rock as shown in Figure 7.12.
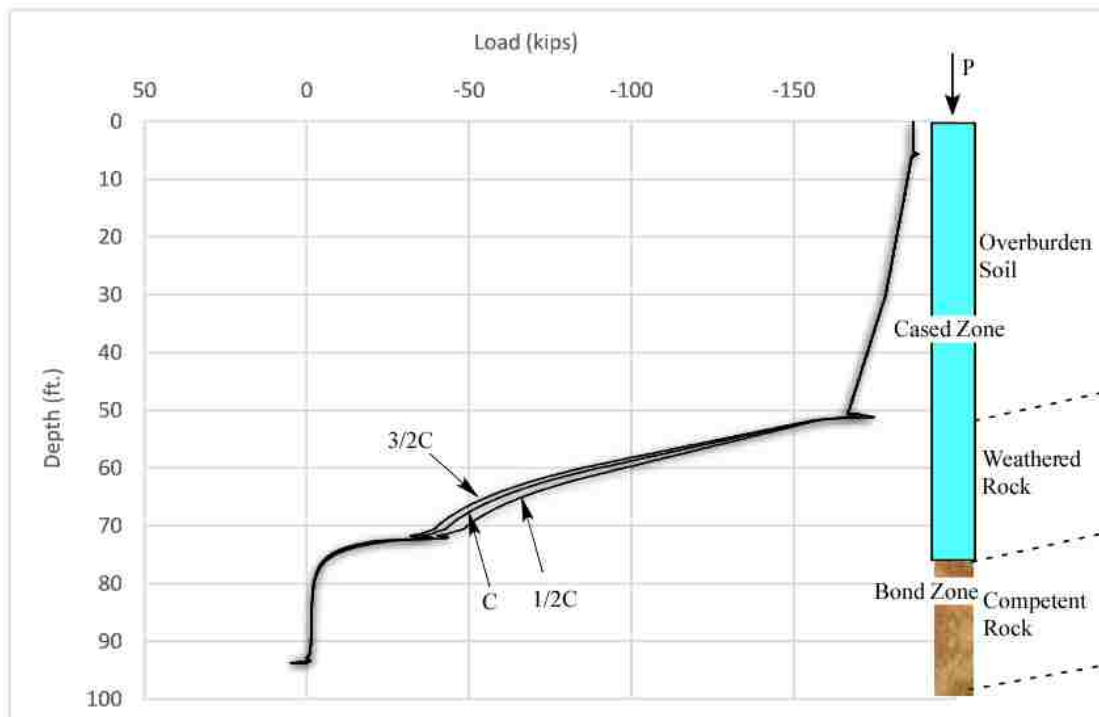
Figure 7.12. Strain Variation with Weathered Rock Cohesion.

Cohesion of competent rock has no effect on the behavior which is similar to Figure 7.12.

Dilation angles sensitivity analysis was conducted at 5º, 10º and 15º of the weathered rock and competent rock separately and they have no effect on the load transfer mechanism. Different friction angles including 25º, 30º and 35º were also conducted separately on the weathered and competent rocks and they are also shows no variation of the strain similar to Figure 7.11. This behavior was expected since the failure is not reached and, therefore, the changes in these parameters, then, will not have significant impact. Summary of the cohesion, friction and dilation angles are shown in Table 7.6.

Table 7.6. Parametric Variations of Cohesion, Friction and Dilation Angles.

Case No.	Parameter	Ground	Observation	Figure No.
9	Cohesion	Weathered Rock	insignificant	5.11
		Competent Rock	No change	5.12
10	Friction and Dilation angles	Weathered Rock	No change	5.12

8. CONCLUSIONS AND RECOMMENDATIONS OF FUTURE WORK

8.1. CONCLUSIONS

Numerical modelling was conducted to understand the load transfer mechanism of micropiles in Bridge No.2 of the foothills smoky mountains in Tennessee. The stratigraphy consists of sandy gravel soil, weathered and competent rock. The bridge consists of four piers; four micropiles were monitored in each of Pier No.1 and Pier No.2. The micropiles in the bridge take two forms; short micropiles that have overburden soil and competent rock and long micropiles that have an additional intermediate weathered rock layer.

The 3D numerical model was developed using ABAQUS standard and it included the following:

• Single micropile analysis (for short and long micropiles). The objective of analyzing both, short and long micropiles, is to understand their load transfer mechanism, particularly, the influence of an intermediate weathered rock layer between the overburden soil and the competent rock.

• Interaction of three micropile without pile cap (for short and long micropiles). The analysis' main objective is to see if there is any overlap in the stresses of the micropiles, particularly, in the bond zone.

• Group Analysis of three micropiles. A group behavior of the micropiles was studied and a cap was included. The main objective is to analyze the stresses transfer from the cap to the micropile and study the load transfer mechanism difference with a loading conditions applied as a pressure on the cap.

- Group Analysis of all micropile. This analysis performs a comprehensive study on the micropiles; including the interface behavior of both the micropile and the ground, the behavior of the ground in all the model, pile cap loading transfer, the group effect and loading quantity in comparison to the real conditions.

After conducting numerical analysis of Bridge No. 2's Micropiles, the conclusions can be stated as the following:

- The numerical simulation as well as the field data showed common load transfer mechanism of Bridge No.2's Micropiles. However, more strain gages are needed to better compare both of them.
- Up to a 0.3 interface friction coefficient in the overburden soil, the load transfer is not significant in the cased zone due to poor interaction between the micropile and the ground and due to the small stiffness of the soil.
- With a 0.3 interface friction coefficient in the weathered rock, most of the load is absorbed in the weathered rock although it has a poor interaction with the ground. The high elasticity modulus of the weathered rock is responsible for most of the load transfer. Therefore, a high stiffness layer can make a good load transfer despite the small interaction with the ground. This conclusion is supported by having two strain gages embedded in the rock in micropile No.16 reading small strain values which matched the numerical analysis.
- The effect of micropiles are negligible at distance greater than one diameter from the micropile. This was verified when section were taken across the micropile and the ground at various locations including the high stress strain concentrations.

- Very small load transfer occurs in the competent rock of the long micropiles and since most of the load transfer has already occurred, the micropile is able to carry further load.

- Based on the group analyses including both with and without cap, it was found that the group effect is negligible. This fact can be supported by the sections taken across the ground and the micropile which show that all readings come back to the normal strain and stresses of the ground at a distance no greater than one diameter. The reasons behind this include the following;

  1. In the overburden soil area; there is a poor interaction with the ground. This will reduce the interaction of the micropiles of each other.

  2. In the rock area, there is a high stiffness layer that also reduces the interaction of the micropiles. Based on Hooke's law, a very high stiffness will have a low strain values and therefore load.

- Also based on the group analysis, it was found that the load transfer of a single micropile matches with a micropile within a group in the overburden soil, weathered and competent rock. At the beginning of the overburden soil, a poor interaction of the micropile and the ground enforces the micropile to behave as a single micropile. It was also shown that the load in the cap and concrete platform is collected and given to the micropile and that matched the best with field instrumentation that has one or two strains gages in the concrete.

- The parametric study was conducted and it was found that the stiffness and the friction are the main factors that govern the load transfer mechanism. In the overburden soil, there is a low friction and low stiffness, so the load transfer is

smaller. In the weathered rock, there is high stiffness and low friction and the overall load transfer is significant. In the competent rock, both of the stiffness and the friction are high and the load transfer is the most significant.

8.2. RECOMMNDATION OF FUTURE WORK

The recommendations of future works are suggested as follows:

1. Development of a more accurate constitutive model that captures the non-linear behavior especially, in the rock. This should include in-situ tests to calibrate the constitutive model

2. Friction along the micropiles should be further studied by installing micropiles in different subsurface conditions.

3. Additional micropiles should be instrumented and monitored and more strain gages should be installed in both cased and bond zones. This can be implemented by, new state of the art sensors, continuous strain gages extending along the whole length of the micropiles. These sensors predict the load transfer at all locations and at different time.

4. Instrumentation can be continued under Bridge No.2 since to understand the long term behavior of load transfer mechanism.

BIBLIOGRAPHY

ABAQUS (2011). ABAQUS Documentation. Dassault Systèmes, Providence, RI.

ACI Committee 318 (2011). Building code requirements for structural concrete (ACI 318-08) and commentary. American Concrete Institute, Farmington Hills, Michigan.

Armour (2001). Micropile Design and Construction Guidelines, Implementation Manual, Springfield, VA, FHWA-SA-97-070.

Barton, N. and V. Choubey (1977). "The shear strength of rock joints in theory and practice." Rock mechanics 10(1-2): 1-54.

Bell & Associates Construction (2012). "Progress meeting, December 18, 2012." Jobsite Trailer, Wears Valley, TN.

Bell, F. (1980). Engineering geology and geotechnics. London: Newnes-Butterworths.

Bowles, J. (1977). Foundation analysis and design. New York: McGraw-Hill.

Bruce, D. A. (2002). "The Basics of Drilling for Specialty Geotechnical Construction Processes." Geotechnical Special Publications 1: 752-771.

Bruce, D. A. and I. Juran (1997). Drilled and grouted micropiles: state-of-practice review, US Department of Transportation, Federal Highway Administration.

Bruce, J., Ruel, M., Janes, M., Ansari, N. (2004). "Design and construction of a micropile wall to stabilize a railway embankment." Proc. 29th, Annual Conference on Deep Foundations, Vancouver, British Columbia, Canada, 1-11.

Cadden, A., Gómez, J., Bruce, D., Armour, T. (2004). Micropiles: Recent advances and future trends. In Current Practices and Future Trends in Deep Foundations, Los Angeles, CA, 140-165.

Coduto, D. P. (2001). Foundation design: Principles and Practices. Prentice Hall, Upper Saddle River, New Jersey.

Coon, R. and A. Merritt (1970). "Predicting in-situ modulus of deformation using rock quality indexes." Determination of the In Situ. Modulus of Deformation'of Rock, ASTM Publication STP 477: 154-173.

Corvern Engineering, Inc. & Palmer Engineering Company, Inc. (2010). "Plans for Proposed Foothills Parkway Project PRA-FOOT 8E17. "Blount County, TN.

Das, B. (1990). Principles of foundation engineering. Boston: PWS-Kent Pub. Co.

Das, B. (2002). Soil mechanics laboratory manual. New York, Oxford university press.

Dixon, D. (2013). "Monitoring Micropile foundations of bridge during construction" thesis presented to Missouri University of Science and Technology, MO, in partial fulfillment of the requirements for the degree of Master of Science.

Donath, F. A. (1968). Experimental study of kink-band development in Martinsburg slate. In Kink Bands and Brittle Deformation (pp. 255-287). Geol. Surv. Canada Ottawa.

Esmaeili, M., Nik, M. G., Khayyer, F. (2012). "Experimental and numerical study of micropiles to reinforce high railway embankments." International Journal of Geomechanics, 13(6), 729-744. Farmer, I. and J. Kemeny (1992). Deficiencies in rock test data. Proc. Int. Conf. Eurock.

Finno, R., Scherer, S., Paineau, B., Roboski, J. (2002). "Load transfer characteristics of micropiles in dolomite". Geotechincal Special Publications, 2, 1038-1053.

Federal Highway Administration (FHWA) (2012). "Post-Tensioning Tendon Installation and Grouting Manual." Ch.1- Bridge Technology.

Foster, R. (1969). General geology. Columbus, Ohio: C.E. Merrill.

FPMP. National Parks Service-Planning, Environment & Public Comment. (NPS PEPC) (1968). "Foothills Parkway Master Plan." US Department of the Interior.

Ghorbani, A., Hasanzadehshooiili, H., Ghamari, E., & Medzvieckas, J. (2014). "Comprehensive three dimensional finite element analysis, parametric study and sensitivity analysis on the seismic performance of soil–micropile-superstructure interaction". Soil Dynamics and Earthquake Engineering, 58, 21-36.

Han, J. S.-L. Ye (2006). "A field study on the behavior of a foundation underpinned by micropiles." Canadian geotechnical journal 43(1): 30-42.

Helwany, S. (2007). Applied soil mechanics with ABAQUS applications. Wiley, New York.

Hoek, E. and M. Diederichs (2006). "Empirical estimation of rock mass modulus." International Journal of Rock Mechanics and Mining Sciences 43(2): 203-215.

Holman, T. P. and B. D. Barkauskas (2007). Mechanics of micropile performance from instrumented load tests. Proc., 7th Int. Symp. on Field Measurements in Geomechanics, ASCE Reston, VA.

Hoskin, P. W. (2005). "Trace-element composition of hydrothermal zircon and the alteration of Hadean zircon from the Jack Hills, Australia." Geochimica et Cosmochimica Acta 69(3): 637-648.

Howe, W. K. (2010). Micropiles for slope stabilization. GeoTrends: The Progress of Geological and Geotechnical Engineering in Colorado at the Cusp of a New Decade, ASCE.

Iai. S, Matsunaga, Y, Kameoka, T "Strain space plasticity model for cyclic mobility" Soils Foundations, 32 (1992), pp. 1–15

Jiang, X. W., Wan, L., Wang, X. S., Wu, X., Zhang, X. (2009). Estimation of rock mass deformation modulus using variations in transmissivity and RQD with depth. International Journal of Rock Mechanics and Mining Sciences, 46(8), 1370-1377.

Juran, I., Benslimane, A., Hanna, S. (2001). Engineering analysis of dynamic behavior of micropile systems. Transportation Research Record: Journal of the Transportation Research Board, 1772(1), 91-106.

Juran, I., Bruce, D. A., Dimillio, A. F., & Benslimane, A. (1999). Micropiles: the state of practice. Part II: design of single micropiles and groups and networks of micropiles. Proceedings of the ICE-Ground Improvement, 3(3), 89-110.

Kershaw, K. A. (2011). "Micropile response to combined loading." thesis, presented to Missouri University of Science and Technology, MO, in partial fulfillment of the requirements for the degree of Doctor of Philosophy.

Kezdi, A. (1974). Handbook of Soil Mechanics. Elsevier, Amsterdam.

Khodair, Y. and A. Abdel-Mohti (2014). "Numerical Analysis of Pile–Soil Interaction under Axial and Lateral Loads." International Journal of Concrete Structures and Materials 8(3): 239-249.

Kulhawy, F. H. and P. W. Mayne (1990). Manual on estimating soil properties for foundation design, Electric Power Research Inst., Palo Alto, CA (USA); Cornell Univ., Ithaca, NY (USA). Geotechnical Engineering Group.

Lade, P. V. (2005). Overview of constitutive models for soils. Calibration of Constitutive Models, ASCE.

Liao, H., Tian, C., & Li, H. (2013). "Analysis of Slope Failure Mechanisms Considering Micropile-Soil Interaction". In Key Engineering Materials, 535: 565-568.

Lizzi, F. (1982). "The static restoration of monuments." International Society for Micropiles & The International Association of Foundation Drilling.

Long, J, Maniaci, M., Menezes, G., Ball, R. (2004). "Results of Lateral Load Tests on Micropiles." Geosupport, 2004: Drilled Shafts, Micropiling, Deep Mixing, Remedial Methods, and Specialty Foundation Systems (Geotechincal Special Publication No. 124), Orlando, FL, 122-133.

Meyerhof, G. (1956). "Penetration tests and bearing capacity of cohesionless soils." Journal of the Soil Mechanics and Foundation Division 82(1): 1-19.

Misra, A. and C.-H. Chen (2004). "Analytical solution for micropile design under tension and compression." Geotechnical & Geological Engineering 22(2): 199-225. Kluwer Academic Publishers, Nehterlands.

Misra, A. and C. Chen (2002). "Load displacement relationships for micropiles." Geotechnical Special Publications 1: 110-125.

Monafared, S. (2012). "Numerical study on the behavior of inclined micropiles." Deep Foundation Institue.

National Park Service (NPS) (1998). "Great Smoky Mountains National Park-Foothills Parkway History." US Department of the Interior.

Ousta, R. and I. Shahrour (2001). "Three-dimensional analysis of the seismic behavior of micropiles used in the reinforcement of saturated soil." International Journal for Numerical and Analytical Methods in Geomechanics 25(2): 183-196.

Peck, R., Hanson, W., Thornburn, T. (1974). Foundation engineering, Wiley, New York.

Prat, M., Bisch, E., Millard, A., Mestat, P., and Cabot, G. (1995). "La modelisation des ouvrages." Hermes, Paris.

Qian, Z., X. L. Lu (2011). "Behavior of micropiles in soft soil under vertical loading." Advanced Materials Research 243: 2143-2150. Trans Tech Publications, Switzerland.

Rahn, P. H. (1996). Engineering geology: an environmental approach. Elsevier, Amsterdam.

Ribacchi, R. (2000). "Mechanical tests on pervasively jointed rock material: insight into rock mass behaviour." Rock mechanics and rock engineering 33(4): 243-266.

Richards, T., M. J. Rothbauer (2004). "Lateral loads on pin piles (micropiles)." Geotechnical Special Publication: 158-174.

Russo, G. (2004). "Full-scale load tests on instrumented micropiles: technology and behavior" Proceedings of the ICE-Geotechnical Engineering 157(3): 127-135.

Sadek, M. and I. Shahrour (2004). "Three-dimensional finite element analysis of the seismic behavior of inclined micropiles." Soil Dynamics and Earthquake Engineering 24(6): 473-485.

Siegel, T. and Brown D. A (2010). "Micropile Design for Pier 1 Bridge No.2 Foothills Parkway Blount County TN" Dan Brown and Associates Consulting Geotechnical Engineers, Sequatchie, TN.

Siegel, T., Graham, D (2010). "Load Test Report for 9 5/8 inch Micropile Bridge No.2 - Foothills Parkway Blount County TN." Dan Brown and Associates Consulting Geotechnical Engineers, Sequatchie, TN.

Siegel, T, Thompson, W.R., III (2010). "Foothills Parkway Bridge No.2 Geotechnical Report." Dan Brown and Associates Consulting Geotechnical Engineers, Sequatchie, TN.

Terzaghi, K (1967). Soil Mechanics in Engineering Practice. New York, John Wiley and Sons.

Ti, K. S., Huat, B. B., Noorzaei, J., Jaafar, M. S., Sew, G. S. (2009). A review of basic soil constitutive models for geotechnical application. Electronic Journal of Geotechnical Engineering, 14, 1-18.

Turan, A., et al. (2008). Lateral behavior of micro-pile groups under static and dynamic loads. Proceedings of the 4th Canadian conference on geohazards.

Vermeer, P. A., & De Borst, R. (1984). Non-associated plasticity for soils, concrete and rock. HERON, 29 (3), 1984.

Wang, M., Han, J. (2010). Numerical Modelling for Ground Improvement of Batter Micropiles on Liquefiable Soils. In Ground Improvement and Geosynthetics, ASCE, 212-219.

Wang, Z., Met, G., Cai, G., Yu, X. (2009). "Dynamic finite element analysis of micropile foundation in subgrade." In Proceedings of Selected Papers from the 2009 GeoHunan International Conference, ASCE, Changsha Hunan, China (pp. 139-144).

West, T. R. (2010). Geology applied to engineering, Waveland Press.

Youssef Abdel Massih, D, Soubra, A. (2008). "Reliability-Based Analysis of Strip Footings Using Response Surface Methodology." Int. J. Geomech., 8(2), 134–143.

Zhang, L. and H. Einstein (2004). "Using RQD to estimate the deformation modulus of rock masses" International Journal of Rock Mechanics and Mining Sciences 41(2): 337-341.

Zienkiewicz, O. C., Chang, C. T., Bettess, P. (1980). Drained, undrained, consolidating and dynamic behaviour assumptions in soils. Geotechnique, 30(4), 385-395.

VITA

Audai K. Theinat was born in Jordan. He earned B.S degree in Civil Engineering from Jordan University of Science and Technology (JUST) in May 2013 where he was ranked as top student among 273 students. Audai then began his M.S degree in Civil Engineering from Missouri University of Science and Technology in August 2013. Audai also taught Geotechnical Engineering Laboratory, six times along three semesters. He also was a research assistant and worked on many civil engineering projects. Audai will be a registered Engineering Intern in the state of Missouri by May 2015.